UNIVERSITÀ
DEGLI STUDI
FIRENZE

Dottorato di Ricerca in Ingegneria Industriale

Ciclo XXVII

Coordinatore del Dottorato
Prof. Ing. Maurizio De Lucia

Development of efficient rotordynamical models to study coupled lateral-torsional vibrations

Settore Scientifico Disciplinare ING/IND 13

Candidata
Ing. Alice Innocenti

Tutor
Dott. Ing. Andrea Rindi

Co-Tutors
Dott. Ing. Enrico Meli
Prof. Ing. Paolo Toni

Anni 2012/2014

Abstract

A correct prediction of the dynamic behaviour of rotors represents a critical issue in the rotating machines field. In the design of rotating systems such prediction is necessary to evaluate if it will accomplish the requirement of safe operating conditions and to prevent systems from working in harmful operating conditions (excessive vibration level, instabilities) that may lead to possible negative consequences such as undesired shut-downs or failures. Hence, the development of accurate and efficient rotordynamical model to be used in the design phase is an important issue in turbo-machinery and rotating machine applications. The current trend in equipping machinery with predictive maintenance systems and the necessity of methods for determining the state of the machine from less intrusive measurements, have led to an increasing need for more reliable mathematical models in rotordynamics. A large amount of research work dealing with rotordynamics modelling can be found in literature and nowadays both traditional simple and complex models may be adopted to investigate the vibration behaviour of rotating equipments.

For a long time most of studies has focused on a single form of vibration, hence lateral and torsional vibrations have been investigated through separate analysis. Current design trends for rotating equipment aim to get higher power transmission and efficiency by reducing weight and increasing the operating speeds, setting the assumption on treating lateral and torsional vibrations by separate and decoupled approaches much less accurate. In fact, this coupling usually exists, as it is caused by the most common malfunction conditions, such as rotor unbalance or shaft misalignment hence, neglecting this coupling may result in inaccurate predictions of the system dynamics. Moreover, complex distributed inertial elements connected to the shaft may determine the coupling of torsional and lateral vibrations as well.

In this thesis an accurate, efficient and fully coupled model for the evaluation of the dynamical behaviour of complex multi-rotor systems is presented. The model has been conceived with the purpose of modelling complex rotors through a systematic and practical approach and with the goal of investigating the bending-torsional interaction in rotor vibrations. The model is based on a finite element rotordynamics formulation and it is able to deal with long rotors characterised by complex topology, such as rotor with distributed inertias or complex connections. This kind of rotor and the way in which they are modelled may deeply influence the predicted dynamics of the system with particular concern to the lateral-torsional vibrations coupling. Thus, through the developed model, complicated shaft-to-rotor connections or particular mounted parts, otherwise not representable with classical models, may be mathematically described. The proposed model represents a systematic and practical approach

to the rotor dynamics modeling issue and its main contribution to the research topic of coupled lateral-torsional vibration in rotors is due to its general topology.

Multi-rotor linking elements (such as couplings) modelled with different levels of detail may be used and non-standard elements may be also adopted for describing particular rotor components, such as rotor with distributed inertias or complex connections. The model is based on a finite element (FE) formulation with 6 degrees of freedom (dofs) for each node and it is therefore suitable to fully coupled studies, in which the existing dependency among longitudinal, lateral and torsional dynamics can be evaluated. Thanks to its numerical efficiency, the proposed model represents a good compromise between accuracy and computational effort, thus it may be used to perform rotordynamical investigation commonly used in rotating machinery design.

The investigated rotor test-case is a dynamometric flywheel test bench for railway brakes that is characterised by a complex geometry formed of several rotors with complex topology (distributed inertias).

The effectiveness of the presented model in predicting the critical behaviour of the considered test-case has been tested by means of experimental vibration data. The experimental data are the results of dedicated vibration tests campaign, performed in collaboration with Politecnico di Milano, Italcertifer (FS) and Simpro S.p.A to assess the vibration behaviour of the machine.

Contents

List of Figures

List of Tables

Introduction

Comprehension and advanced modelling of the complicated dynamic and vibration phenomena involved in rotating machines applications represent a critical issue in the rotordynamics field. A correct prediction of the dynamical behaviour of a rotating machine is indeed an important issue to identify safe operating conditions and to avoid instability operating range that may lead to possible catastrophic consequences for machine. Recent design trends for rotating equipment aim to get higher power and efficiency through optimised weights and increased operating speeds. To this aim, the development and the adoption of advanced rotordynamics models enable designers and engineers to make precise assessment of the significant parameters of rotors and accurate identification of their critical speeds and dynamical behaviour. Furthermore, the current trend in equipping rotating machinery with predictive maintenance systems and the necessity of methods for determining the state of the machine from less intrusive measurements, have led to an increasing demand for more accurate and reliable mathematical models in rotordynamics.

A large amount of research work can be found in literature dealing with rotordynamics modeling and nowadays both traditional simple models (such as the Jeffcott or Stodola-Green rotor models [2, 3]) or more complex ones (transfer-matrix or finite-element (FE) approaches [4, 5, 6, 7, 8]) can be used to investigate the vibration behaviour of a rotor system. Both traditional and complex approaches use systematic discretisation to create an approximated model of the investigated rotor with a finite number (but possibly large) of coordinates. While in the past transfer-matrix methods [4, 8] were used to this aim, nowadays, with the recent fast increase in computing power, FE method represent the standard approach adopted to analyse the dynamics of structure, considering also rotating machines [9].

In the case of rotating machines, for a long time most of studies has focused on a single form of vibration, hence lateral and torsional vibrations were usually modelled and studied in a separate way [4, 6, 9] until some real applications [10] exhibited unpredicted critical resonances on the lateral vibrations characterised by the torsional mode frequency, demonstrating that decoupled lateral and torsional studies could not correctly predict some vibrations.

Current trends in rotordynamics design resulting in more and more complex rotors and high rotational speeds, set the assumption on treating lateral and torsional vibrations by separate and decoupled analysis much less accurate. In fact, this coupling usually exists, as it is caused by the most common malfunction conditions, such as rotor unbalance, shaft misalignment or rotor-to-stator rubbing [11, 12, 13]. Hence, neglecting this coupling may result in inaccurate predictions of the system dynamics. Coupling mechanisms in lateral-torsional

dynamics may lead to rotor unstable behaviours, which mainly arise for rotor speed value where maps of lateral and torsional natural frequencies intersect each other. Hence, in those types of rotating machinery where the angular speed is subjected to high rate of changes, a correct identification of unstable regimes by means of coupled models is required [14]. The coupling of the rotor lateral and torsional motion also becomes significant when the driving or load torques applied to the rotor are unsteady. Torsional vibrations are *quiet* and do not usually propagate to other elements of the machine [10, 15]: only dedicated instrumentation may detect the torsional vibrations and machine operators often do not recognize their presence. In such situations, accurate coupled lateral-torsional models may be useful in detecting torsional vibrations from more standard measurements (such as lateral vibrations).

Vibration analysis represents so a crucial issue in the preliminary design and analysis of rotating machines. The majority of vibrations are caused by rotation related sources (normally unbalance) and consequently excitation forces are synchronous with the rotational speed. Therefore, the forced vibration study is a fundamental aspect in design and analysis of rotating equipments. Since certain effects, such as gyroscopic or fluid-bearings characteristics, are dependent on the rotational speed, common analysis methods require computational assembly and inversion of large matrices at each frequency step. In such a context the development of an accurate and efficient rotordynamics models is highly demanded to accomplish the design and acceptance criteria required by rotating machines standards [16, 17, 18].

Dynamical properties of rotor systems are hence derived through advanced mathematical models representing all the rotordynamics elements present in real rotor applications. Such elements may be classified in two groups: *single-rotor elements* (shafts, mounted parts, bearings, seals) and *multi-rotor elements* (couplings and gearboxes). It is worth noticing that while the mathematical representations of the elements belonging to the former group are almost standardised in the technical literature [1, 4, 10, 17], modelling issues characterising the components of the latter group are still open and their influence on multi-rotors vibration behaviour is yet not well-understood [19, 20, 21, 22].

Critical systems from the modelling standpoint are represented by complex topology rotors, such as rotor with distributed inertial elements or connected simultaneously in several points to the shaft. In this case, a substantial lack concerning models suitable for the coupled bending-torsional analysis of complex rotors is observed in the literature.

Flexible couplings are widely used in rotating machines for power transmission, to compensate the residual misalignment between shafts that rotating equipments may exhibit because of improper machine assembly, thermal distortion or asymmetries in the applied loads. Misalignment represents the second most common malfunction cause after unbalance [10, 19], thus an accurate knowledge of this kind of phenomenon is useful in each application related to the rotating machines diagnosis and prognosis. An extensive overview of the most important papers dealing with this topic can be found in [19]. Since the presence of coupling-misalignment may lead to several problem such as vibration, noise, power losses, wear of bearings or seals and fatigue failures, an accurate modelling of the flexible-coupling in multi-rotor assembly is required to correctly evaluate their dynamical effects in real shaft-lines [21].

Gearboxes are components commonly adopted in multi-rotor systems to in-

crease or reduce the transmitted torque and consequently to reduce or increase shafts angular velocity. The dynamical behaviour induces complex coupled lateral and torsional vibrations phenomena through gear meshing effect, hence, in geared rotors, a correct modelling of gear components is fundamental to predict the vibration behaviour and to achieve a highly reliable design of the investigated machine [22, 23].

Mechanical looseness or improper fit between components parts is common machine malfunction [10] and it generally produces very characteristic modifications of rotor dynamic responses [24] (i.e. long string of frequency harmonics in the FFT at abnormally high amplitudes). A mathematical model capable to reproduce the dynamical properties of loosing parts is very useful to investigate the rotor response to looseness-related dynamic phenomena.

The majority of rotordynamics studies are linear and they are performed in the frequency domain. However, linearity is an idealization of the actual behaviour of real rotors that always deviates to a certain extent from linearity [25]. Rotors may be indeed considered linear in their nominal conditions (small displacements) other components like bearings, dampers, and seals may exhibit severe nonlinear behaviours.

When the linear analysis techniques commonly adopted in design phase are not accurate enough [26] to predict the critical behaviour and to evaluate the amplitude response of nonlinear rotor systems, nonlinear computational strategies like transient analysis must be adopted. Moreover, when forcing functions becomes time dependent, steady-state frequency domain analysis are not sufficient to provide adequate analysis capability and to correctly represent the dynamical behaviour of the considered rotor system [27]. Also in such cases time transient analysis are required since the system response has to be computed as a function of time, especially when rotordynamics analysis are concerned with stresses and fatigue life of the investigated machine.

In literature, several models concerning classical rotordynamics elements may be found [4, 6, 9, 10, 26] while there is a substantial lack concerning distributed elements modelling for the development of general and multi-purpose rotordynamics models. In the present thesis, a rotordynamics model developed with the aim of studying complex phenomena ruling rotor vibrations is introduced. The developed model aims at overcoming modelling limitations relative to complex topology rotors, such as rotors with distributed inertias or connected simultaneously in several points. The modelling of this kind of rotors may affect the dynamical behaviour of the system with particular concern to lateral-torsional vibrations coupling.

The model studies the dynamic behaviour of rotating equipments by means of a FE formulation characterised by 3D beams with 2 nodes and six degrees of freedoms for each node [28, 29]. Based on the finite element formulation a dedicated tool has been developed in the MatLab with Comsol 4.4a environment. The developed model is established to perform rotordynamics analysis of rotor systems characterised by complex topology, such as distributed rotors. The tool has the capability to automatically cover all the typical steps required in a generic rotordynamics design analysis such as undamped and damped critical speeds,harmonic response and instability analysis [17]. Classical or distributed rotordynamics elements may be adopted to execute both linear or nonlinear analysis respectively in the frequency or in the time-domain. Due to its computational efficiency, the model introduced in this work is a good compromise

between accuracy and computational load, hence it is suitable to execute common dynamical studies in the design of rotating equipments.

The rotor test-case studied and modelled in the present work is a flywheel masses test bench for railway brakes, which has been designed for the dynamic testing of railway brakes components. During the tests, railway discs or pads must dissipate the relative quota of the total kinetic energy characterising a single vehicle. Therefore, to produce such huge amount of energy the test bench is composed of a group of shafts, linked each other through flexible couplings and driven by an electrical motor, and of five shiftable flywheel masses, which are used during tests to vary the simulated mass of vehicle. The maximum operating speed of the test bench is equal to 3000 rpm.

The brake test bench has been chosen as case study for several reasons. The first motivation consists in its complex topology configuration. The shaft-line is made up of a *multi-rotor* configuration, formed of multiple shaft groups presenting several distributed inertial elements and linked together through flexible-couplings. Secondly, the particular operating conditions (transient characterised by high torsional and bending applied moments) of the test bench may induce harmful stress state in the rotor structure and may also determine complex modes and coupled lateral-torsional vibrations.

The activity on the selected test-case has been performed in collaboration with RFI (Rete Ferroviaria Italiana) and Simpro S.P.A.

A correct identification of the critical speeds of the machinery is necessary to assure safe working conditions and to prevent the system from working with large amplitude vibrations that may be harmful for the system integrity (rolling bearing, flexible couplings) and for the operation of the test bench. In fact, since the test bench must be used for certification purposes, vibration levels allowed during brake components tests must respect the vibration limits prescribed in international standards [18]. Moreover, during the verification tests the test bench showed some unpredicted vibrations phenomena. Furthermore, after simple rotordynamics models failed to predict the critical speeds in the operating range, a comprehensive model accounting for all flexible systems is required.

Since measured axial motions of the test bench are small if compared both with torsional and lateral ones, in the present state of the research activity the longitudinal displacements have not been taken into account.

The rotordynamics model developed in this work has been validated in a preliminary way by means of experimental data coming from a test campaign aimed at the evaluation of the vibration behaviour of the machine. The test campaign has been performed by Politecnico di Milano, thanks to the instrumentation of the test bench by means of accelerometers to measure mechanical vibration signals in terms of acceleration characterising the non-rotating parts of the machinery [18]. More specifically, accelerometers have been installed on the bearings housing to capture radial vibrations and servo-accelerometers have been used to measure the vibrations of the baseplate, foundation and of the civil structure.

Structure of the thesis

This thesis starts with an initial chapter presenting a survey of the modelling approaches commonly used to study uncoupled lateral and torsional vibrations in rotordynamics applications.

In the second chapter the state-of-the-art on the topic of lateral-torsional vibrations coupling in rotors is presented. Both the phenomenological and the modelling aspects are treated.

The third chapter deals with the description of the Rotordynamical model developed during the Ph.D research activity. A preliminary validation of the model based on a numerical rotor benchmark is also presented.

In the fourth chapter the structure and several components of the rotating machine investigated as test-case are presented.

The experimental activities performed to characterise the dynamical behaviour of the test-case is described in the fifth chapter.

Finally, in the sixth chapter numerical results are compared to experimental data to validate the developed Rotordynamical model by means of measurements coming from the studied test-case.

Chapter 1

Rotordynamics modelling

Rotating machines exhibit complex torsional and bending dynamics for which analytical models may be obtained in the simple cases. Nowadays, thanks to the recent increase in computational power, complex numerical 2D or 3D analysis may also be performed to predict the critical behaviour of rotors. Neverthless, thanks to their step-to-step derivation, analytical models are still employed for understanding physical phenomena determining the peculiar dynamics of rotating systems. For a long time most of studies has focused on a single form of vibration, hence separate lateral and torsional analysis were usually performed [4, 9, 6] through appropriate uncoupled models. These models can be classified in two groups: classical and modern methods. Classical models [2, 3] are based on the study of oversimplification of real-world rotors to gain a qualitative insight into important phenomena typical of rotordynamics, while being much simpler than more realistic models. Such methods provide analytical close solutions to assess the basic critical behaviour of rotors but, due to the geometry semplification, cannot represent real-rotors with complex geometries. Modern rotordynamics models are instead used to investigate the dynamics behaviour of real rotors and they can be based on both transfer-matrix [30] or finite element (FE) [4, 9] formulations.

1.1 Lateral Vibrations

Lateral vibrations are a serious concern in rotors and, if not accurately predicted and corrected, can determine trips, noise, fatigue failure and reduced efficiency of machine. Therefore, analysis of lateral dynamical behaviour of rotors represents a critical issue for the design of turbomachinery and other rotating equipments.

The most important classical and modern methods developed for the study of uncoupled lateral vibrations of rotor are presented in the following sections.

1.1.1 Jeffcott's rotor

The first attempts in defining a mathematical model for the comprehension of rotordynamics were made by Föppl in 1895 and Jeffcott [2] in 1919. Their results can be summed up in the so-called Jeffcott's model where the dynamical

behaviour of a simple rotor-bearings system is investigated and the basic theory for prediction and attenuation of rotor vibrations is established.

Figs. 1.1(a)- 1.1(b) illustrate a flexible rotor with rigid bearings. A rigid disk is located at the axial mid-span of the shaft. Considering the reference frame $Oxyz$ shown in Fig. 1.1(b) the instantaneous position of the rotation axis (geometric center of the rotor) is denoted with the letter C, and it is located in the point of lateral coordinates x_C and y_C; due to a residual unbalance in the disk, the coordinates of the center of mass G are x_G and y_G.

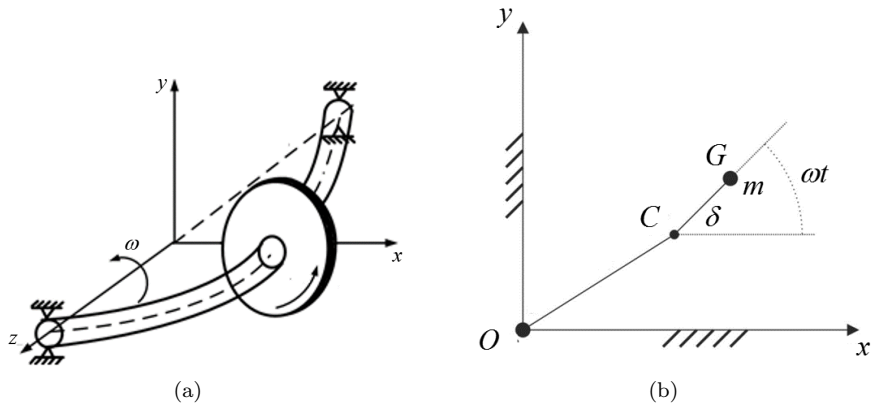

(a) (b)

Fig. 1.1: Jeffcott's rotor (a): scheme (b): back view.

The Jeffcott's model is based on the following assumptions:

- the disk may only translate and it cannot tilt around x or y axis; thus gyroscopic effects can be neglected;
- the disk mass value m is noticeably higher than the shaft mass; the shaft is thus considered massless;
- the shaft is supposed to be isotropic and characterised by a bending stiffness value k;

The studied system is planar and the position of the center of mass G at a generic time t is given by:

$$x_G = x_C + \delta \cos \omega t \tag{1.1}$$
$$y_G = y_C + \delta \sin \omega t \tag{1.2}$$

Time derivatives of Eqs. 1.1 and 1.2 can be obtained:

$$\dot{x}_G = \dot{x}_C - \delta\omega \sin \omega t \tag{1.3}$$
$$\dot{y}_G = \dot{y}_C + \delta\omega \cos \omega t \tag{1.4}$$
$$\ddot{x}_G = \ddot{x}_C - \delta\omega^2 \cos \omega t \tag{1.5}$$
$$\ddot{y}_G = \ddot{y}_C - \delta\omega^2 \sin \omega t \tag{1.6}$$

By applying the Newton's second law through the projection of the force vectors on the plane perpendicular to the rotor undeformed axis the following expressions can be written:

$$m\ddot{x}_G + kx_C = f_x(t) \tag{1.7}$$
$$m\ddot{y}_G + ky_C = f_y(t) \tag{1.8}$$

and considering a free motion Eqs. 1.7 and 1.8 become:

$$m\ddot{x}_G + kx_C = 0 \tag{1.9}$$
$$m\ddot{y}_G + ky_C = 0 \tag{1.10}$$

Introducing the acceleration expressions defined in Eq. 1.5 and 1.6 into the equations of motion it results:

$$m\ddot{x}_C + kx_C = m\delta\omega^2 \cos\omega t \tag{1.11}$$
$$m\ddot{y}_C + ky_C = m\delta\omega^2 \sin\omega t \tag{1.12}$$

The previous equations prove that horizontal (x) and vertical (y) motions of the geometric center C of the shaft consist in forced vibrations, that are the response to the x and y components of the centrifugal force. Moreover, when rigid bearings are assumed, lateral responses are decoupled in the x and y lateral directions and they do not affect each other.

Through the adoption of a complex coordinates formalism [25], as the shaft geometrical center C moves in a plane variable, a vector $(\mathbf{C} - \mathbf{O})$ may be defined through the following complex variable:

$$r_C = x_C + jy_C \tag{1.13}$$

By multiplying Eq. 1.12 for the imaginary unit j, adding it to Eq. 1.11 and introducing the complex variable r_C, it leads to the single complex equation:

$$m\ddot{r}_C + kr_C = m\delta\omega^2 e^{j\omega t} \tag{1.14}$$

thus the Jeffcott's rotor equation is analogous to a single-dof mass equation where the excitation magnitude is function of ω^2. The solution of the previous equation is given by the sum of the homogeneous solution and the particular integral.

The homogeneous solution describes the free motion of the considered rotor and it may be derived by solving the homogeneous algebraic equation obtained introducing a general form of the solution in the homogeneous form of Eq. 1.14 [25]. It results that free whirling of the Jeffcott's rotor is ruled by the expression:

$$r_C^{hom}(t) = R_1 e^{j\omega_n t} + R_2 e^{-j\omega_n t} \tag{1.15}$$

where $\omega_n = \sqrt{k/m}$ is the natural frequency in rad/s and R_1, R_2 are complex constants depending on the initial conditions.

The particular solution defines the response to the harmonic forcing term $m\delta\omega^2 e^{j\omega t}$. Accordingly to the system linearity, the solution has to be harmonic at the same frequency ω of the forcing term:

$$r_C^{for}(t) = r_0 e^{j\omega t} \tag{1.16}$$

Velocity and acceleration responses are given by time derivatives of the previous expression:

$$\dot{r}_C^{for}(t) = j\omega r_0 e^{j\omega t} \tag{1.17}$$

$$\ddot{r}_C^{for}(t) = -\omega^2 r_0 e^{j\omega t} \tag{1.18}$$

By introducing Eqs. 1.16, 1.17 and 1.18 in Eq. 1.14 and simplifying, the unbalance amplitude response can be obtained:

$$r_0^{for} = \frac{m\delta\omega^2}{k - m\omega^2} \tag{1.19}$$

with $r_0^{for} \in \Re$, $\forall\omega$ and $\omega \neq 0$.

Considering a damped motion, where for instance air drag on disks, bearings or shaft damping is modelled through a viscous damping coefficient c, the unbalance response amplitude is instead given by the complex expression [1, 25]:

$$r_0 = \frac{m\delta\omega^2}{k - m\omega^2 + j\omega c} \tag{1.20}$$

In this case, the maximum value of the unbalance amplitude response is given when the shaft speed ω is equal to the critical speed $\omega_{cr} = \omega_{cr}/(1 - 2\xi^2)$, where $\xi = c/(2\sqrt{km})$ is called the damping factor.

1.1.2 Stodola-Green's model

The Jeffcott's model helps in the introduction of elementary rotordynamics concepts as critical speeds and synchronous response. The heaviest assumption made in the Jeffcott's model consists in concentrating the whole mass in a point mass located at the mid-span of the shaft, consequently the contribution of the moments of inertia is not taken into account. This limitation precludes the study of phenomena that considerably affect lateral dynamics, such as those causing the lateral natural frequencies to depend on the rotor spin speed. To overcome this limitation, a first step was made by the so-called Stodola-Green's model. This model is the final output of the research activity performed by Stodola (1927) [3], Green (1948) and Den Hartog (1952) [8].

The model can be derived starting from the following hypotheses:

- the rotor mass is uniformly distributed in a disk;
- the disk can be placed at any axial location of the shaft (Fig. 1.2(a));
- the rotation axis is coincident with the geometrical shaft line and it is inertial central and principal;
- the longitudinal displacement may be neglected;
- rotor spin speed is constant.

An analytical response of the rotor system may be derived through the application of the rigid-body dynamics equations [6] leading to a model with six degrees of freedom (dofs): three translations x_G, y_G and z_G of the center of mass G of the disk and three rotational displacements. Due to the adopted working

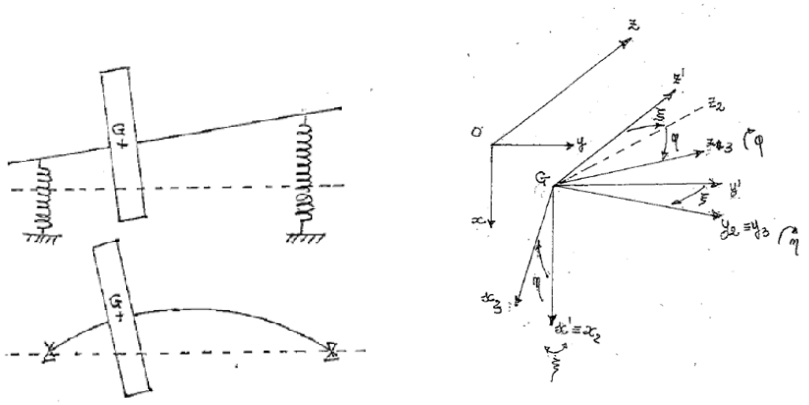

(a) (b)

Fig. 1.2: Stodola-Green's model (a): rotor scheme (b): reference systems.

hypotheses, only four degrees of freedom have to be considered: the lateral translations (x_G and y_G) of the center of mass G and two rotations α and β around appropriate axes. These rotations may be defined considering that, in a reference system with central axes x', y_2 and z_3 illustrated in Fig. 1.2(b), that are parallel to those of the undeformed system, the angular position of the disk may be defined through an α rotation around x' axis, a β rotation around y_2 and finally a ϕ rotation around the z_3 axis.

By hypothesizing that the vibration motion is characterised by a synchronous pulsation ω and neglecting damping effects, the existence of a rotating plane around the z axis that contains the deformed system can be assumed (Fig. 1.3(a)) and the disk equilibrium in the rotating plane can be studied to obtain an analytical solution of the problem [31].

The forces acting on the rotating plane are the centrifugal force $F_C = m\omega^2 x_G \mathbf{i}$ and the centrifugal momentum $M_C = I_{xz}\omega^2 \mathbf{j}$ where it can be proved that $I_{xz} \cong (I_P - I_T)\alpha$. In the case of small deformations the beam theory establishes that deformations (Fig. 1.3(b)) are linear functions of the applied loads:

$$x_G = a_{11}F_C + a_{12}M_C \tag{1.21}$$

$$\alpha = a_{21}F_C + a_{22}M_C \tag{1.22}$$

where, from the Maxwell's theorem $a_{12} = a_{21}$ and the coefficients a_{ij} with $i, j = 1, 2$ depend only on the beam geometry and material's property. Introducing the expressions of the centrifugal force F_C and momentum M_C and re-arranging, the following homogeneous system may be obtained:

$$(a_{11}m\omega^2 - 1)x_G + a_{12}(I_P - I_T)\omega^2\alpha = 0 \tag{1.23}$$

$$a_{21}m\omega^2 x_G + \left[a_{22}(I_P - I_T)\omega^2 - 1\right]\alpha = 0 \tag{1.24}$$

Non-trivial solution of the previous system may be obtained setting the determinant of the coefficient matrix equal to zero and solving the resulting characteristic equation:

$$(a_{11}m\omega^2 - 1)\left[a_{22}(I_P - I_T)\omega^2 - 1\right] - a_{12}(I_P - I_T)\omega^2 m a_{21} = 0 \tag{1.25}$$

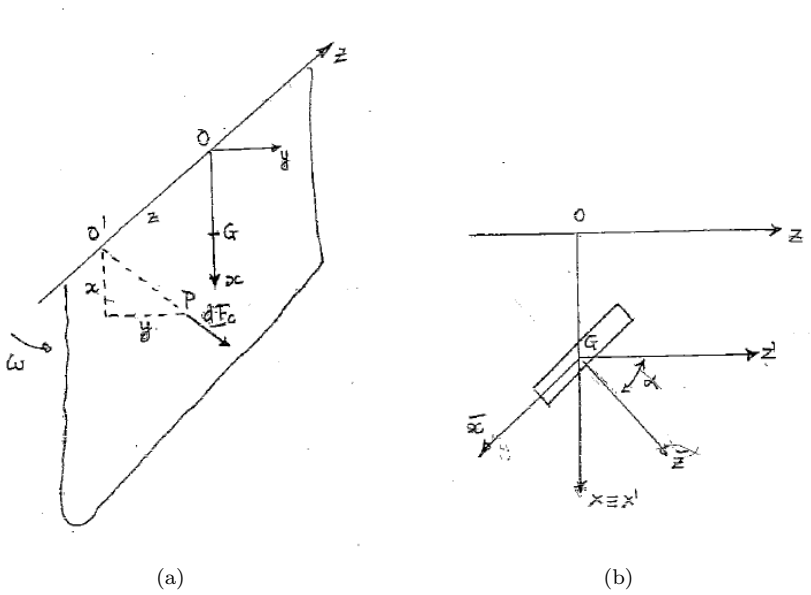

(a) (b)

Fig. 1.3: Solution on the rotating plane (a): centrifugal force and momentum (b): deformed state.

The two values of the variable ω satisfying the previous equation are the two critical speeds of the investigated rotor. The complete solution of Eq. 1.25 is formed of two pairs of values, presenting by the same module and opposite sign, each one relative to the opposite whirling directions of the rotor.

1.1.3 Myklestad-Prohl Transfer Matrix Approach

Transfer-matrix formulations have been historically employed to develop lumped-parameters structural models for rotordynamics analysis [8]. Three different formulations belonging to this group are: the first one is the Myklestad's [32] approach for predicting critical speeds of non-rotating constrained beam (particularly cantilever aircraft wing). The second is the Myklestad-Prohl's method [30, 33] for the critical speeds computation in a isotropic rotor; it extends the application of the previous one to rotating structures by including gyroscopic moments. The third approach is the so-called Lund method [6], representing a generalization of the second one to include complex motion and generalized bearings. In the present section the approach developed almost simultaneously by Myklestad and Prohl is introduced. The investigated rotor system, depicted in Fig. 1.4(a), is lumped in a number of rigid disks located at specific nodes, called stations. Following the conventional transfer-matrix notation, the $i-th$ disk element is placed at the $i-th$ station and the massless beam element connecting two succeeding stations (i and $i+1$) is the $i-th$ field. Fields are the elements to which the elastic characteristics of the investigated rotor are assigned. Superscripts r and l refer respectively to left and right side of a station. The properties necessary to represent the $i-th$ disk are: mass m_i, polar J_{Pi} and transverse J_{Ti} inertia values.

The mathematical development of the present model is based on the assump-

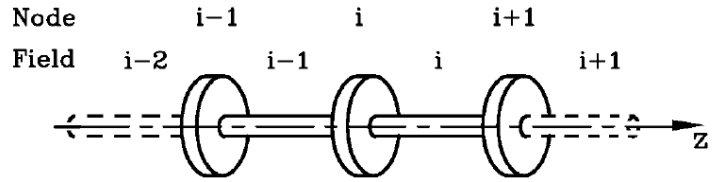

(a)

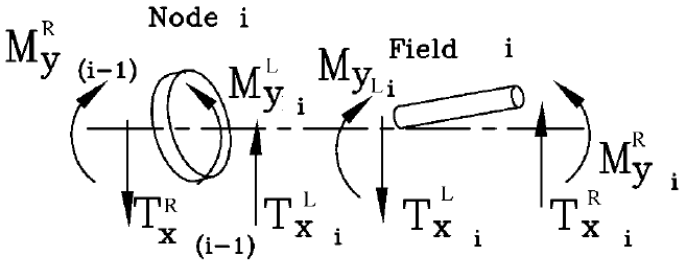

(b)

Fig. 1.4: Myklestadt-Prohl approach (a): scheme of the discretisation (b): external forces and moments.

tion that the deformed shape of the investigated structure, due to shear forces T_x and bending moments M_y ,lies in the xz plane as illustrated in Fig. 1.4(b). A deformed configuration is thus defined through the deflection x_i and slope β_i values. The $i-th$ state vector $\mathbf{s}_i$ can be thus defined:

$$\mathbf{s}_i = \begin{bmatrix} x_i & \beta_i & T_{xi} & M_{yi} \end{bmatrix}^T \tag{1.26}$$

Relationships that relate the shear forces and moment of the left and right side of the $i-th$ station can be derived through continuity:

$$x_i^r = x_i^l \tag{1.27}$$

$$\beta_i^r = \beta_i^l \tag{1.28}$$

$$T_{xi}^r = T_{xi}^l - m_i x_i \omega^2 \tag{1.29}$$

$$M_{yi}^r = M_{yi}^l - I_i \beta_i \omega^2 \tag{1.30}$$

or in matrix arrangement:

$$\begin{bmatrix} x_i \\ \beta_i \\ T_{xi} \\ M_{yi} \end{bmatrix}^r = \begin{bmatrix} 1 & 0 & 0 & 0 \\ 0 & 1 & 0 & 0 \\ -\omega^2 m_i & 0 & 1 & 0 \\ 0 & -\omega^2 I_i & & 1 \end{bmatrix} \begin{bmatrix} x_i \\ \beta_i \\ T_{xi} \\ M_{yi} \end{bmatrix}^l \tag{1.31}$$

Considering the state vector expression in Eq. 1.26, Eq. 1.31 can be written in a more compact form;

$$\mathbf{s}_i^r = T_{si} \mathbf{s}_i^l \tag{1.32}$$

where T_{si} represents the $i-th$ station transfer matrix.

Analogous relationships may be written to relate variables on left and right-hand sides of the $i-th$ field element. The deflection x_{i+1} at the right-hand side of the considered field is evaluated as the characteristic deflection of a l_i length cantilever beam, loaded on its right-hand side by the shear force T_{xi+1} and bending moment M_{xi+1} and subjected on its left-hand side to the initial constraint displacement x_i and rotation β_i. Taking into account the bending moment and shear force equilibrium requirements:

$$\frac{\partial M}{\partial z} = T \tag{1.33}$$

$$\frac{\partial^2 x}{\partial z^2} = \frac{M}{EI} \tag{1.34}$$

equations relating right and left-hand side of the $i-th$ field result:

$$x^l_{i+1} = x^r_i + \beta_i l_i - \frac{l_i^3}{6EI_i} T^l_{xi+1} + \frac{l_i^2}{2EI_i} M^l_{yi+1} \tag{1.35}$$

$$\beta^l_{i+1} = \beta^r_i - \frac{l_i^2}{2EI_i} T^l_{xi+1} + \frac{l_i^2}{EI_i} M^l_{yi+1} \tag{1.36}$$

$$T^l_{xi+1} = T^r_{xi} \tag{1.37}$$

$$M^l_{yi+1} = M^r_{yi} + l_i T^r_{xi} \tag{1.38}$$

where I_i is the area moment of inertia of the $i-th$ shaft station.
In matrix form it can be written:

$$\begin{bmatrix} x_{i+1} \\ \beta_{i+1} \\ T_{xi+1} \\ M_{yi+1} \end{bmatrix}^l = \begin{bmatrix} 1 & l_y & \frac{l_i^3}{6EI_i} & \frac{l_i^2}{2EI_i} \\ 0 & 1 & -\frac{l_i^2}{2EI_i} & +\frac{l_i^2}{EI_i} \\ 0 & 0 & 1 & 0 \\ 0 & 0 & -l_i & 1 \end{bmatrix} \begin{bmatrix} x_i \\ \beta_i \\ T_{xi} \\ M_{yi} \end{bmatrix}^r \tag{1.39}$$

or more compactly:

$$\mathbf{s}^l_{i+1} = T_{fi} \mathbf{s}^r_i \tag{1.40}$$

where T_{fi} represents the field transfer matrix. The combination of Eq. 1.40 with Eq. 1.32 yields to the overall transfer matrix:

$$\mathbf{s}^l_{i+1} = T_{fi} T_{si} \mathbf{s}^l_i = T_i \mathbf{s}^l_i \tag{1.41}$$

Through the recursive application of the previous equation from station 1 to station n, where n is the number of stations forming the rotor discretisation, the system global transfer matrix can be obtained:

$$\mathbf{s}^r_n = T_{sn} T_{n-1} T_{n-2} ... T_1 \mathbf{s}^l_1 = T \mathbf{s}^l_1 \tag{1.42}$$

Since the elements of the global transfer matrix T matrix are functions of ω, the values of the natural frequencies of the system can be obtained by introducing the boundary conditions (e.g free-free boundary conditions) of the system and then imposing the mathematical conditions to get non-trivial solutions [31].

1.1.4 Finite Element Models for Lateral Vibrations

In the past, methods based on transfer matrices were used to predict the dynamical behaviour of rotating machines because they could work with tabular manual computations or implemented on very small computers. Due to the fast increase in computational power registered in the last thirty-years, finite element (FE) method has become the *de facto* standard approach to model rotordynamics systems [8, 9]. The FE approach was firstly applied to a rotor structure by Ruhl and Booker [34], with subsequent main contributions by Nelson and McVaugh [8, 35, 36].

A lot of works has been done and several models can be found in literature dealing with the development of finite element formulations for lateral vibration analysis. In the following part of the section, a mathematical model based on the work of Lalanne [4] and Friswell [9] is described. The FE formulation is obtained by a Lagrangian approach.

Conceptually, to apply the FE approach to an investigated structure, this one must be preliminary discretised into simple elements. The mathematical formulations describing these elements can be derived and then assembled together yielding, with acceptable accuracy, to the equations of motion of the entire studied structure. For modelling purposes, rotors are discretised into shaft elements. Each element is characterised by two nodes where disks, bearings or other concentrated elements may be attached.

FE elements models developed for lateral analysis are focused only on lateral vibrations, hence four generalized coordinates for each node are employed to represent the significant degrees of freedom: two transverse displacements and two rotations about the lateral X and Y axes.

The following hypotheses hold:

- XYZ is an inertial frame;
- rotations are defined such that θ is a positive rotation around X axis and ψ is a positive rotation around the Y axis;
- small displacements and rotations of the rotor from its equilibrium assumptions are considered.

Disk element

The equations of motion of disk elements may be derived through an energetic lagrangian approach: because the disk is supposed to be rigid, kinetic energy must be evaluated and strain energy can be neglected. The expression of the translational kinetic energy of the $i-th$ disk, neglecting axial motions, may be derived as:

$$T_{Di}^{t} = \frac{1}{2} m_{Di} \left(\dot{u}_i^2 + \dot{v}_i^2 \right) \tag{1.43}$$

with m_{Di} is the mass of the $i-th$ disk and $\dot{u}_i$,$\dot{v}_i$ are the translational velocities in the X and Y directions.

For a simmetric disk, the kinetic energy related to the rotational motion, may be computed as:

$$T_{Di}^{r} = \frac{1}{2} I_{Di} \left(\widetilde{\omega}_{xi}^2 + \widetilde{\omega}_{yi}^2 \right) + \frac{1}{2} I_{Pi} \widetilde{\omega}_{zi}^2 \tag{1.44}$$

where I_{Pi} and I_{Ti} are respectively the polar and transverse moments of inertia of the disk; $\widetilde{\omega}_{xi}$, $\widetilde{\omega}_{yi}$ and $\widetilde{\omega}_{zi}$ are the instantaneous angular speeds around the $\widetilde{x}$, $\widetilde{y}$ and $\widetilde{z}$ axes of a reference frame attached to the disk. The expressions $\widetilde{\omega}_{xi}$, $\widetilde{\omega}_{yi}$ and $\widetilde{\omega}_{zi}$ can be derived considering an appropriate set of subsequent rotations relating the orientation of the disk reference system to the fixed one. It is easy to obtain [9] the following expression:

$$\begin{bmatrix} \widetilde{\omega}_{xi} \\ \widetilde{\omega}_{yi} \\ \widetilde{\omega}_{zi} \end{bmatrix} = \begin{bmatrix} \dot{\theta}\cos\phi + \dot{\psi}\sin\phi\cos\theta \\ -\dot{\theta}\sin\phi + \dot{\psi}\cos\phi\cos\theta \\ \Omega - \dot{\psi}\sin\theta \end{bmatrix} \tag{1.45}$$

By substituting the previous definitions in Eq. 1.44 and assuming small values for the rotations θ and ψ, the rotational kinetic energy of the disk is defined through the following expression:

$$T_{Di}^{r} = \frac{1}{2} I_{Di}\left(\dot{\theta}_i^2 + \dot{\psi}_i^2\right) + \frac{1}{2} I_{Pi}\left(\Omega^2 - 2\dot{\psi}_i \Omega\theta\right) \tag{1.46}$$

At this point the total kinetic energy of the disk can be evaluated:

$$\begin{aligned} T_{Di} = T_{Di}^{t} + T_{Di}^{r} = & \frac{1}{2} m_{Di}\left(\dot{u}_i^2 + \dot{v}_i^2\right) + \frac{1}{2} I_{Di}\left(\dot{\theta}_i^2 + \dot{\psi}_i^2\right) + \\ & \frac{1}{2} I_{Pi}\left(\Omega^2 - 2\dot{\psi}_i \Omega\theta\right) \end{aligned} \tag{1.47}$$

Re-arranging the local coordinates defining the motion of the $i-th$ disk element in the state vector $\mathbf{u}_i \in \Re^{4\times 1}$:

$$\mathbf{u}_i = \begin{bmatrix} u_i & v_i & \theta_i & \psi_i \end{bmatrix}^T \tag{1.48}$$

the application of Lagrange's equations to Eq. 1.47 leads to:

$$\frac{d}{dt}\left(\frac{\partial T_{Di}}{\partial \dot{\mathbf{u}}_\mathbf{i}}\right) - \frac{\partial T_{Di}}{\partial \mathbf{u}_i} = M_{Di}\ddot{\mathbf{u}}_\mathbf{i} + \Omega G_{Di}\mathbf{u}_\mathbf{i} \tag{1.49}$$

where the expressions of the $i-th$ disk mass $M_{Di} \in \Re^{4\times 4}$ and gyroscopic $G_{Di} \in \Re^{4\times 4}$ matrices result:

$$M_{Di} = \begin{bmatrix} m_{Di} & 0 & 0 & 0 \\ 0 & m_{Di} & 0 & 0 \\ 0 & 0 & I_{Di} & 0 \\ 0 & 0 & 0 & I_{Di} \end{bmatrix} \qquad G_{Di} = \begin{bmatrix} 0 & 0 & 0 & 0 \\ 0 & 0 & 0 & 0 \\ 0 & 0 & 0 & I_{Pi} \\ 0 & 0 & -I_P & 0 \end{bmatrix} \tag{1.50}$$

Shaft element

Shaft elements contribute both on stiffness and inertial property of the rotor finite element model, thus both kinetic and strain energy must be evaluated to determine shaft element matrices.

Shaft elements are usually represented as beam-like structure with circular or circular hollow cross-section. Several beam theories have been employed in rotordynamics analysis. The Euler-Bernoulli [9, 25] beam element is the most simple as it neglects shear effects and rotary inertia contribution. Mass and stiffness matrices derived through this beam formulation are usually accurate enough for the description of slender beams. For relatively thick shafts

both shear effects and rotary inertia must be considered and to this aim the Rayleigh's beam model [9], which takes into account shear effects, and Timoshenko's formulation [9, 25, 37], including both shear and rotary inertia effects, can be employed.

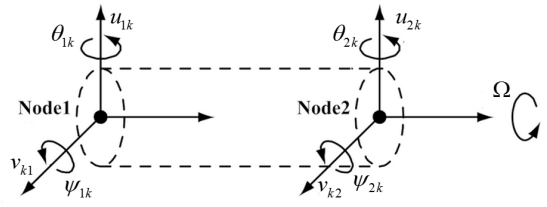

Fig. 1.5: Timoshenko's beam.

In the following part of the section, the derivation of the mass and stiffness matrices for a Timoshenko beam element (Fig. 1.5) is presented. The $k-th$ Timoshenko beam element is delimited by two nodes with six dofs for each node: three displacements and three rotations. As the Timoshenko's beam properties lead to uncoupled axial, torsional and bending behaviour, lateral analysis in each of the coordinate planes may be performed considering only four degrees for each node namely two transverse displacement u and v along respectively x and y axes and two rotations θ and ψ around the same axes. Hence, the vectors of generalized coordinates $\mathbf{u}_{1k}$ and $\mathbf{u}_{2k}$ containing the nodal displacement for the $k-th$ shaft element result:

$$\mathbf{u}_{1k} = \begin{bmatrix} u_{1k} & \theta_{1k} & v_{1k} & \psi_{1k} \end{bmatrix}^T \tag{1.51}$$

$$\mathbf{u}_{2k} = \begin{bmatrix} u_{2k} & \theta_{2k} & v_{2k} & \psi_{2k} \end{bmatrix}^T \tag{1.52}$$

The deflections and rotations within the $k-th$ element may be expressed as function of the nodal variables:

$$\begin{bmatrix} u_k(\xi,t) \\ \psi_k(\xi,t) \end{bmatrix} = \begin{bmatrix} N_{11}(\xi) & N_{12}(\xi) & N_{13}(\xi) & N_{14}(\xi) \\ N_{21}(\xi) & N_{22}(\xi) & N_{23}(\xi) & N_{24}(\xi) \end{bmatrix} \begin{bmatrix} u_{1k}(t) \\ \psi_{1k}(t) \\ u_{2k}(t) \\ \psi_{2k}(t) \end{bmatrix} = N\mathbf{q}_x \tag{1.53}$$

$$\begin{bmatrix} v_k(\xi,t) \\ -\theta_k(\xi,t) \end{bmatrix} = \begin{bmatrix} N_{11}(\xi) & N_{12}(\xi) & N_{13}(\xi) & N_{14}(\xi) \\ N_{21}(\xi) & N_{22}(\xi) & N_{23}(\xi) & N_{24}(\xi) \end{bmatrix} \begin{bmatrix} v_{1k}(t) \\ \theta_{1k}(t) \\ v_{2k}(t) \\ \theta_{2k}(t) \end{bmatrix} = N\mathbf{q}_y \tag{1.54}$$

and the expression of the adopted shape functions can be easily found in literature [9, 25].

The potential energy consists of the contribution given by bending and shear deformations:

$$dU_k = \frac{1}{2} EI_{yk} \left[\left(\frac{\partial \psi_k}{\partial z} \right)^2 + \left(\frac{\partial \theta_k}{\partial z} \right)^2 \right] dz + \frac{1}{2} \frac{GA_k}{\chi_k} \left(\gamma_{xz}^2 + \gamma_{yz}^2 \right) dz \tag{1.55}$$

with E and G respectively denoting the Young's and tangential modulus of the shaft material, I_{yk} and A_k represents the diametral cross-section inertia and

area. Shear deformations γ_{xz} and γ_{yz} are related to displacements through the following expressions:

$$\gamma_{xz} = \psi - \frac{\partial u}{\partial z} \qquad \gamma_{yz} = -\theta - \frac{\partial v}{\partial z} \tag{1.56}$$

The expression of the strain energy of the element may be computed integrating Eq. 1.55 over the whole beam:

$$\begin{aligned} U_k = &\frac{EI_{yk}}{2l_k}\int_0^1 \mathbf{q}_x^T \frac{\partial \mathbf{N}_2^T}{\partial z}\frac{\partial \mathbf{N}_2}{\partial z}\mathbf{q}_x d\zeta + \frac{EI_{yk}}{2l_k}\int_0^1 \mathbf{q}_y^T \frac{\partial \mathbf{N}_2^T}{\partial z}\frac{\partial \mathbf{N}_2}{\partial z}\mathbf{q}_y d\zeta \\ &+ \frac{6EI_{yk}}{\Phi l_k}\int_0^1 \mathbf{q}_x^T \mathbf{N}_3^T \mathbf{N}_3 \mathbf{q}_x d\zeta + \frac{6EI_{yk}}{\Phi l_k}\int_0^1 \mathbf{q}_y^T \mathbf{N}_3^T \mathbf{N}_3 \mathbf{q}_y d\zeta \end{aligned} \tag{1.57}$$

where:

- $\mathbf{N}_1$ and $\mathbf{N}_2$ denote respectively the first and second row of the shape function matrix N;
- $\mathbf{N}_3$ is given by the expression $\mathbf{N}_2 - \partial \mathbf{N}_1^T/\partial z$;
- $\Phi = 12EI_{yk}/GA_k l_k^2 \chi$ and χ represents the shear factor.

Eq. 1.57 can be re-arranged by introducing the stiffness matrix K:

$$U_k = \frac{1}{2}\mathbf{q}_x^T K \mathbf{q}_x + \frac{1}{2}\mathbf{q}_y^T K \mathbf{q}_y \tag{1.58}$$

and introducing the expressions of the shape functions [9] in the potential energy expression and through integrations, the bending stiffness matrix K results:

$$K = \frac{EI_{yi}}{l^3\left(1+\Phi\right)}\begin{bmatrix} 12 & 6l_k & -12 & 6l_k \\ & \left(4+\Phi\right)l_k^2 & -6l_k & \left(2-\Phi\right)l_k^2 \\ & & 12 & -6l_k \\ & symm. & & \left(4+\Phi\right)l_k^2 \end{bmatrix} \tag{1.59}$$

The expression of the kinetic energy can be computed as:

$$dT_{Sk} = \frac{1}{2}\rho A_k\left(\dot{u}^2 + \dot{v}^2\right) + \frac{1}{2}\rho\left[I_y\left(\dot{\theta}^2 + \dot{\psi}^2\right) + J_P\left(\Omega^2 + \Omega\psi\theta\right)\right] \tag{1.60}$$

Substituting into the previous equation the expressions of the shape function [9], it yields to:

$$\begin{aligned} T_k = &+ \frac{1}{2}\rho A l_k \int_0^1 \left(\dot{\mathbf{q}}_x^T N_1^T N_1 \dot{\mathbf{q}}_x + \dot{\mathbf{q}}_y^T N_1^T N_1 \dot{\mathbf{q}}_y\right) d\zeta \\ &+ \frac{1}{2}\rho I_y l_k \int_0^1 \left(\dot{\mathbf{q}}_x^T N_2^T N_2 \dot{\mathbf{q}}_x + \dot{\mathbf{q}}_y^T N_2^T N_2 \dot{\mathbf{q}}_y\right) d\zeta \\ &+ \rho J_y l_k \Omega^2 - 2\rho J_y l_k \Omega \int_0^1 \mathbf{q}_y^T N_2^T N_2 \mathbf{q}_x d\zeta \end{aligned} \tag{1.61}$$

Through the introduction of the the mass matrix M, the following expression holds:

$$T_{Si} = + \frac{1}{2}\dot{\mathbf{q}}_x^T M_t \dot{\mathbf{q}}_x + \frac{1}{2}\dot{\mathbf{q}}_y^T M_t \dot{\mathbf{q}}_y + \frac{1}{2}\dot{\mathbf{q}}_x^T M_r \dot{\mathbf{q}}_x + \frac{1}{2}\dot{\mathbf{q}}_y^T M_r \dot{\mathbf{q}}_y \tag{1.62}$$

$$+ \rho J_y l_i \Omega^2 - 2\Omega \dot{\mathbf{q}}_y^T M_r \mathbf{q}_x \tag{1.63}$$

where M_t and M_r represents respectively the translational and rotational mass matrices.

Bearing elements

All types of bearings that can be adopted in rotating machines are characterised by a certain amount of flexibility and a certain quantity of adsorbed energy; hence, in FE models, they can be represented by means of stiffness and damping elements connecting the nodes of the rotor and the supporting structure. For most types of bearings, the load-deflection characteristic is nonlinear and it is function of the shaft speed, leading, from a modelling standpoint, to more difficult dynamical analysis. A widely spread simplified approach consists in assuming a linear load-deflection relationship that holds when the dynamical displacements are small.

In industrial applications, bearing elements are usually taken into account only for lateral translational motions. Therefore, the mathematical expression of the X and Y components of the $j-th$ force acting on the rotor due to bearing can be written starting from velocities and displacements of the $j-th$ shaft node:

$$\begin{bmatrix} F_{Xj} \\ F_{Yj} \end{bmatrix} = - \begin{bmatrix} K_{XX} & K_{XY} \\ K_{YX} & K_{YY} \end{bmatrix} \begin{bmatrix} u_j \\ v_j \end{bmatrix} - \begin{bmatrix} C_{XX} & C_{XY} \\ C_{YX} & C_{YY} \end{bmatrix} \begin{bmatrix} \dot{u}_j \\ \dot{v}_j \end{bmatrix} \tag{1.64}$$

or in matrix form:

$$\mathbf{F}_j^{brg} = -K_j^{brg}\mathbf{u}_j^{brg} - C_j^{brg}\dot{\mathbf{u}}_j^{brg} \tag{1.65}$$

Bearing stiffness and damping matrices are commonly asymmetrical and their terms may be noticeably vary in function of rotor speed.

From a rotordynamics modelling standpoint, seals act essentially as bearings acting forces on the rotors and they can be taken into account as extra-bearings.

Assembly of the full equations of motion

The global equation of motion for a n degrees of freedom rotor system can be obtained through the assembly of the equations of motion of the single elements:

$$M\ddot{\mathbf{u}} + (C - \Omega G)\,\dot{\mathbf{u}} + K\mathbf{u} = \mathbf{F} \tag{1.66}$$

where $\mathbf{u} \in \Re^{n\times 1}$ is the vector of displacements and rotations of the nodes. M, C, G and K are respectively the mass, damping, gyroscopic and stiffness global matrices and F is the vector of the external forces acting on the discretised system.

1.2 Torsional Vibrations

All rotating machines experience torsional vibrations of a certain degree during startup, operating conditions and shutdown, thus the torsional response must be predicted and investigated to ensure operation reliability of rotating equipments [15]. Torsional vibration is an oscillatory twisting motion of the shaft of a rotating system that is superimposed on its steady rotational motion. The time-dependent twist in the shaft line induces pulsating torques acting

both on the shafts of the machines and on couplings or gearboxes in multi-rotor configurations [4, 38].

Torsional shaft vibrations may cause gear noise and wear, gear teeth failures, damages on couplings, shrink-fit slip and keys failures. Tipically single turbomachinery rotors are characterised by high torsional stiffness values, hence the natural frequencies of torsional vibrations are out of the possible torsional excitations range; in multi-rotor configurations the torsional stiffness values characterising shaft-couplings may be low enough to set the torsional natural frequencies of the considered system in the range of excitation frequencies [39]. Moreover, coupling of turbomachinery with other type of rotating machines (e.g., electrical motors) or the presence of complex distributed inertial elements with multi-points and asymmetric rotor-to-shaft connections may results in torsional vibrations phenomena.

Mechanical reliability of rotating machines represents a crucial aspect in the design phase of every train element and sufficient analysis and investigation has to be done to ensure reliable operating condition of the designed machine throughout its service life [17]. When several rotor units are assembled together to form a multi-rotor configuration, an investigation of the torsional response of the complete train is highly required with the purpose of studying the torsional behaviour of individual units when coupled together and ensuring reliability of the coupled system.

The torsional response of a rotor system can be considered acceptable when it does not exhibit any coincidence between operating speeds or torsional excitations harmonic with the torsional natural frequency. For instance, API codes for turbomachinery applications [16, 17] establish that the torsional frequency values of a complete unit have to be lower at least 10 percent of any operating speed or 10 percent higher than the trip speed value.

Torsional natural frequencies may be evaluated through uncoupled analysis focused on torsional vibrations only or also by means or more complex coupled lateral-torsional models.

Detailed methodology and modelling recommendations for uncoupled train torsional analysis (such as rotor discretisation, dimensions and number of elements) can be found in API standards [16, 17].

In the present section the mathematical modelling of uncoupled torsional vibration is introduced; this kind of approach may be employed when the rotor lateral response is substantially absent (whenever the rotor is characterised by a high value of the flexural stiffness or supported by adequately spaced bearing), or when torsional-lateral coupling is negligible.

1.2.1 Direct Approach

In lumped parameters models [10, 25], the torsional behaviour of rotors can be investigated using a direct approach. The rotor is lumped into a set of rigid inertias, connected by means of massless visco-elastic elements. Damping elements may represent *internal damping* phenomena (related to relative motion between rotor sections) or *external damping* caused by the shaft-case relative motion [38].

Inertias representing disk elements are located at specific positions called nodes. Each node is characterised by a single degree of freedom, namely, the

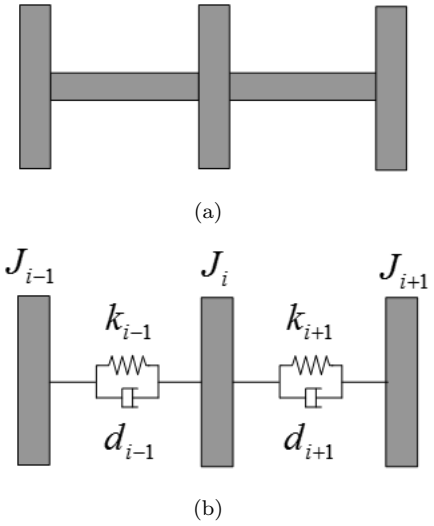

Fig. 1.6: Direct approach (a): disk-shaft system (b): lumped parameters model.

torsional rotation, and a single generalized force, the torsional moment, is acting on it.

The generic rotor train illustrated in Fig. 1.6(a) is formed of n massive disks connected by $n-1$ torsionally flexible rotors, the corresponding lumped parameters model is shown in Fig. 1.6(b). Each torsionally flexible section is represented by a torsional stiffness k_i that is evaluated by means of the following expression:

$$k_i = \frac{\pi G(d_{i,ext}^4 - d_{i,int}^4)}{32 l_i} \tag{1.67}$$

with G representing the shear modulus of the rotor material, l_i is the length of the section, $d_{i,ext}$ and $d_{i,int}$ are respectively the external and internal diameter. The polar inertia of the $i-th$ shaft section J_i can be computed through the relation:

$$J_i = \frac{\rho \pi l_i (d_{i,ext}^4 - d_{i,int}^4)}{32} \tag{1.68}$$

where ρ is the density of the material. The inertia J_i is divided in two equal parts that are respectively concentrated in the two nodes delimiting the section. The linear equations of motion of the lumped model are given by:

$$J_i \ddot{\vartheta}_i + d_{i-1}(\dot{\vartheta}_i - \dot{\vartheta}_{i-1}) + d_{i+1}(\dot{\vartheta}_i - \dot{\vartheta}_{i+1}) \tag{1.69}$$

$$+ k_{i-1}(\vartheta_i - \vartheta_{i-1}) + k_{i+1}(\vartheta_i - \vartheta_{i+1}) = T_i(t) \tag{1.70}$$

where ϑ_i is the angular position of the $i-th$ node, $T_i(t) \in \Re^{n\times 1}$ include the contribute of an external torque on the $i-th$ disk and $i = 1,..,n$. These equations may be assembled in a matrix formulation:

$$J\ddot{\boldsymbol{\vartheta}} + D\dot{\boldsymbol{\vartheta}} + K\boldsymbol{\vartheta} = \mathbf{T} \tag{1.71}$$

where $J, D, K \in \mathbb{R}^{n\times n}$ denote respectively the inertia, damping and stiffness matrix, $\mathbf{T}$ is the vector of the applied torques and $\boldsymbol{\vartheta} \in \mathbb{R}^{n\times 1}$ is the vector representing the degrees of freedom of the lumped model, the nodes rotation around the shaft axis. The solution of Eqs. 1.71 consists of free and forced responses of the rotor. The main purpose of assessing free vibrations is to obtain the natural frequency spectrum and the corresponding mode shapes. Forced vibrations are usually studied to evaluate the system response to constant torque or variable torque.

Modal analysis to investigate the free response can be done starting from the homogeneous equations of motion:

$$J\ddot{\boldsymbol{\vartheta}} + K\boldsymbol{\vartheta} = 0 \tag{1.72}$$

where the external torque and damping contribution of Eq. 1.71 is neglected. The harmonic time solution and its derivatives can be written in the form:

$$\boldsymbol{\vartheta}(t) = \boldsymbol{\vartheta}_0 e^{j\omega t} \tag{1.73}$$

$$\dot{\boldsymbol{\vartheta}}(t) = j\omega\boldsymbol{\vartheta}_0 e^{j\omega t} \tag{1.74}$$

$$\ddot{\boldsymbol{\vartheta}}(t) = -\omega^2\boldsymbol{\vartheta}_0 e^{j\omega t} \tag{1.75}$$

Introducing Eqs. 1.73 and 1.75 in Eq. 1.72, eliminating the exponential term (that is always non-zero) and re-arranging, the formulation of the problem can be obtained by multiplying each term for J^{-1}, thus resulting in:

$$(-\omega^2 I + J^{-1}K)\boldsymbol{\vartheta}_0 = 0 \tag{1.76}$$

where $I \in \mathbb{R}^{n\times n}$ is the identity matrix. From the previous expression it clearly results that the computation of non-trivial solutions for $\boldsymbol{\vartheta}_0$ correspond to the eigenvalue analysis of matrix $J^{-1}K$:

$$det(-\omega^2 J + K) = 0 \tag{1.77}$$

The square-root values of the non-zero eigenvalues represent the torsional natural frequencies ω_i in rad/s. The eigenvector associated to the $i-th$ torsional natural frequency is the corresponding torsional mode shape of the investigated rotor.

1.2.2 Holtzer's method

The generic rotor train shown in Fig. 1.7 is lumped in a number of rigid disks located at specific nodes, called stations. Following the conventional transfer-matrix notation, the $i-th$ disk element is placed at the $i-th$ station and the massless torsional flexible element connecting two succeeding stations (i and $i+1$) is the $i-th$ field. Each station has one degree of freedom, namely the rotation around rotor axis ϕ_z
The $i-th$ state vector $\mathbf{s}_i$ is can be expressed as:

$$\mathbf{s}_i = \begin{bmatrix}\phi_{zi} & M_{zi}\end{bmatrix}^T \tag{1.78}$$

where M_{zi} is the applied moment at the $i-th$ station.

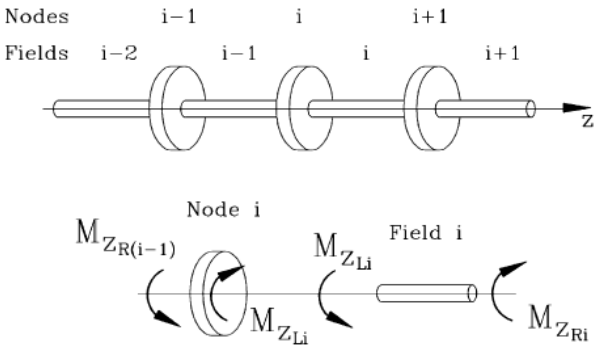

Fig. 1.7: Holtzer's method: scheme of the discretisation and external moments.

The general expression of the field transfer matrix is obtained considering that the moment at the left is equal to the moment at the right end of the field and that the rotation at the right is given by the sum of the rotation at the left end and the twisting of the field:

$$\phi_{zi}^r = \phi_{zi}^l + \Delta\phi_{zi} = \phi_{zi}^l + \frac{l_i}{G_i I_{Pi}} M_{zi}^l \tag{1.79}$$

$$M_{zi}^r = M_{zi}^l \tag{1.80}$$

or in matrix form:

$$\begin{bmatrix} \phi_{zi} \\ M_{zi} \end{bmatrix}^r = \begin{bmatrix} 1 & \frac{l_i}{G_i I_{Pi}} \\ 0 & 1 \end{bmatrix} \begin{bmatrix} \phi_{zi} \\ M_{zi} \end{bmatrix}^l \tag{1.81}$$

Considering the state vector expression, Eq. 1.81 can be written as:

$$\mathbf{s}_i^r = T_{fi} \mathbf{s}_i^l \tag{1.82}$$

where T_{fi} represents the field transfer matrix.

Analogous relationships may be written to relate variables on the left and right-hand sides of the $i-th$ station. The rotations at the left and right side of the $i-th$ station are equal, while the moment at the right of the station is equal to the one at the left increased by the concentrated moments acting on the station due to torsional spring constraints and to inertia reactions. The equations relating right and left-hand side of the $i-th$ station result:

$$\begin{bmatrix} \phi_{zi} \\ M_{zi} \end{bmatrix}^l = \begin{bmatrix} 1 & 0 \\ -\omega^2 J_{zi} + K_t & 1 \end{bmatrix} \begin{bmatrix} \phi_{zi} \\ M_{zi} \end{bmatrix}^{r-1} \tag{1.83}$$

or more compactly:

$$\mathbf{s}_i^r = T_{st} \mathbf{s}_i^{r-1} \tag{1.84}$$

where T_{st} represents the station transfer matrix. The recursive multiplication of Eq. 1.82 with Eq. 1.84 yields to the overall transfer matrix and it can be written:

$$\begin{bmatrix} \phi_z \\ M_z \end{bmatrix}_n = \begin{bmatrix} T_{11} & T_{12} \\ T_{21} & T_{22} \end{bmatrix} \begin{bmatrix} \phi_z \\ M_z \end{bmatrix}_1 \tag{1.85}$$

As it has been stated for lateral transfer-matrix formulations, the value of the torsional natural frequencies of the system can be obtained by introducing the boundary conditions (e.g free-free boundary conditions) of the system and then imposing the mathematical conditions to get non-trivial solutions.

1.2.3 Finite Element Models for Torsional Vibrations

Accuracy in torsional response calculations may be improved through finite element (FE) formulations. In FE torsional mathematical models, disks are modelled through rigid elements thus they only add discrete inertias to FE model, as it occurrs in the direct approach. Torsional stiffness is instead taken into account with energy distributed inertia matrices for each shaft element [9, 15].

FE formulations can be derived using shape functions of arbitrary order. In the present work distributed inertia matrices defined by means of linear shape functions are briefly presented.

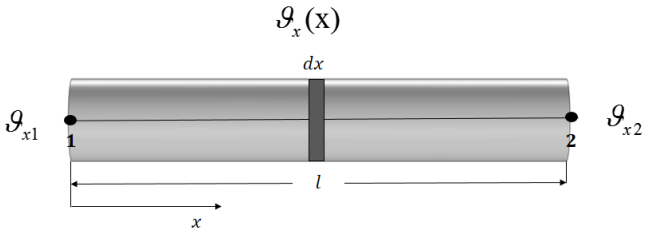

Fig. 1.8: Torsional shaft element.

Fig. 1.8 illustrates a circular cross-section torsional element with 1 dof per node, namely the rotational displacement ϑ_x about the longitudinal axis x of the shaft.

The kinetic energy of the the $k-th$ element is computed as the integral of the product of the velocity and mass squared, resulting for a rotational motion in the product of the angular velocity squared and second moment of area:

$$T_k = \frac{1}{2}\int_0^{L_k} \rho_k J_k \left(\frac{\partial \vartheta_{xk}(x,t)}{\partial t}\right)^2 dx \tag{1.86}$$

where L_k is the element length, ρ_k is the density of the material and J_k represents the torsional constant that for a circular cross section is equal to $\pi(d_{i,ext}^4 - d_{i,int}^4)/32$.

The strain energy within a bar due to torsion is evaluated through the integration of the product of stress and strain, resulting for uncoupled torsional analysis in the following expression [9]:

$$U_k = \frac{1}{2}\int_0^{L_k} GJ_k \left(\frac{\partial \vartheta_{xk}(x,t)}{\partial x_{xk}}\right)^2 dx \tag{1.87}$$

where G denotes the shear modulus.

Introducing in Eqs. 1.86 1.87 and the displacement model obtained through the adoption of a linear shape functions:

$$\vartheta_{xk}(x,t) = \left(1 - \frac{x}{L}\right)\vartheta_{x1k}(t) + \frac{x}{L}\vartheta_{x2k}(t) \tag{1.88}$$

the expressions of the element mass and stiffness matrix may be respectively derived:

$$M = \frac{\rho_k J_k L}{6}\begin{bmatrix} 2 & 1 \\ 1 & 2 \end{bmatrix} \qquad K_k = \frac{G_k J_k}{L}\begin{bmatrix} 1 & -1 \\ -1 & 1 \end{bmatrix} \tag{1.89}$$

Chapter 2

Coupled Lateral-Torsional Vibrations

In the rotating machines field, lateral and torsional dynamics affect each other depending on the amount of the coupling effect [10, 14]. Coupling between torsional and lateral modes of vibration, to a certain degree, usually exists in rotating machines, as it is caused by the most common malfunction conditions such as rotor unbalance and shaft anisotropy [10]. This coupling can also occur by means of gyroscopic effects, radial constant forces, tangential forces and in presence of a gearbox [8, 40] (Fig. 2.1). Coupled lateral-torsional vibrations may occur in long flexible shaft systems due to long span or in complex structure such as rotors with distributed inertial elements. Bending-torsional coupling may lead to rotor unstable behaviour [14] that may cause problems and faults of rotating machines.

For long time rotordynamics studies and research activities have been focused on a single form of vibration: lateral and torsional vibrations were investigated through uncoupled separate models. However, this kind of approach is correct as long as the coupling effect is weak and recent trends in turbomachinery design, with higher performance and more sophisticated systems, set the uncoupled approach to be less and less accurate.

To assure rotor systems stability and reliability, more accurate mathematical advanced models are required to take into account all external or internal factors that may affect the dynamical behaviour, such as the bending-torsional vibrations coupling [41].

Furthermore, the necessity of more advanced rotordynamics models is highly demanded for monitoring and diagnostic purposes. In fact, although vibrations problems occurring in rotating machines may be detected through diagnostic dedicated tools (accelerometers, proximity probes), these systems are usually intrusive and require penetration and machinery access. Advanced model could then be employed to determine state of machines from simpler and more convenient measurement devices [42].

In the present section an extended review of literature dealing with lateral-torsional vibrations coupling in rotors is presented and the most significant mathematical models developed by researchers for the comprehension of the problem are briefly introduced.

2.1 Literature survey

Several research activities may be found in literature on the topic of coupling between lateral and torsional vibration in rotors. These works are focused on both the physical investigation of the mechanisms inducing the vibrations coupling (*phenomenological aspect*) and on the development of innovative mathematical formulations, able to represent lateral-torsional dynamics (*modelling aspect*).

The attention of researchers to this particular topic arose due to real case-studies [10] relative to rotating machines that exhibited unpredicted critical resonances on the lateral vibrations characterised by the torsional mode frequency.

From a chronological standpoint, to the author's knowledge, the first work in literature addressing the *phenomenological aspect* of lateral-torsional vibration coupling in rotating machines is the paper by Tondl [43], where the stability of a steam coupled turbo-generator is investigated. More specifically, thanks to an analytical model, results are given about the rise of some instability regions when torsional-lateral coupling is caused by rotor unbalance. The model consists of a massless shaft with two rigid disks and the torsional vibrations are described through the superimposition of the torsional angle to the rigid body rotational motion.

In the research by Rabkin [44], the forced lateral-torsional vibration response of an unbalanced multi-disk rotor is mathematically derived.

The paper by Smith [45] analyses rotor instability caused by the interaction between $2X$ torsional vibration with lateral vibrations at frequency $1X$ or $3X$. In the studied test-case the main mechanism inducing the lateral-torsional coupling is represented by unbalanced blade vibrations.

Diken [46] investigates the effect of coupling with torsion on the lateral response of unbalanced flexible rotors, supported by isotropic damped bearings. Bending torsional coupling of the shaft-disk system occurs through mass eccentricity. A modified Myklestad-Prohl method is employed to solve numerically the equations of motion of the continuous system. Both constant and harmonic torques are applied to the investigated system and gyroscopic effects, rotary inertia, shear deformation, external and internal damping effects are taken into account.

A reference work is represented by the study of Bernasconi [47]. In this study the dynamical behaviour of unbalanced rotors is considered and it is found out that gyroscopic effects induce torsional vibrations at 2X frequency (bisynchronous vibrations). The nonlinear term which represents this coupling is characteristic of the asymmetrical aspect of the rotating shaft kinematics. The analytical results obtained in this study have been confirmed through experimental tests.

In Cohen's research [48] a model of an unbalanced rotor, driven by a torsional-flexible and lateral rigid shaft by means of a constant velocity joint, is employed for studying the combination-resonance effect in coupled torsional-lateral vibration. The nonlinear equations of motion are solved by means of an asymptotic method that determines the instability zones of the system but does not yield to a closed solution. Results also show that superimposed lateral and torsional damping may cause enlargement of the instability zones.

The problem of torsional and transverse deformations of a shaft rotating at

a constant speed is also addressed by Nataraj in [49]. The displacements are expressed through a perturbation series in terms of a small parameter. Energy expressions are computed for each order and Hamilton's principle is then applied to obtain the equations of motion and the boundary conditions governing the displacement functions of different orders. This work clearly shows that the interaction of torsion and lateral vibration occurs at second order. Previous results of torsional vibration caused at a 2X frequency due to this interaction are confirmed.

In the work by Plaut [50] coupled bending and torsional displacements are investigated considering three coupling mechanisms: unbalance, gravitational effects and time-dependent angular velocity. The linearised equations for the two transverse deflections and the torsional vibration are derived using the Euler-Bernoulli beam theory and solved through the application of the Galerkin's method.

The coupled dynamics of actively controlled drillstrings is studied by Yigit and al. in [51]. In this work the effect of axial forces and torques on the system bending stiffness is investigated.

Another mechanism representing a source of lateral and torsional vibrations is rotor anisotropy, condition occurring when cracks are present in the shaft. This kind of mechanism has been extensively addressed in the rotordynamics literature [52, 53, 54, 55]. In [53], for instance, the presence of a transverse shaft crack is modelled through a 3x3 flexibility matrix describing local flexibility due to crack. Due to the shear terms of the Timoshenko beam equation of the shaft, lateral vibration results coupled to torsional vibration and the influence of crack depth and slenderness ratio is investigated. A finite element procedure developed to simulate the dynamic characteristics of a rotor system with transverse cracks is introduced in [56].

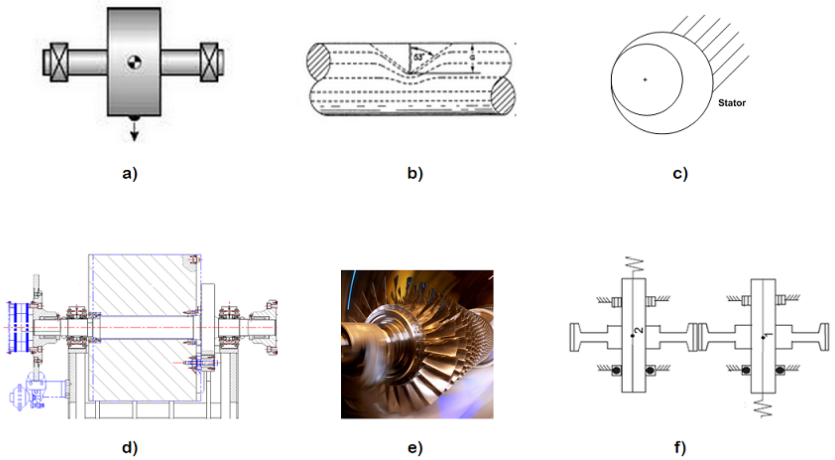

Fig. 2.1: Mechanisms inducing coupled torsional lateral vibrations (a): unbalance (b): rotor anisotropy (c): rubbing (d): blade dynamics (e): gearbox (f): complex rotors.

An important source of torsional-lateral coupling is the presence of a gearbox

in geared multi-rotors, where lateral and torsional vibrations get coupled due to the tooth force resulting in coupled lateral-torsional or lateral-torsional-axial vibrations not found in non-geared shafts. The problem of lateral-torsional vibrations in geared multi-rotor systems has been extensively addressed in the rotordynamics literature [12, 22, 40]. Significant discussions and information on publications on different topics of geared rotordynamics, such as torsional-lateral vibration coupling modelling, may be found in [57]. The research activity presented in [58] studies the influence of torsional-lateral coupling on the stability behaviour of a simple geared system supported by oil film bearings. The coupling effect due to the gear system is investigated through parametric studies and sensitivity analysis for both uncoupled and coupled system. The influence of torsional excitations on coupled torsional-lateral response of geared rotors is also studied by Rao in [22]. In this work, a turbo-alternator example is investigated through a coupled torsional-lateral finite element approach. The influence of axial torques and the response to short circuit torques is analysed. The coupling among the axial, torsional and lateral vibrations due to bevel gear transmission is addressed in [59]. In [60] an estimation of dynamic gear tooth loading caused by coupled torsional-lateral vibrations in a geared rotor-hydrodynamic bearing system is given. The effects of mass unbalance and geometrical eccentricity of the pinion and the combined effects of manufacturing errors, profile modifications of gear teeth, gear mesh compliance and damping have been taken into account. Journal lateral motions are shown to be related with variations in the angular velocity ratio of meshing gears and with the dynamic loading of gear teeth.

The coupling between lateral and torsional vibrations in rotors can also be determined by the dynamics of blades in bladed rotors [13]. In [61] a dynamical model considering elastic blade attached to a disk mounted on a torsional flexible shaft is introduced. Lateral-torsional coupling in rotors may also arise due to rotor-to-stator rubbing [10, 20]. In [62] a model for the coupled torsional and lateral vibrations of unbalanced rotors that considers for the rotor-to-stator rubbing is presented. Lagrangian dynamics is used to obtain the equation of motions for the rotor rigid-body rotation, the rotor torsional deformation and two orthogonal lateral deflections of the rotor. The rubbing condition is modelled through an elastic impact-contact idealization, consisting of normal and tangential forces at the rotor-to-stator contact point. A mathematical model of an impacting-rub rotor system is also developed in [63]. In this work the influence of lateral-torsional coupling on the dynamical response of the studied response is discussed. The vibration characteristics of a rotor in presence of unbalance, rotor-to-stator rub and transverse crack are investigated in [20] through a fully coupled finite-element model.

Several sources causing the excitation of lateral-torsional vibrations are also analysed in [10]. More specifically mathematical models are derived for the description of the lateral-torsional dynamic coupling due to unbalance, variable torques and rotor anisotropy.

2.2 Modelling aspect

Rotordynamics analysis have been performed for more than 140 years [8]. To this purposes, appropriate mathematical models have been developed coherently

on current computational technology and rotordynamics knowledge. Thanks to the elementary models such as Jeffcott's rotor, simple mathematical formulations and closed analytical solution may be used for educational purposes or to investigate particular phenomena [64].

Nowadays, the study of complex rotating machines requires the application of more advanced models able to represent all the significant property of a real system (e.g., multi-rotors configuration, distributed inertial elements and lateral-torsional vibrations coupling).

In the present section an overview of the modelling aspect of the coupled lateral-torsional vibrations in literature is given and the most significant models developed by rotordynamics researchers are briefly introduced. Such models can be classified into: elementary models, transfer-matrix formulations, finite element approaches, distributed models and models based on flexible multi-body formulations.

Elementary models [10, 11] are derived from the simple Jeffcott's rotor and they are employed for studying the basic mechanisms inducing the lateral-torsional coupling. For instance, a rotordynamical model of an unbalanced Jeffcott rotor is derived in [65]. Three degrees of freedom are considered, namely two lateral displacement and the torsional angle. The solution of the nonlinear equations of motions is obtained using the Wilson-Θ method.

Both analytical and numerical methods are used in [41] to study internal and external lateral-torsional coupling effects of an unbalanced rotor. More specifically, static, dynamical and comprehensive unbalance effects on the lateral torsional coupling are studied. External and internal bending torsion coupling effects of a rotor system with comprehensive unbalances are studied by analytical analysis and numerical simulations. Based on Lagrangian approach, a full-degree-of-freedom dynamic model of a Jeffcott rotor is developed. The harmonic balance method and the Floquet theory are combined to analyse the stability of the system equations. Numerical simulations are conducted to observe the lateral-torsional coupling effects. In the formulation of rotordynamic model, two bending torsion coupling patterns, external coupling and internal coupling, are suggested. By analytical analysis, it is concluded that the periodic solution of the system is asymptotically stable. From numerical simulations, three bending torsion coupling effects are observed in three cases. Under static unbalance, synchronous torsional response is observed, which is the result of external coupling under unbalanced force. Under dynamic unbalance, two-time synchronous frequency torsional response is observed, which is the result of internal coupling under unbalanced moment. Under comprehensive unbalance, synchronous and two-time synchronous frequency torsional components are observed, which are the results of both external and internal couplings under unbalanced force and moment. These observations agree with the analytical analysis.

The aim of the work described in [66] consists in studying the characteristics of torsional vibration of a rotor with unbalance by numerical simulation. It can be concluded that synchronous torsional vibration accompanying with small higher harmonic components are excited, except when the speed of rotation is near, or equal to, half the natural frequency of torsional vibration, the bisynchronous component is much more remarkable than other harmonic components including the degraded synchronous one, and torsional vibration of the shaft can result in lateral vibration with bisynchronous frequency. Especially, when the rotating frequency is near the natural torsional frequency, where torsional vi-

bration is strongest, the bisynchronous vibration becomes rather strong.

In [67] the nonlinear response of a rotor system in coupled lateral torsional vibrations is studied through a nonlinear mathematical model.

The transfer-matrix approaches is used in [68] where an extended method to investigate coupled lateral and torsional vibrations of symmetric rotor-bearing system subject to time-varying torques is presented. Results of the introduced model show that, when unbalance and torque excitation are applied to the system, the steady-state lateral response consists of a forward and a backward whirl at $(n+1)\,x$ and $(n-1)\,x$ (with nx spin frequency) whirls arise together with the synchronous whirl.

Finite element formulation is used in [69], wherein a finite element model with 5 degrees of freedom for each node is established for investigating coupled lateral-torsional vibration of shaft system.

A model based in discrete-continuos approach for the study of coupled lateral torsional vibration of rotor system is presented in [64]. The paper investigates coupled linear or nonlinear lateral torsional vibrations of rotors in steady-state and transient operations.

Recent developments in rotorcraft and wind turbine industry have led to the adoption of flexible multibody modelling approaches for the prediction of the dynamical behaviour of rotating systems [70]. Particularly, flexible multibody modelling is starting to be employed to address the limitations of the classical equations of motion and to provide a comprehensive model for rotating shafts. To this purpose, Brown and Shabana [71] derived the general equations of motion for a flexible body through the application of the principle of virtual work in rotating shaft dynamics. The equations include both the Coriolis and centrifugal inertia forces, and in the work the effect of the inertia terms on the system dynamic stability is studied. The effect of the rotary inertia on the axial and lateral deformations is also formulated and the coupling terms are obtained. The results presented in the study show that the general flexible body formulation can be used to study rotating shafts. As a consequence, general purpose flexible multibody computer algorithms can be adopted to systematically solve more general rotating shaft problems.

In the following sections the mathematical formulations of the most representative models are briefly introduced.

2.2.1 Anisotropic rotor with one massive disk (3 dofs)

An extensive investigation on several mechanisms inducing lateral-torsional coupling in rotors has been made by Muszynska [10]. In particular she studied the torsional-lateral response and stability of a simple Jeffcott's rotor when subjected to different source of couplings such as unbalance, constant radial force and variable/unsteady driving or load torque applications and rotor anisotropy).

Muszynska's model represents the dynamical behaviour of a 3 degrees of freedom undamped Jeffcott's rotor; the flexible rotor is assumed to be mass-less and the total mass M is concentrated in a point mass representing the unbalanced disk that is placed at the midspan of the flexible shaft, thus gyroscopic effects may be neglected.

The classical 3 dofs mathematical model in the xyz fixed reference system

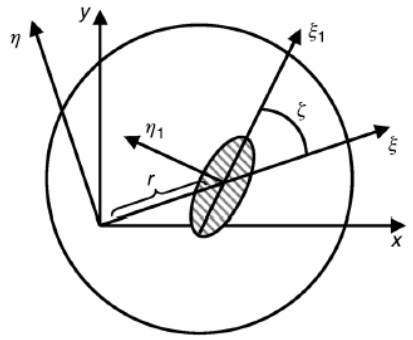

Fig. 2.2: Coordinate reference systems and rotor main stiffness axes.

(Fig. 2.2) is formulated through the following equations of motion:

$$M\ddot{x} + Kx = Mr\left(\dot{\psi}^2 \cos\psi + \ddot{\psi}\sin\psi\right) \tag{2.1}$$

$$M\ddot{y} + Ky = Mr\left(\dot{\psi}^2 \sin\psi - \ddot{\psi}\cos\psi\right) - Mg \tag{2.2}$$

$$I\ddot{\psi} + Kr\left(\psi - \psi_e\right) + Kr\left(x\sin\psi - y\cos\psi\right) = T(t) + Mgr\cos\psi \tag{2.3}$$

where K is the rotor lateral stiffness, K_t is the torsional flexibility, I represents the disk polar inertia, $\psi(t)$ and ψ_e are the twist angles at respectively the disk and the driving end sections. $T(t)$ is the applied torque and g is the gravity acceleration. Lateral (Eqs. 2.1- 2.2) and torsional (Eq. 2.3) equations are nonlinear and coupled through the disk mass eccentricity r.

A more suitable form of the previous system of equations may be obtained according to the following assumptions:

- the angle of twist ψ of the rotor is given by the sum of two terms: the angle due to the rotational rigid body motion Ωt and the torsional vibration ϕ;
- after linearisation in the inertial coordinate system, Eqs. 2.1- 2.3 can be transformed into the rotating coordinates ξ and η attached to the rotor.

The resulting equations of motion are as follows:

$$M\left(\ddot{\xi} - 2\Omega\dot{\eta} - \Omega^2\xi\right) + K_\xi\xi - 2Mr\Omega\dot{\phi} = Mgr\Omega^2 - Mg\sin\Omega t \tag{2.4}$$

$$M\left(\ddot{\eta} + 2\Omega\dot{\xi} - \Omega^2\eta\right) + K_\eta\eta + Mr\left(\ddot{\phi} - \Omega\phi\right) = -Mg\cos\Omega t \tag{2.5}$$

$$I\ddot{\phi} + K_t\phi - K_\eta r\eta = T(t) + Mgr\cos\Omega t \tag{2.6}$$

where K_ξ and K_η are the anisotropic lateral stiffness values along the main stiffness axes ξ_1 and η_1 as shown in Fig. 2.2.

Eqs. 2.4-2.6 represent the model of coupled lateral-torsional vibrations of anisotropic rotors with one unbalanced disk. It must be noticed that if the disk is perfectly balanced ($r = 0$), the equations describing lateral and torsional models result decoupled. The solution of this set of equations consist of the

modal response and forced vibrations due to the unbalance force or gravity force and to the application of an unsteady torque $T(t)$.

Concerning the free response, Muszynska solves the eigenvalue problem associated to Eqs. 2.4-2.6 through a numerical procedure to find the rotor natural frequencies and she studied the existence of instability ranges. The Campbell's plot (Fig. 2.3) illustrates the resulting natural frequencies plotted versus the rotational speed Ω values and also the natural frequencies of the uncoupled system are shown. The first instability range is shown to be approximately between two natural frequencies of the rotor lateral modes and it is determined by the inequality of the stiffness components. It can also be noticed that the uncoupled natural frequencies represent asymptotes for the coupled natural frequencies and an additional instability zone may arise in the vicinity of the intersection between torsional and lateral uncoupled modes.

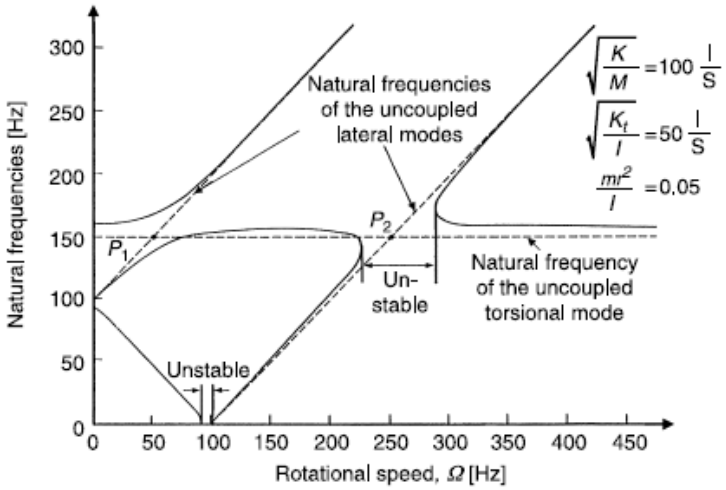

Fig. 2.3: Rotor natural frequencies of the coupled lateral and torsional vibrations versus rotational speed expressed in the rotating coordinates.

A mathematical explanation of when intersections in the map of uncoupled frequencies determines instability ranges is given by Gosiewski in [14]. He firstly investigates lateral-torsional coupling effects by means of an approach similar to Muszynska's model, then he studies the system stability through a model derived from the control theory.

By solving the forced response [10], Muszinska finds out that, even if the unbalance is a mechanism determining lateral-torsional coupled modes, the unbalance force does not directly excite torsional response in elementary models. The application of a variable torque to the rotor coupled model excites lateral vibrations with frequencies being sums and differences of the torque frequencies and rotational speeds. These vibrations are particularly critical when the excitation frequencies coincide with the coupled lateral/torsional natural frequencies.

2.2.2 Anisotropic rotor with one massive disk (4 dofs)

A further step in the investigation of lateral-lateral coupling due to unbalance has been made by Al-Bedoor in [11], wherein a coupled lateral-torsional mathematical formulation of a Jeffcott's rotor is derived. The main novelty of this work w.r.t to most of the studies previously cited, consists in assuming the torsional vibration motion as a separate degree of freedom. The studied system is a driven shaft rotor, composed of a motor and a driven disk-shaft element illustrated in Fig. 2.4(a), and the adopted notation is shown in Fig. 2.4(b).

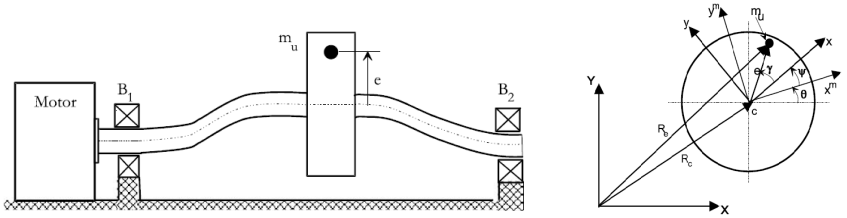

(a) (b)

Fig. 2.4: Disk-shaft system (a): scheme of the motor-disk-shaft system (b): the adopted coordinate reference system configuration.

The mathematical formulation is derived according to the following hypotheses:

- the model is based on the Jeffcott's approach [2], therefore gyroscopic effects due to spinning motion of the rotor are neglected;
- the total mass M corresponds to the modal mass of the first lateral mode of the model;
- the considered range of operating conditions includes speeds lower than the second critical speed value of the system;
- lateral stiffness of the shaft is small if compared with the bearings stiffness;
- bearings are characterised by viscous damping;

The reference systems adopted for the development of the present model are illustrated in Fig. 2.4(b), where X and Y are the lateral coordinates in the inertial reference frame XYZ, while x^m and y^m are the lateral coordinates in a body coordinate system $x^m y^m z^m$ rigidly attached to the motor shaft thus rotating with the torsionally undeformed system; xyz is instead the rotating system attached to the disk.

The system has 4 degrees of freedom lumped at the disk:

- two lateral displacements X and Y of the disk geometrical center C;
- one rigid rotation θ around the axle of the rotor Z;
- one torsional deflection angle ψ;

The unbalance mass m_u is located at the position defined by the vector $\mathbf{e}$ from the shaft geometric center C. The position of m_u with respect to the inertial reference system can be written as:

$$\mathbf{R_e} = A(\theta)\, A(\psi)\, \mathbf{e} \tag{2.7}$$

where $A(\theta)$ and $A(\psi)$ are the rotational transformation matrices respectively from the motor coordinate system $x^m y^m z^m$ and from the disk coordinate system xyz to the inertial frame XYZ. By assuming small values for the torsional deflection ψ, the expression of the transformation matrices result:

$$A(\theta) = \begin{bmatrix} \cos\theta & -\sin\theta \\ \sin\theta & \cos\theta \end{bmatrix} \qquad A(\psi) = \begin{bmatrix} 1 & -\psi \\ \psi & 1 \end{bmatrix} \tag{2.8}$$

The equations of motion describing the dynamic behaviour of the system are obtained through the application of the Lagrangian approach in the inertial frame. The kinetic energy of the system, which is formed of three contributes: the disk kinetic energy T_d, the motor kinetic energy T_m and the mass unbalance kinetic energy T_{mu}, is given by the following expression:

$$\begin{aligned} T &= T_d + T_m + T_{mu} \\ &= \frac{1}{2}M(\dot{X}^2 + \dot{Y}^2) + \frac{1}{2}J_d(\dot{\Theta} + \dot{\psi})^2 + \frac{1}{2}J_m\dot{\theta}^2 + \frac{1}{2}m_u\dot{\mathbf{R}}_e^T\dot{\mathbf{R}}_e^T \end{aligned} \tag{2.9}$$

where J_m is the motor inertia (kgm^2) and $\dot{\mathbf{R}}_e$ is the velocity vector of the unbalance mass m_u in the inertial reference frame.

The potential energy of the studied system is formed of the bending and torsional strain energy contribution of the shaft:

$$U = U_{ben} + U_{tors} = \frac{1}{2}K_{XX}X^2 + \frac{1}{2}K_{YY}Y^2 + \frac{1}{2}K_{\psi\psi}\psi^2 \tag{2.10}$$

where K_{XX}, K_{YY} and $K_{\psi\psi}$ represent the lateral and torsional stiffness values.

It is assumed that the system has modal viscous damping, thus the corresponding Rayleigh's dissipation function may be expressed as:

$$R = \frac{1}{2}C_{XX}\dot{X}^2 + \frac{1}{2}C_{YY}\dot{Y}^2 + \frac{1}{2}C_{\psi\psi}\dot{\psi}^2 \tag{2.11}$$

with C_{XX}, C_{YY} and $C_{\psi\psi}$ are the lateral and torsional damping values. By introducing the extended expression of $\dot{\mathbf{R}}_e$ in Eq. 2.9 and applying Lagrange's approach to Eq. 2.9 and 2.10, the equations of motion of the system may be written as:

$$M\ddot{\mathbf{q}} + C\dot{\mathbf{q}} + K\mathbf{q} + \mathbf{Q} = \mathbf{F} \tag{2.12}$$

where $\mathbf{q} = \begin{bmatrix} X & Y & \theta & \psi \end{bmatrix}^T$ is the vector containing the system degrees of freedom, $\mathbf{Q}$ is the vector of nonlinear terms and $\mathbf{F}$ represents the external forces vector. The matrices M, C and K are symmetrical and contain respectively mass, damping and stiffness properties of the studied rotor and they are defined according to the following expressions:

$$M = \begin{bmatrix} m_{XX} & 0 & m_{X\theta} & m_{X\psi} \\ 0 & m_{YY} & m_{Y\theta} & m_{Y\psi} \\ m_{\theta X} & m_{\theta Y} & m_{\theta\theta} & m_{\theta\psi} \\ m_{\psi X} & m_{\psi Y} & m_{\psi\theta} & m_{\psi\psi} \end{bmatrix} \tag{2.13}$$

$$C = \begin{bmatrix} c_{XX} & 0 & 0 & 0 \\ 0 & c_{YY} & 0 & 0 \\ 0 & 0 & 0 & 0 \\ 0 & 0 & 0 & c_{\psi\psi} \end{bmatrix} \tag{2.14}$$

$$K = \begin{bmatrix} k_{XX} & 0 & 0 & 0 \\ 0 & k_{YY} & 0 & 0 \\ 0 & 0 & 0 & 0 \\ 0 & 0 & 0 & k_{\psi\psi} \end{bmatrix} \tag{2.15}$$

The following relationships hold:

$$m_{XX} = m_{YY} = M + m_u \tag{2.16}$$
$$m_{\theta\theta} = J_M + J_D + m_u e^2(1 + \psi^2) \tag{2.17}$$
$$m_{\psi\psi} = m_u e^2 + J_D \tag{2.18}$$
$$m_{x\psi} = -m_u \left(e_x \sin\theta + e_y \cos\theta\right) \tag{2.19}$$
$$m_{y\psi} = m_u \left(e_x \cos\theta - e_y \sin\theta\right) \tag{2.20}$$
$$m_{x\theta} = -m_u \left[(e_x - \psi e_y)\sin\theta + (e_x\psi + e_y)\cos\theta\right] \tag{2.21}$$
$$m_{y\theta} = m_u \left[(e_x - \psi e_y)\cos\theta - (e_x\psi + e_y)\sin\theta\right] \tag{2.22}$$
$$m_{\psi\theta} = m_u e^2 + J_D \tag{2.23}$$
$$k_{\psi\psi} = K_t - m_u e^2 \dot{\theta}^2 \tag{2.24}$$

The main results of the model presented by Al-Bedoor show that inertial coupling among lateral and torsional degrees of freedom exists, as it is can be deduced from the form of the mass matrix M (see Eq. 2.13). Eq. 2.17 prooves that the inertia of the rotational rigid motion is influenced by the unbalance mass and it is nonlinearly affected by the torsional vibration ψ. Coupling also exists among the rigid body rotation θ and torsional motion ψ due to the disk inertia J_D and to unbalance. Eqs. 2.21 and 2.22 shows the periodic inertial coupling among lateral and rotational motion caused by the unbalance and torsional vibration. Finally, periodic inertial couplings of the lateral and torsional motions is shown by the expressions in Eqs. 2.18 and 2.20. The model predicts also a softening effect on the torsional stiffness $k_{\psi\psi}$ due to the rigid body rotation, as it can be seen in Eqs. 2.24 and highlights the presence of coupling nonlinear terms. More specifically, lateral-torsion coupling is contained in the Q_X and Q_Y terms of the nonlinear terms vector:

$$\begin{aligned} Q_X = {} & 2m_u\dot{\theta}\dot{\psi}\left(e_y \sin\theta - e_x \cos\theta\right) \\ & - m_u\dot{\theta}^2\left[(e_x - \psi e_y)\cos\theta - (e_x\psi + e_y)\sin\theta\right] \end{aligned} \tag{2.25}$$

$$\begin{aligned} Q_Y = {} & -2m_u\dot{\theta}\dot{\psi}\left(e_x \sin\theta + e_y \cos\theta\right) \\ & - m_u\dot{\theta}^2\left[(e_x - \psi e_y)\sin\theta - (e_x\psi + e_y)\cos\theta\right] \end{aligned} \tag{2.26}$$

where nonlinear terms due to Coriolis and centrifugal effects appear. In the final part of the paper [11], thanks to the developed model, the dependence of the energetic interaction between lateral and torsional modes to the values of the uncoupled lateral frequencies is investigated through a set of numerical analysis.

The previous model has been further extended by Sukkar and Yigit in [42] to include the effect of axial forces.

2.2.3 Finite Element Models for Torsional-Lateral Vibrations

In the last decades finite element formulations have become the standard method employed for rotordynamics and during the last 50 years many different mathematical formulations have been proposed [8]. To the author's knowledge the finite element method for rotors was first developed by Ruhl and Booker [34]. Their model includes only translational inertia and bending effects. Nelson and McVaugh [35] extended this model to include gyroscopic effects. The effects of axial torque were included by Zorzi and Nelson [36] and Nelson [72] defined rotor dynamics elements with the Timoshenko beam theory.

The coupling between lateral and torsional deformations is not included nor in the works previously cited neither in the numerous formulations that have been developed starting from them. To obtain information on coupled torsional and lateral behaviour, adequate finite element approaches have been proposed by in [5, 22, 69] where the effects of torsional and bending deformation coupling have been taken into account.

In the present section the FE formulation presented by Mohiuddin in [5] is described. As it holds for uncoupled lateral FE formulations, coupled finite element models are based on the adoption of an inertial XYZ and a rotating xyz reference frame. Considering the notation adopted by Mohiuddin in [5] , the X and x axes are coincident with the undeformed centerline of the investigated rotor. By defining the angular displacement between the two axes as $\theta(t)$, the rotational speed of the rotor can be expressed as $\dot{\theta}(t)$.

The vector of generalized coordinates $\mathbf{e}$, representing the deformation of a generic shaft element delimited by a left i and a right j node, is defined through the following expression:

$$\mathbf{e} = \begin{bmatrix} v_i & w_i & \beta_i & \gamma_i & \phi_i & v_j & w_j & \beta_j & \gamma_j & \phi_j \end{bmatrix}^T \tag{2.27}$$

where five degrees for each node have been considered: two lateral displacement v and w along respectively Y and Z directions and three rotational deformations β, γ and ϕ about Y, Z and X respectively.

The translation, rotation and the torsional deflection of a point within the shaft element can be expressed as function of the nodal variables:

$$\begin{aligned}
\begin{bmatrix} v(x,t) \\ w(x,t) \end{bmatrix} &= N_v(x)\mathbf{e}(t) = \begin{bmatrix} N_{vv}(x) \\ N_{vw}(x) \end{bmatrix} \mathbf{e}(t) \\
&= \begin{bmatrix} N_{v1} & 0 & 0 & N_{v2} & 0 & N_{v3} & 0 & 0 & N_{v4} & 0 \\ 0 & N_{v1} & -N_{v2} & 0 & 0 & 0 & N_{v3} & -N_{v4} & 0 & 0 \end{bmatrix} \mathbf{e}(t) \\
\begin{bmatrix} \beta(x,t) \\ \gamma(x,t) \end{bmatrix} &= N_\beta(x)\mathbf{e}(t) = \begin{bmatrix} N_{\beta\beta}(x) \\ N_{\beta\gamma}(x) \end{bmatrix} \mathbf{e}(t) \\
&= \begin{bmatrix} 0 & -N_{\beta1} & 0 & 0 & 0 & -N_{\beta3} & N_{\beta4} & 0 & 0 & 0 \\ N_{\beta1} & 0 & 0 & N_{\beta2} & 0 & N_{\beta3} & 0 & 0 & N_{\beta4} & 0 \end{bmatrix} \mathbf{e}(t)
\end{aligned}$$

$$\phi(x,t) = N_\phi(x)\mathbf{e}(t) = \begin{bmatrix} 0 & 0 & 0 & 0 & N_{\phi1} & 0 & 0 & 0 & 0 & N_{\phi1} \end{bmatrix} \mathbf{e}(t) \tag{2.28}$$

where the extended expressions of the adopted shape functions can be found in [5]. Referring to Fig. 2.5, the position vector $\bar{\mathbf{r}}_\mathbf{p}$ of a generic point p_i in the

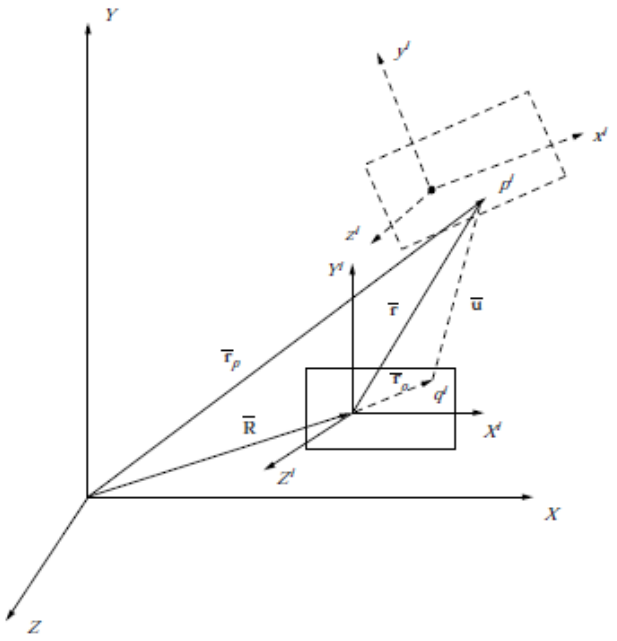

Fig. 2.5: Generalized coordinates of the $i-th$ element.

deformed shape element can be defined as:

$$\bar{\mathbf{r}}_{\mathbf{p}} = \overline{\mathbf{R}} + \bar{\mathbf{r}}_{\mathbf{0}} + \bar{\mathbf{u}} \tag{2.29}$$

where $\overline{\mathbf{R}}$ defines the coordinates of the origin of the $X^iY^iZ^i$ frame in the global reference frame XYZ and $\bar{\mathbf{r}}_{\mathbf{0}}$ is the position vector of the point p_i in the local frame $X^iY^iZ^i$. The deformation vector $\bar{\mathbf{u}}$ can be written as:

$$\bar{\mathbf{u}} = N\mathbf{e} \tag{2.30}$$

with $N \in \Re^{5\times 10}$ representing the shape functions matrix

$$N = \begin{bmatrix} N_v \\ N_\beta \\ N_\phi \end{bmatrix} \tag{2.31}$$

The kinetic energy T_i of the $i-th$ shaft element can be obtained by integrating the kinetic energy of an infinitesimal volume at point p_i over the element volume V and it results:

$$T = \frac{1}{2}\dot{\mathbf{e}}^T M\dot{\mathbf{e}} + \frac{1}{2}C^*\dot{\theta}^2 - \dot{\theta}\dot{\mathbf{e}}^T G^*\dot{\mathbf{e}} \tag{2.32}$$

where the composite mass matrix M is:

$$M = M_t + M_r + M_\phi - 2M_e \tag{2.33}$$

The matrix M_e contains the coupling terms between torsional and lateral vibrations and, since it is a function of the nodal vector, it results time-dependent. The extended expressions of the M matrix may be found in [5].

The strain energy of the $i-th$ shaft can be written as:

$$\begin{aligned} U = &+ \frac{1}{2}\int_0^l EI\left\{\left(\frac{\partial\beta}{\partial x}\right)^2 + \left(\frac{\partial\gamma}{\partial x}\right)^2\right\}dx \\ &+ \frac{1}{2}\int_0^l \kappa GA\left\{\left(\frac{\partial v}{\partial x} - \gamma\right)^2 + \left(\frac{\partial\gamma}{\partial x} + \beta\right)^2\right\}dx \\ &+ \frac{1}{2}\int_0^l GJ\left(\frac{\partial\phi}{\partial x}\right)^2 dx \end{aligned} \tag{2.34}$$

where G is the shear modulus of the shaft material, I is the second moment of cross-sectional area, J is the polar moment of inertia and κ is the shear factor. In a matrix form this equation results:

$$U = \frac{1}{2}\mathbf{e}^T K\mathbf{e} \tag{2.35}$$

where the K matrix is the composite stiffness matrix that is equal to:

$$K = K_e + K_s + K_\phi \tag{2.36}$$

with K_e, K_s and K_ϕ represent respectively the elastic, shear and torsional stiffness matrices.

Through the Lagrangian approach, the equations of motion of a generic shaft element can be derived as:

$$M\ddot{\mathbf{e}} + \dot{\theta}G\dot{\mathbf{e}} + K\mathbf{e} = \mathbf{Q} \tag{2.37}$$

where $G = G^* - G^{*T}$ is the element gyroscopic matrix and $\mathbf{Q}$ is the vector of generalized forces.

Finally, considering the equations of motion of disk elements and the expressions of generalized forces due the bearings action, the equation of motion of a general rotor-bearing system may be written:

$$\overline{M}\ddot{\overline{\mathbf{e}}} + \overline{C}\dot{\overline{\mathbf{e}}} + \overline{K}\overline{\mathbf{e}} = \overline{Q} \tag{2.38}$$

.

An analogous 5 dofs formulation has been derived by Qin in [69], through the application of the extended Hamilton's principle. In this work, the effects of internal viscous and hysteretic damping and of mass unbalance are also included. The finite element proposed by Qin is assessed through three numerical examples of rotor systems taken from the literature.

2.2.4 Discrete-continuous models

The continuous modelling of rotating machines is based on the assumptions of uniform axial mass distribution and stiffness of rotor shafts. Inertial disks data and visco-elastic properties of bearings and seals are considered as uniformly distributed along the shaft or through distributions of the Dirac type. Bladed disks, impellers, gears, coupling disks, flywheels can be represented by rigid bodies fixed in appropriate sections of the stepped shafts. In many applications, to take into account the lateral flexibility of these components when

they influence the lateral response of shafts, they are modelled as rigid disks connected to shafts by massless isotropic membranes.

In the work by Szolc [64], the discrete-continuos modelling of the rotor-shaft system illustrated in Fig. 2.6(a) is presented.

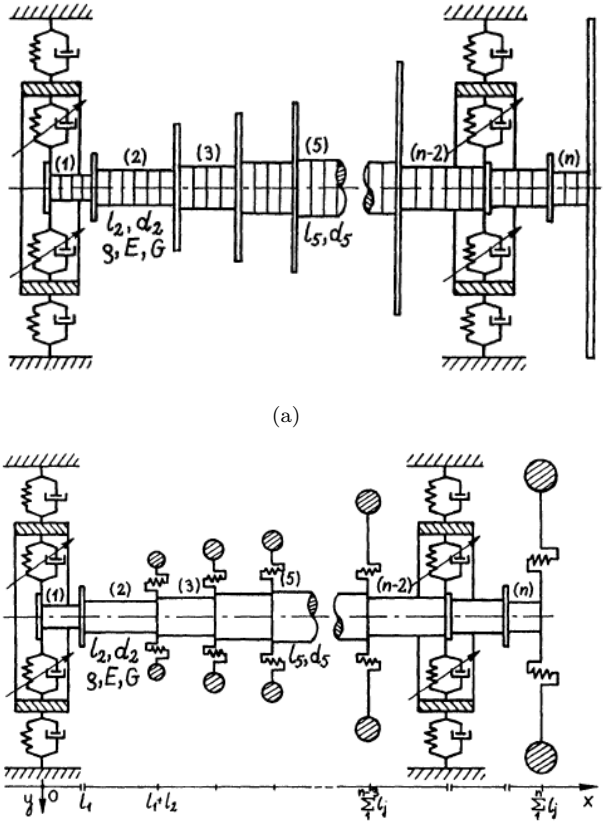

Fig. 2.6: Shaft-rotor system (a): finite-element model (b): discrete-continuous model.

Each $i-th$ (with $i = 1, ..., n$) cylindrical element of the stepped shaft is treated as a lateral and torsional flexible continuous visco-elastic element. Shaft elements are characterised by the same parameters of finite-elements models: element length l_i, cross-sectional mass density ρA_i, lateral EI_i and torsional GJ_{0i} stiffness, mass eccentricities $\delta_i(x)$ and phases Γ_i. Each rigid body is or ring is characterised by mass m_i, diametral J_i and polar I_{0i} inertia, radial eccentricity ϵ_i and phase Δ_i and by the centrifugal inertias I_{xyi}, I_{xzi} and I_{yzi} with $i = 1, ..., n+1$. Bearings are modelled with the same visco-elastic approach used in finite-elements models.

Both external distributed or concentrated loads, damping forces and torques can be added to the model as arbitrary time functions or as functions of the system response.

Considering an orthogonal non-rotating coordinate system $Oxyz$ where the x

axis is parallel to the rotation axis of the undeformed shaft with the origin set at the shaft left-most cross-section, as shown in Fig. 2.6(b). The y axis is vertical, directed downwards. The shaft is assumed slender enough to neglect shear effects in the considered frequency range. Thus, for small lateral vibrations vertical and horizontal motions of circular cross-sections of the $i-th$ elastic segment of the stepped shaft are described by means of the rotating Rayleigh beam equation:

$$\begin{aligned} &EI_i\left[\frac{\partial^4 v_i(x,t)}{\partial x^4}+e\frac{\partial^5 v_i(x,t)}{\partial x^4\partial t}\right]-\rho I_i\left[\frac{\partial^4 v_i(x,t)}{\partial x^2\partial t^2}+2j\Omega\frac{\partial^3 v_i(x,t)}{\partial x^2\partial t}\right] \\ &+\rho A_i\frac{\partial^2 v_i(x,t)}{\partial t^2}=\rho A_i\delta_i(x)\,\Omega^2\exp(\Omega t+\Gamma_i) \end{aligned} \tag{2.39}$$

where $v_i(x,t)=u_i(x,t)+jw_i(x,t)$, with $u_i(x,t)$ lateral displacement in the vertical direction and $w_i(x,t)$ in the horizontal direction and j is the imaginary unit.

Torsional motions is given by the following equation:

$$G\left[\frac{\partial^2\theta_i(x,t)}{\partial x^2}+\tau\frac{\partial^3\theta_i(x,t)}{\partial x^2\partial t}\right]-\rho\frac{\partial^2\theta_i(x,t)}{\partial t^2}=q_i(x,t) \tag{2.40}$$

with $\theta_i(x,t)$ angular displacement with respect of the shaft rotational motion with the constant velocity Ω and $q_i(x,t)$ representing the external torque distribution. The material damping in the shaft is represented by the viscosity coefficients for τ torsion and bending e, respectively.

Eqs. 2.39-2.40 can be solved with appropriate boundary conditions (geometrical conformity for displacements and inclinations of extreme cross-sections), linear and nonlinear equilibrium equations for the external forces and torques, static and dynamic unbalance forces and moments, inertial, elastic and external damping forces, supports forces and gyroscopic moments [14].

The analytically derived mathematical model formed of Eqs. 2.39-2.40 can be solved using the separation-of-variable approaches to evaluate both free and forced vibration behaviours. Results show that an increase in the unbalance values (eccentricity of static unbalances or inertia describing dynamic unbalance) cause a proportional rise of the lateral-torsional vibrations interaction. For relatively small static or dynamic unbalance the coupling between lateral and torsional vibration is small enough to treat them in an uncoupled way. Neverthless, a rapid increase in unbalance induce strong lateral and torsional vibrations that may lead to fatigue damage or rotor failures.

2.2.5 Flexible-multibody models for rotating shafts

Flexible-multibody techniques can be used to address the limitations of the classical equations of motion and provide a comprehensive model for rotating shafts. To this aim, Brown and Shabana [71] derived the general equations of motion for a flexible body through the application of the principle of virtual work in rotating shaft dynamics. The mathematical model developed in [71] aims at overcoming the limitations of classical formulations of the equations of motion of a rotating shaft, taking into account both the Coriolis and centrifugal inertia forces, and the effect of the inertia terms on the system dynamic stability

is studied. The effect of the rotary inertia on the axial and lateral deformations is also formulated and the coupling terms are obtained.

Classical formulation of rotating shaft problems

The working hypotheses for the derivation of classical formulation of rotating shaft applications are:

- a shaft rotating about its axis at a constant angular velocity is considered;
- cross sectional dimensions of the shaft are small in comparison to its length;
- shear deformation is neglected.

The equations of motion are derived by applying Newton-Euler equations to a cross-section characterised by an infinitesimal length of a rotating shaft (see Fig. 2.7. The gyroscopic moment effect is studied using the definition of the angular momentum as it applies to the rotation of the cross-section of the shaft.

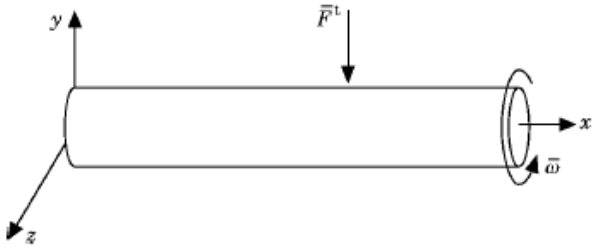

Fig. 2.7: Rotating shaft.

Starting from the Euler's equation

$$\mathbf{T} = \rho \mathbf{I} \frac{\partial \Psi}{\partial t^2} \tag{2.41}$$

where $\mathbf{T}$ represents the vector of applied moments, $\mathbf{I}$ is the inertia tensor of an infinitesimal cross-section of the shaft defined as:

$$\begin{bmatrix} 2I & 0 & 0 \\ 0 & I & 0 \\ 0 & 0 & I \end{bmatrix} \tag{2.42}$$

with I moment of inertia of the cross-section about the y and z axes, ρ is the shaft density. The angular displacement of the shaft is given by

$$\Psi = \begin{bmatrix} 0 & \psi_2 & \psi_3 \end{bmatrix}^T \tag{2.43}$$

where ψ_2 and ψ_3 are rotations about respectively the y and z axes. Due to the assumption of constant angular velocity ω_1 about the x axis its angular acceleration about the x axis is identically equal to zero The angular displacements can be written as:

$$\psi_2 = -\frac{\partial u_3}{\partial x} \qquad \psi_3 = \frac{\partial u_2}{\partial x} \tag{2.44}$$

where u_1 and u_2 are the displacements in the y and z directions. The angular momentum of the shaft is expressed as:

$$\bar{\mathbf{H}} = \rho \mathbf{I} \boldsymbol{\omega} \tag{2.45}$$

with

$$\boldsymbol{\omega} = \begin{bmatrix} \omega_1 & 0 & 0 \end{bmatrix}^T \tag{2.46}$$

Using the rate of change of the angular momentum and following the procedure described in references the classical equations of motion for the rotating shaft can be obtained [71]. In obtaining the classical equations of motion several assumptions are made, limiting the use of this formulation in the analysis as follows:

1. The angular velocity of the shaft is assumed constant and hence classical formulation cannot be used in the analysis of shafts that have non-zero angular accelerations.

2. The effect of the longitudinal displacement resulting from the transverse applied load is neglected. As a result of the rotary inertia effect, bending deformations affect the longitudinal displacement of the rotating shaft and this effect cannot be examined using the classical approach.

3. The classical formulation does not take into account the support vibration resulting from support movements or bearing looseness and joint clearances. Therefore the use of this formulation is limited to special rotating shaft problems where base excitations and joint and bearing flexibility are ignored.

4. In the classical formulation the complete effect of the deformation on the expression of the angular momentum is not taken into consideration. At high speed rotations such as those encountered in modern rotating spindle applications, a more precise definition for the inertia forces must be used.

Flexible-multibody models for rotating shafts

Through the adoption of the principle of virtual work in dynamics, the equations of motion of a deformable body that undergoes an arbitrary displacement can be written as:

$$M\ddot{\mathbf{q}} + K\mathbf{q} = \mathbf{Q}_v + \mathbf{Q}_c \tag{2.47}$$

where M is the body mass matrix, K is the stiffness matrix, $\mathbf{Q}_v$ is the vector of Coriolis and centrifugal forces and $\mathbf{Q}_e$ is the vector of generalized applied forces. The vector of generalized coordinates $\mathbf{q}$ can be written in a partitioned form as:

$$\mathbf{q} = \begin{bmatrix} \mathbf{R}^T & \boldsymbol{\theta}^T & \mathbf{q}_f^T \end{bmatrix}^T \tag{2.48}$$

with $\mathbf{R}$ reference displacement, $\boldsymbol{\theta}$ represents the set of parameters defining the body orientation and $\mathbf{q}_f$ is the vector of elastic coordinates.

According to the coordinate partitioning, the equation of motion can be written as:

$$\begin{bmatrix} m_{RR} & m_{R\theta} & m_{Rf} \\ m_{\theta R} & m_{R\theta} & m_{\theta f} \\ m_{fR} & m_{f\theta} & m_{ff} \end{bmatrix} \begin{bmatrix} \ddot{\mathbf{R}} \\ \ddot{\boldsymbol{\theta}} \\ \ddot{\mathbf{q}}_\mathbf{f} \end{bmatrix} + \begin{bmatrix} 0 & 0 & 0 \\ 0 & 0 & 0 \\ 0 & 0 & k_{ff} \end{bmatrix} \begin{bmatrix} \mathbf{R} \\ \boldsymbol{\theta} \\ \mathbf{q}_\mathbf{f} \end{bmatrix} = \begin{bmatrix} (\mathbf{Q_v})_R \\ (\mathbf{Q_v})_\theta \\ (\mathbf{Q_v})_f \end{bmatrix} + \begin{bmatrix} (\mathbf{Q_e})_R \\ (\mathbf{Q_e})_\theta \\ (\mathbf{Q_e})_f \end{bmatrix} \tag{2.49}$$

where the elements of the stiffness matrix, quadratic velocity vector ($\mathbf{Q_v}$) and the vector of generalized external forces ($\mathbf{Q_e}$) are defined in explicit form in [71]. The elements of the mass matrix are defined as

$$M = \begin{bmatrix} m_{RR} & m_{R\theta} & m_{Rf} \\ m_{\theta R} & m_{R\theta} & m_{\theta f} \\ m_{fR} & m_{f\theta} & m_{ff} \end{bmatrix} = \int \begin{bmatrix} \mathbf{I} & \mathbf{A}\tilde{\bar{\mathbf{u}}}\bar{\mathbf{G}} & \mathbf{AS} \\ & \bar{\mathbf{G}}^\mathbf{T}\tilde{\bar{\mathbf{u}}}^\mathbf{T}\tilde{\bar{\mathbf{u}}}\bar{\mathbf{G}} & \bar{\mathbf{G}}^\mathbf{T}\tilde{\bar{\mathbf{u}}}\mathbf{S} \\ Sym & & \mathbf{S}^\mathbf{T}\mathbf{S} \end{bmatrix} dV \tag{2.50}$$

where the integration is taken over the volume of the body V, $\mathbf{A}$ is the transformation matrix defining the orientation of the body coordinate system $\tilde{\bar{\mathbf{u}}}$ is the skew symmetric matrix associated with the vector $\bar{\mathbf{u}}$ that gives the position of an arbitrary point on the body with respect to the body coordinate system, $\mathbf{S}$ is the shape function matrix and $\bar{\mathbf{G}}$ is the matrix relating the angular velocity vector to the vector of time derivatives of the orientation coordinates. That is

$$\bar{\mathbf{u}} = \bar{\mathbf{u}}_\mathbf{0} + \bar{\mathbf{u}}_\mathbf{f} = \bar{\mathbf{u}}_\mathbf{0} + \mathbf{S}\mathbf{q}_\mathbf{f} \quad \bar{\omega} = \bar{\mathbf{G}}\dot{\theta} \tag{2.51}$$

where $\bar{\mathbf{u}}_\mathbf{0}$ is the position of an arbitrary point on the body in the undeformed state, $\bar{\mathbf{u}}_\mathbf{f}$ is the time-space dependent deformation vector and $\dot{\boldsymbol{\theta}}$ is the angular velocity vector in the body coordinate system. The expressions describing the vector of the Coriolis and centrifugal forces can be found in [71]. This general formulation can be applied to the rotating shaft problem to investigate the dynamics of accelerating shafts, the effect of rotary inertia and of the Coriolis coupling [71].

The results presented in the study show that the general flexible body formulation can be used to study rotating shafts. As a consequence, general purpose flexible multibody computer algorithms can be adopted to systematically solve more general rotating shaft problems.

Chapter 3

Architecture of the Rotordynamical Model

Modelling approaches for coupled lateral-torsional rotordynamics are mainly based on elementary formulations and applied to simple theoretical rotor schemes for a qualitative investigation on the mechanisms inducing the coupling. For real applications, an improvement of rotordynamical models is still highly demanded, in order to make them able to model the combined torsional-lateral dynamics and to properly predict the critical behaviour of complex rotor systems, such as rotors with distributed elements and with multi-point connections. As far as the author knows, in the literature, there is a substantial lack concerning models suitable for the coupled lateral-torsional analysis of multi-rotor systems characterised by complex topology. In such a context a rotordynamical model is introduced in this thesis; the model has been specifically developed to be suitable for the analysis of coupled lateral-torsional vibrations in complex multi-rotor configurations.

3.1 General architecture of the model

The proposed rotordynamical model represents a systematic and efficient approach to various rotor dynamics modelling issues and its main contribution to the state-of-the-art in rotordynamics research is due to its general topology. In fact, the presented model is general-purpose and it is able to reproduce all the main mechanisms inducing vibration phenomena in rotating machinery. More particularly, it allows complex topology rotors to be modelled through a general approach. Innovative rotor elements are available to characterise the dynamic behaviour of non-standard components that cannot be represented with any classical rotordynamics elements such as disks, shafts or concentrated elasto-damping elements. For instance, the model is particularly useful for the mathematical modelling of distributed rotors with complex rotor-to-shaft connections to accurately reproduce their contributions to the dynamical response of rotor systems or eventually, to consider moments and forces due to mechanical looseness or improper assembly. Multi-rotor linking elements such as couplings and gearboxes can be represented with elements defined by according to several levels of detail. The rotordynamical model is based on an accurate FE formulation

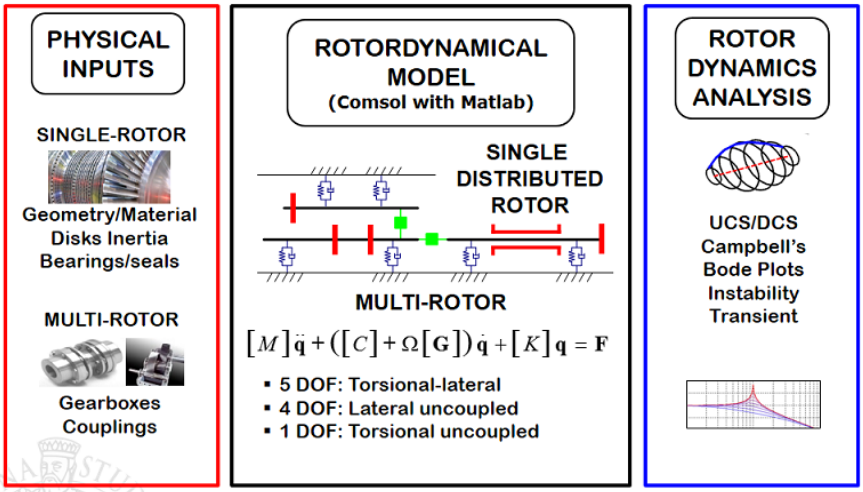

Fig. 3.1: General architecture of the proposed model.

with 6 degrees of freedom for each node. Because of its numerical efficiency, it represents a good compromise between accuracy and computational effort, thus it may be used to perform the common dynamical investigation used in the rotordynamics design phase.

The general architecture of the model developed in this work is illustrated in Fig. 3.1. The model is formed of three succeeding parts:

- the *Physical Inputs* module, involving the pre-processing phase;
- the *Rotordynamical Model*, representing the core of the proposed model;
- the *Rotordynamics Analysis* module, conceived for the post-processing of the results.

The *Physical Inputs* part is the module that includes all the physical inputs that must be provided to the model to perform the rotor discretisation and the dynamical analysis. It represents the collecting process of the significant physical features and modeling choices that must be specified to the model to ensure that it accurately portrays the dynamics of the investigated test-case (such as geometry and material of the shafts, disk inertias and bearing or seals data) for *single-rotor* systems and also data relative to coupling components (i.e. flexible couplings) in *multi-rotor* configurations.

The core of the innovative model is the second part of the general architecture, the *Rotordynamical Model*, which is the module responsible for the model set-up and for the dynamical analysis. The Rotordynamical Model is able to reproduce the dynamics of a generic multi-shaft rotor assembly, taking into account all the components that influence the response of the investigated rotor system (Fig. 3.2).

The elementary unit of the Rotordynamical Model is represented by an accurate FE model of a *single-rotor* formed of basic building blocks (rotordynamics elements). More specifically, it is the module responsible for describing the rotor mass-elastic properties by means of both classical and non-standard rotor FE

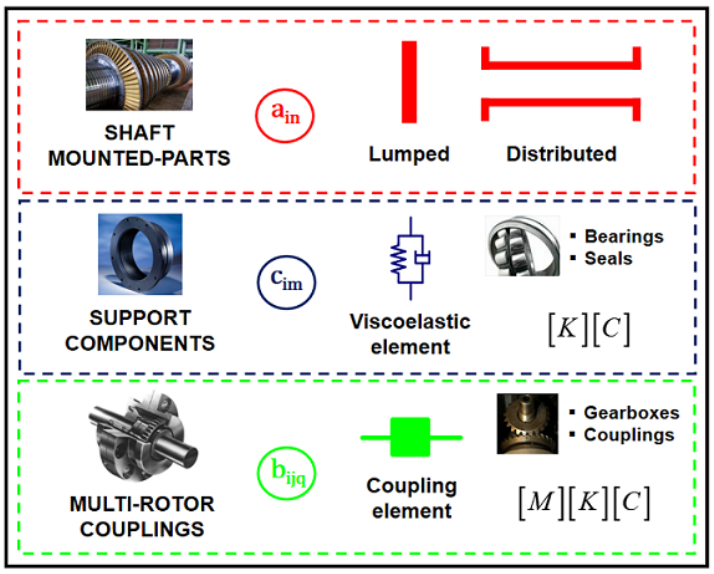

Fig. 3.2: Rotordynamics elements.

elements such as shafts, disks, distributed inertias with multi-point connections, bearings and seals [4].

The building blocks that must be joined together to obtain a complete *single rotor* model may be distinguished according to the physical characteristics of a generic rotating assembly:

1. *Shaft elements* that contribute both on stiffness and inertial properties of the rotor model. Typical shaft elements include beam characterised by circular or hole-circular cross-sections. In the presented model rotating beams characterised by generic user-defined cross-section can also be adopted.

2. *Mounted elements*, representing disks or other massive components shrunk onto the shaft. Due to the high complexity characterising modern rotating systems, the necessity of generating detailed inertia distribution models and other non-standard components has increased. In the Rotordynamical Model, mounted elements may be represented through both classical lumped and non-standard distributed inertial elements. Lumped elements give contribution only to inertial properties thus representing disk elements of classical modelling approaches. Inertial distributed elements are instead employed when particular mounted elements have to be reproduced and they may be used to easily represent different types of connection, which can be adopted to take into account the elastic effects of massive components. In general, distributed elements may be adopted to correctly model elements characterised by more complex shaft-to-rotor multiple-points connections. The non-standard elements previously described have been developed to overcome modelling limitations relative to complex rotor with distributed inertias, such kind of component may in fact affect the dynamical behaviour of the system with particular concern

to the lateral-torsional coupled vibrations.

3. *Elasto-damping lumped elements* that are commonly employed to take into account the contribution that seals or bearings can give to rotor vibrations. The elements are based on stiffness and damping matrices [4, 6, 9] that are computed through the linearised models (obtained starting from more complex FE or CFD models) of bearings and seals, assuming that they act on the centerline of the associated shaft element.

A *multi-rotor* configuration can be assembled starting from several *single rotors*, connected each other through innovative elements that model the common devices used for the power transmission. Linking elements used to drive rotating machines such as flexible couplings can be represented through the presented Rotordynamical Model. More specifically, generic power transmission systems linking the different shafts of a multi-rotor configuration to be investigated, can be easily taken into account by means of both static or dynamical 6 dofs models [21]. This kind of approach leads to equivalent, accurate and simple models, starting from data computed by means of more sophisticated analysis (e.g. solid 3D finite element models).

The presented model is able to study the influence of distributed rotors on the dynamics of an investigated system, thanks to a FE formulation with 3D beam that may shift among formulations characterised by 1, 4, 5 or 6 degrees of freedom for each node [28, 29]. In such a way, traditional uncoupled, such as lateral (4 dofs) or torsional (1 dof) studies, or coupled such as axial-lateral-torsional (6 dofs) or lateral-torsional (5 dofs) approaches can be chosen for the rotordynamics analysis.

The Rotordynamical Model has been specifically developed to perform classical rotordynamics analysis, commonly performed in the design, operating, and troubleshooting phases of rotating equipments. Thanks to the proposed model, the most significant rotordynamics analysis can be performed and for each studied rotor assembly all the relevant results can be obtained in a reasonable computational time.

The rotordynamics outputs of the developed model are:

- *Undamped Critical Speed UCS*: it determines how modifications in some design parameters (i.e. bearing stiffness) affect the critical speed values of the considered system;
- *Damped Critical Speed DCS*: it allows the Campbell's plot to be defined and the evaluation of the torsional natural frequencies of the studied rotor;
- *Forced Response* to assess the amplitudes of synchronous, sub-synchronous and super-synchronous vibration caused by the rotor unbalance or other harmonic forcing functions;
- *Transient analysis* to study nonlinear or local effects.

The third part of the general architecture, the *Rotordynamics analysis*, is the module responsible for the post-processing (i.e. the outputs of the Rotordynamical Model). The specific output of each feasible analysis can be assessed and the typical results are automatically generated. In the following sections the Rotordynamical Model developed in the present activity is described in detail.

3.2 The Physical Inputs module

The *Physical Inputs* module is the part responsible for the pre-processing phase and it represents the first step in a rotordynamics analysis when the studied equipment is reproduced by means of a theoretical scheme according to the chosen modelling elements. The starting point of each rotordynamical analysis consists in fact in defining a FE model of the rotating assembly that has to be investigated. The model is totally defined when the geometrical characteristics and the significant mechanical properties are given.

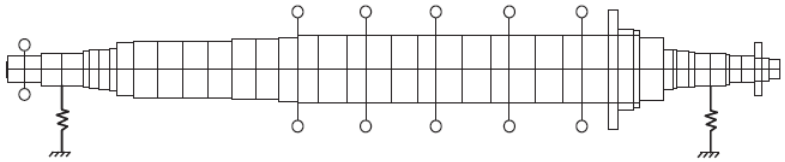

Fig. 3.3: An example of FE discretisation [1].

The *Physical Inputs* is hence the module where both geometrical-physical properties and discretisation data, needed for the definition of the mathematical model, are provided. More specifically the inputs that must be specified for a generic model are:

- node positions (stations);
- cross-section areas and inertia moments;
- material properties (density, elastic and tangential modulus);
- inertial characteristics of the mass elements;
- stiffness and damping parameters of bearings and seals;
- non-standard components features and mechanical properties;
- multi-rotor couplings parameters.

It must be noticed that the necessary physical inputs for the mathematical description of the investigated system are strictly related to the particular analysis task and elements chosen for the discretisation.

The *Physical Inputs* module is implemented in tha Matlab environment.

3.3 The Rotordynamical Model

The finite element approach provides a methodical approach for the discretisation of a continuum [73]. It can provide a solution for many types of complicated systems including fluid flows, static or dynamic mechanical systems. In each case the system is divided into smaller contacting regions called elements that can be described mathematically. For rotordynamics applications, finite elements models aim to describe them mathematically using a system of differential equations. Thanks to the increase in computing power in the last

decades, this kind of method became the *de facto* standard for the static and dynamic analysis of rotor systems [9].

In the present section the core of the developed model is introduced. The Rotordynamical Model is based on a FE formulation using 3D 2 nodes beams with 6 dofs at each node [28, 29]. Thanks to this formulation the following coupled or uncoupled analysis may be performed:

- axial-lateral-torsional (6 dofs);
- lateral-torsional (5 dofs);
- lateral (4 dofs);
- torsional (1 dof).

The finite element method for rotordynamics analysis is based on the discretization of the considered rotor into a series of *rotor elements* [4, 8, 9]. More specifically, in rotordynamics applications several kinds of elements can be adopted for the system modelling and the standard ones that may be implemented in a single rotor unit of the introduced model are:

- rigid disk element;
- shaft element;
- bearing element;
- non-standard component.

The model described in this thesis enables the representation of non-standard elements (distributed inertial elements, solid 3D components and elements characterised by complex connections). The general rotor equations of motion are provided by applying the Lagrange's equation to the expressions of the kinetic energy (disk elements, shafts and unbalanced mass), of strain energy (shaft elements) and of the virtual work done by the forces acting on the shaft (bearings, seals and complex connections).

The presented Rotordynamical Model allows the modelling of *multi-rotor elements* representing coupling components that link the single rotor units and that are commonly adopted in multi-shaft configurations such as flexible couplings and gear-boxes.

A subset of the possible rotordynamics elements has been adopted for the study of the test-case presented in this thesis, thus, for sake of brevity, the mathematical formulation of the elements employed in the present application is described in the following parts of the work.

The entire Rotordynamical Model has been implemented in the *Matlab with Comsol v.4.4a* environment [74].

Working hypotheses

The mathematical formulation of the Rotordynamical Model is based on the following working hypotheses:

- XYZ is a fixed reference frame with the origin in the point O;

- $X_dY_dZ_d$ is a rotating reference frame attached to the symmetric disk and placed in its center of mass G;
- the X and X_d axes are coincident with the rotor axis in the undeformed configuration;
- small-deformation and small-rotation problems are considered.

Rigid disk element

The disk is a rigid element containing the inertial properties of the rotor system. It does not contribute to the stiffness of the model since it is taken into account as a rigid body, free from elastic deformations. The dynamics of the disk may be described starting from an energy standpoint. The strain energy may be neglected and only its kinetic energy contributes to the definition of the equations of motion.

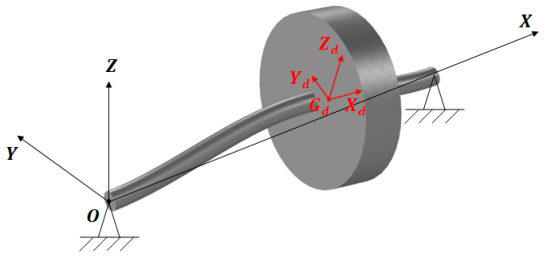

Fig. 3.4: Typical rotor deformed configuration and reference systems.

According to the rotating $G_dX_dY_dZ_d$ reference system illustrated in Fig. 3.4, the general expression of the kinetic energy T_i^D of the $i-th$ disk element considering a complete 6 dofs motion is given by the sum of the translational $T_i^{D\ t}$ and rotational $T_i^{D\ r}$ contributions:

$$T_i^D = T_i^{D\ t} + T_i^{D\ r} = \frac{1}{2} m_i^D \left(\dot{\mathbf{v}}_i^D\right)^2 + \frac{1}{2} \boldsymbol{\omega}_i^{D\,T} \Gamma_i^D \boldsymbol{\omega}_i^D \tag{3.1}$$

where $\mathbf{v}_i^D = \left[\dot{u}_i^D \ \ \dot{v}_i^D \ \ \dot{w}_i^D\right]^T$ is the velocity vector of the center of mass G_i^D of the $i-th$ disk with $\dot{u}_i^D$, $\dot{v}_i^D$ and $\dot{w}_i^D$ translational velocities respectively in the X,Y and Z directions.

The vector $\boldsymbol{\omega}_{xi}^D = \left[\omega_i^D \ \ \omega_{yi}^D \ \ \omega_{zi}^D\right]^T$ is the angular speed of the disk expressed in the rotating reference system $X_dY_dZ_d$, m_i^D is the mass of the disk and Γ_i^D is the inertial tensor. Assuming that the disk is symmetric, then $X_dY_dZ_d$ are principal directions of inertia and the Γ_i^D tensor is given by:

$$\begin{bmatrix} J_{Pi}^D & 0 & 0 \\ 0 & J_{Ti}^D & 0 \\ 0 & 0 & J_{Ti}^D \end{bmatrix} \tag{3.2}$$

with J_{Pi}^D and J_{Ti} defining respectively the polar and the transverse inertial moments of the disks.

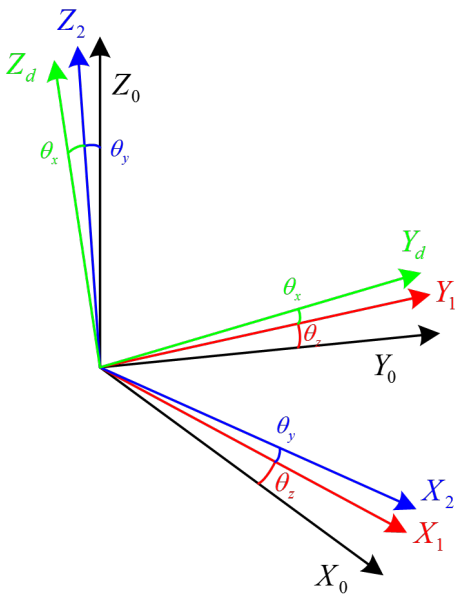

Fig. 3.5: Rotation angles.

To find an expression of the vector $\boldsymbol{\omega}_i^D$ in the fixed reference frame, the inertial $OXYZ$ and the disk $G_dX_dY_dZ_d$ reference systems orientation can be related through a set of rotations shown in Fig. 3.5.

The rotations are applied in the following order: θ_z about Z_0 axis, θ_y about the new Y_1 axis and finally θ_x about the so obtained X_2 axis, thus θ_x represents the angle of rotation about the rotor shaft.

Assuming that $\dot{\theta}_y$ and $\dot{\theta}_z$ are the rotational velocity of the disk with respect to respectively the Y and Z fixed axes, the angular velocity $\boldsymbol{\omega}_i^D$ is given by:

$$\begin{aligned}\boldsymbol{\omega}_i^D = &\begin{bmatrix}\dot{\theta}_{xi}\\0\\0\end{bmatrix} + \begin{bmatrix}1 & 0 & 0\\0 & \cos\theta_{xi} & \sin\theta_{xi}\\0 & -\sin\theta_{xi} & \cos\theta_{xi}\end{bmatrix}\begin{bmatrix}0\\\dot{\theta}_{yi}\\0\end{bmatrix}\\ &+ \begin{bmatrix}1 & 0 & 0\\0 & \cos\theta_{xi} & \sin\theta_{xi}\\0 & -\sin\theta_{xi} & \cos\theta_{xi}\end{bmatrix}\begin{bmatrix}\cos\theta_{yi} & 0 & -\sin\theta_{yi}\\0 & 1 & 0\\\sin\theta_{yi} & 0 & \cos\theta_{yi}\end{bmatrix}\begin{bmatrix}0\\0\\\dot{\theta}_{zi}\end{bmatrix}\end{aligned} \tag{3.3}$$

Hence it results:

$$\boldsymbol{\omega}_i^D = \begin{bmatrix}\omega_{xi}\\\omega_{yi}\\\omega_{zi}\end{bmatrix} = \begin{bmatrix}\dot{\theta}_{xi} - \dot{\theta}_{zi}\sin\theta_{yi}\\\dot{\theta}_{yi}\cos\theta_{xi} + \dot{\theta}_{zi}\sin\theta_{xi}\cos\theta_{yi}\\-\dot{\theta}_{yi}\sin\theta_{xi} + \dot{\theta}_{zi}\cos\theta_{xi}\cos\theta_{yi}\end{bmatrix} \tag{3.4}$$

Substituting the previous expressions in Eq.3.1, and assuming the hypothesis of small rotation angle (thus neglecting terms higher than second order derivatives) an extended formulation of the kinetic energy of the disk in the fixed reference

system may be calculated [4, 8, 28, 9]:

$$\begin{aligned} T_i^D = T_i^{D\ t} + T_i^{D\ r} =& \frac{1}{2} m_i^D \left[\left(\dot{u}_i^D\right)^2 + \left(\dot{v}_i^D\right)^2 + \left(\dot{w}_i^D\right)^2 \right] \\ &+ \frac{1}{2} J_{Pi}^D \left(\dot{\theta}_{xi}^2 - 2\dot{\theta}_{zi}\dot{\theta}_{xi}\theta_{yi} \right) + J_{Ti}^D \left(\dot{\theta}_{yi}^2 + \dot{\theta}_{zi}^2 \right) \end{aligned} \tag{3.5}$$

In the present research activity a complete 6 dofs formulation is considered, thus at the $i-th$ disk node the rotor has six degrees of freedom: three translations u_i^D ,v_i^D,w_i^D and three rotations θ_{xi}^D, θ_{yi}^D and θ_{zi}^D. Then, if the $i-th$ displacement vector of the disk center in the fixed reference frame is:

$$\mathbf{q}_i^D = \begin{bmatrix} u_i^D & v_i^D & w_i^D & \theta_{xi}^D & \theta_{yi}^D & \theta_{zi}^D \end{bmatrix}^T \tag{3.6}$$

the application of the Lagrange's equations to the expression of the kinetic energy determines the matrices describing the dynamics of the $i-th$ disk element.

$$\frac{d}{dt}\left(\frac{\partial T}{\partial \dot{\mathbf{q}}_i^D}\right) - \frac{\partial T}{\partial \mathbf{q}_i^D} = M_i^D \ddot{\mathbf{q}}_i^D + \Omega G_i^D \dot{\mathbf{q}}_\mathbf{i}^\mathbf{D} = \mathbf{F}_i^D \tag{3.7}$$

where M_i^D and G_i^D represent respectively the mass and the gyroscopic matrices and $\mathbf{F}_i^D$ represents the vector of external forces. The rotation θ_{xi}^D around the spin axle is related to the spin speed Ω according to the relation $\theta_{xi}^D = \Omega t + \phi$ where ϕ is the vibration contribute.

Shaft element

Shaft elements contribute both on stiffness and inertial property of the rotor finite element model. They are represented as beam with circular or circular hollow cross-section with 6 dofs for each node [28, 29]. In this case the vector of the generalized coordinates of the $k-th$ shaft element is given by:

$$\mathbf{q}_k^s = \begin{bmatrix} u_1^s & v_1^s & w_1^s & \theta_{x1}^s & \theta_{y1}^s & \theta_{z1}^s & u_2^s & v_2^s & w_2^s & \theta_{x2}^s & \theta_{y2}^s & \theta_{z2}^s \end{bmatrix} \tag{3.8}$$

where, the subscript k has been dropped out for notational simplicity.

The deformation vector $\mathbf{u}$ describing axial $u(x,t)$, transverse $v(x,t)$, $w(x,t)$ deflections, $\theta_y(x,t)$ and $\theta_z(x,t)$ rotations and torsional $\theta_z(x,t)$ deformation of a point within the element can be expressed as:

$$\begin{bmatrix} u(x,t) \\ v(x,t) \\ w(x,t) \\ \theta_x(x,t) \\ \theta_y(x,t) \\ \theta_z(x,t) \end{bmatrix} = \begin{bmatrix} N_u \\ N_v \\ N_w \\ N_{\theta_x} \\ N_{\theta_y} \\ N_{\theta_z} \end{bmatrix} \mathbf{q}^s = N\mathbf{q}^s \tag{3.9}$$

where the shape function matrix N is:

$$N = \begin{bmatrix} N_{u1} & 0 & 0 & 0 & 0 & 0 & N_{u2} & 0 & 0 & 0 & 0 & 0 \\ 0 & N_{v1} & 0 & 0 & 0 & N_{v2} & 0 & N_{v3} & 0 & 0 & 0 & N_{v4} \\ 0 & 0 & N_{w1} & 0 & N_{w2} & 0 & 0 & 0 & N_{w3} & 0 & -N_{w4} & 0 \\ 0 & 0 & 0 & 0 & 0 & N_{\theta_{x1}} & 0 & 0 & 0 & 0 & 0 & N_{\theta_{x2}} \\ 0 & 0 & -N_{\theta_{y1}} & 0 & N_{\theta_{y2}} & 0 & 0 & 0 & -N_{\theta_{y3}} & 0 & N_{\theta_{y4}} & 0 \\ 0 & N_{\theta_{z1}} & 0 & 0 & 0 & N_{\theta_{z2}} & 0 & N_{\theta_{z3}} & 0 & 0 & 0 & N_{\theta_{z4}} \end{bmatrix}$$

where the extended expressions of the shape functions are given in appendix **??**.

For shaft elements both kinetic and strain energy contribute to the determination of the shaft element matrices [4, 9, 28, 22]. The expression of the kinetic energy of the $k-th$ shaft element of length l_k, (Fig 3.6) comes from an extension of the disk equation:

$$\begin{aligned} T_k^S =& \frac{1}{2}\int_0^{l_k} \rho A_k \left(\dot{u}^2 + \dot{v}^2 + \dot{w}^2\right) ds + \frac{1}{2}\int_0^{l_k} I_{Tk}\left(\dot{\theta}_y^2 + \dot{\theta}_z^2\right) ds \\ &+ \frac{1}{2}\int_0^{l_k} I_{Pk}\left(\dot{\theta}_x^2 - 2\Omega\dot{\theta}_z\theta_y\right) ds \end{aligned} \tag{3.10}$$

where ρ is the density of the material, A_k is the $k-th$ section area, I_{Pk} and I_{Tk} define respectively the polar and transverse inertial moments for length unit. The potential energy is given by:

$$\begin{aligned} U_k^S =& \frac{1}{2}\int_0^{l_k} EI_k \left[\left(\frac{\partial\theta_y}{\partial x}\right)^2 + \left(\frac{\partial\theta_z}{\partial x}\right)^2\right] ds \\ &+ \frac{1}{2}\int_0^{l_k} K_k G A_k \left[\left(\frac{\partial v}{\partial x} - \theta_z\right)^2 + \left(\frac{\partial v}{\partial w} - \theta_y\right)^2\right] ds \\ &+ \frac{1}{2}\int_0^{l_k} GJ_k \left(\frac{\partial\theta z}{\partial x}\right)^2 ds + \frac{1}{2}\int_0^{l_k} EA_k \left(\frac{\partial u}{\partial x}\right)^2 ds \end{aligned} \tag{3.11}$$

where E is the Young's modulus, I_k represent the second area moment of the $k-th$ shaft section, G is the shear modulus, K_k is the shear form factor and J_k is the polar second moment of area.

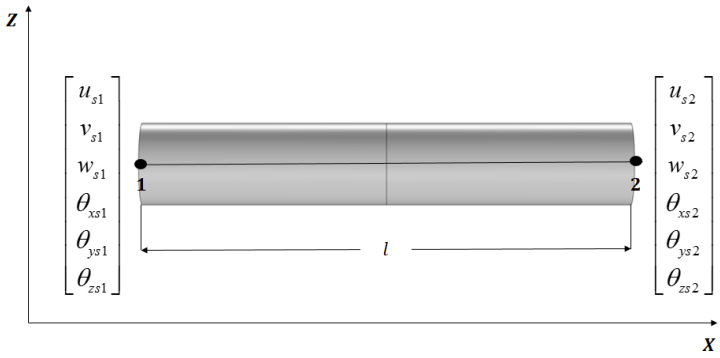

Fig. 3.6: Shaft beam element.

Substituting the relationships defined by Eq. 3.9 into the previous expression and applying the Lagrange's equations to the expression of the kinetic and strain energies, the equationss describing the dynamics of the $k-th$ shaft element may be written as:

$$\frac{d}{dt}\left(\frac{\partial L}{\partial \dot{\mathbf{q}}_i^S}\right) - \frac{\partial L}{\partial \mathbf{q}_i^S} = M_k^S \ddot{\mathbf{q}}_k^S + \Omega G_k^S \dot{\mathbf{q}}_\mathbf{k}^\mathbf{S} + K_k^S \mathbf{q}_k^S = \mathbf{F}_k^S \tag{3.12}$$

where M_k^s, G_k^s and K_k^s represent respectively the mass, gyroscopic and stiffness matrices and $\mathbf{F}_k^s$ is vector of the generalized forces applied to the shaft beam element.

Bearing element

In rotor systems the bearing forms a link between the rotor and the support structure representing one of the most critical components in turbomachinery and rotating machines applications. Bearings have a deep influence on the rotordynamics performance and their contribution must be accurately taken into account for the dynamical behaviour prediction.

Several types of bearings (Fig. 3.7) are employed in rotordynamics applications: rolling-elements bearings, fluid-dynamic journal bearings, hydrostatic journal bearings and magnetic bearings. Rolling bearings are characterised by an isotropic behaviour and they exhibit very low damping values. Stiffness properties are almost independent on the spin speed, while they depend on the housing geometry. Cost is relatively low but they require accurate maintenance operations.

Fig. 3.7: Bearing examples.

Hydrostatic journal bearings may support the rotor in low rotational speed regimes, avoiding the contact between the rotor and housing. To this purpose, they require a lubricant supplying system. In fluid-dynamic journal bearings, usually adopted in heavy and large machine, a film of oil is present in the clearance between static and rotating elements. The rotor creates a hydrodynamic pressure distribution within the oil film supporting weight and unbalance forces of the rotor. In the last decades magnetic bearings have been introduced in rotordynamics application. The peculiarity of such type of bearings is that the separation between rotor and stator is obtained through a magnetic field, thus rotor to stator contact is removed.

In classical FE uncoupled lateral formulation [4, 9], they are usually specified through stiffness and damping elements connecting the transverse v and w degrees of freedoms of rotor nodes to the supporting structure or the four bending dofs (v, w translations and θ_y, θ_z rotations). Furthermore, stiffness and damping values are usually evaluated considering only the linear part of the load-deflection characteristics.

In the Rotordynamical Model developed in the present activity, classical bearing formulations have been extended to consider all the six components of the load exerted by a generic bearing element on the shaft. More specifically, the action of the $p-th$ bearing element on the investigated rotor in compact

form is defined as:

$$\mathbf{F}_p^{brg} = -K_p^{brg}(N,\Omega)(\mathbf{q}_{p1}^{brg} - \mathbf{q}_{p2}^{brg}) - C_p^{brg}(N,\Omega)(\dot{\mathbf{q}}_{p1}^{brg} - \dot{\mathbf{q}}_{p2}^{brg}) \tag{3.13}$$

where the stiffness $K_p^{brg}(N,\Omega)$ and damping $C_p^{brg}(N,\Omega)$ matrices may depend on both the rotational shaft speed Ω and the load N. The extended expressions of the stiffness and damping matrices are given by:

$$K_p^{brg} = \begin{bmatrix} k_{xxp}^{brg} & k_{xyp}^{brg} & k_{xzp}^{brg} & k_{x\theta_x p}^{brg} & k_{x\theta_y p}^{brg} & k_{x\theta_z p}^{brg} \\ k_{yxp}^{brg} & k_{yyp}^{brg} & k_{yzp}^{brg} & k_{y\theta_x p}^{brg} & k_{y\theta_y p}^{brg} & k_{y\theta_z p}^{brg} \\ k_{zxp}^{brg} & k_{zyp}^{brg} & k_{zzp}^{brg} & k_{z\theta_x p}^{brg} & k_{z\theta_y p}^{brg} & k_{z\theta_z p}^{brg} \\ k_{\theta_x xp}^{brg} & k_{\theta_x yp}^{brg} & k_{\theta_x zp}^{brg} & k_{\theta_x\theta_x p}^{brg} & k_{\theta_x\theta_y p}^{brg} & k_{\theta_x\theta_z p}^{brg} \\ k_{\theta_y xp}^{brg} & k_{\theta_y yp}^{brg} & k_{\theta_y zp}^{brg} & k_{\theta_y\theta_x p}^{brg} & k_{\theta_y\theta_y p}^{brg} & k_{\theta_y\theta_z p}^{brg} \\ k_{\theta_z xp}^{brg} & k_{\theta_z yp}^{brg} & k_{\theta_z zp}^{brg} & k_{\theta_z\theta_x p}^{brg} & k_{\theta_z\theta_y p}^{brg} & k_{\theta_z\theta_z p}^{brg} \end{bmatrix} \tag{3.14}$$

$$C_p^{brg} = \begin{bmatrix} c_{xxp}^{brg} & c_{xyp}^{brg} & c_{xzp}^{brg} & c_{x\theta_x p}^{brg} & c_{x\theta_y p}^{brg} & c_{x\theta_z p}^{brg} \\ c_{yxp}^{brg} & c_{yyp}^{brg} & c_{yzp}^{brg} & c_{y\theta_x p}^{brg} & c_{y\theta_y p}^{brg} & c_{y\theta_z p}^{brg} \\ c_{zxp}^{brg} & c_{zyp}^{brg} & c_{zzp}^{brg} & c_{z\theta_x p}^{brg} & c_{z\theta_y p}^{brg} & c_{z\theta_z p}^{brg} \\ c_{\theta_x xp}^{brg} & c_{\theta_x yp}^{brg} & c_{\theta_x zp}^{brg} & c_{\theta_x\theta_x p}^{brg} & c_{\theta_x\theta_y p}^{brg} & c_{\theta_x\theta_z p}^{brg} \\ c_{\theta_y xp}^{brg} & c_{\theta_y yp}^{brg} & c_{\theta_y zp}^{brg} & c_{\theta_y\theta_x p}^{brg} & c_{\theta_y\theta_y p}^{brg} & c_{\theta_y\theta_z p}^{brg} \\ c_{\theta_z xp}^{brg} & c_{\theta_z yp}^{brg} & c_{\theta_z zp}^{brg} & c_{\theta_z\theta_x p}^{brg} & c_{\theta_z\theta_y p}^{brg} & c_{\theta_z\theta_z p}^{brg} \end{bmatrix} \tag{3.15}$$

As it will be explained in the following sections, in case of complex rotor-to-structure connections, the elements of the previous matrices can be previously evaluated starting from more complex models (solid FEM,CFD) and then stored in look-up tables as function of the spin speed Ω or of the load N. The vectors $\mathbf{q}_{p1}^{brg}$ and $\mathbf{q}_{p2}^{brg}$ are the vectors describing the generalized coordinates of the connected nodes respectively on the rotor and on the structure:

$$\mathbf{q}_{p1}^{brg} = \begin{bmatrix} u_{p1}^{brg} & v_{p1}^{brg} & w_{p1}^{brg} & \theta_{xp1}^{brg} & \theta_{yp1}^{brg} & \theta_{zp1}^{brg} \end{bmatrix}^T \tag{3.16}$$

$$\mathbf{q}_{p2}^{brg} = \begin{bmatrix} u_{p2}^{brg} & v_{p2}^{brg} & w_{p2}^{brg} & \theta_{xp2}^{brg} & \theta_{yp2}^{brg} & \theta_{zp2}^{brg} \end{bmatrix}^T \tag{3.17}$$

Obviously, if the supporting structure is assumed to be rigid the $\mathbf{q}_{p2}^{brg}$ vector is set to zero.

The presented formulation is used to model through a practical and simple approach the dynamical characteristics of the most common bearing types.
It is worth noticing that the same modelling approach may be employed adopted also for seals [4, 9].

Non-standard components

The main feature of the Rotordynamical Model developed in the present research activity consists in its capability of modelling and investigating complex topology rotors through a general and systematic approach. Innovative models have been developed to characterise the dynamic behaviour of non-standard

components that cannot be reproduced with any classical rotordynamical element such as disks, shafts or concentrated elasto-damping elements. For instance, the model is particularly useful for the mathematical modelling of distributed rotors with complex rotor-to-shaft connections to accurately reproduce their contributions to the dynamical response of rotor systems or eventually, to consider moments and forces due to mechanical looseness or improper assembly in general.

Distributed elements may be adopted to correctly model elements characterised by more complex shaft-to-rotor multiple-points connections. Such elements have been developed to overcome modelling limitations relative to complex rotor with distributed inertias, that may affect the dynamical behaviour of the system with particular concern to the lateral-torsional.

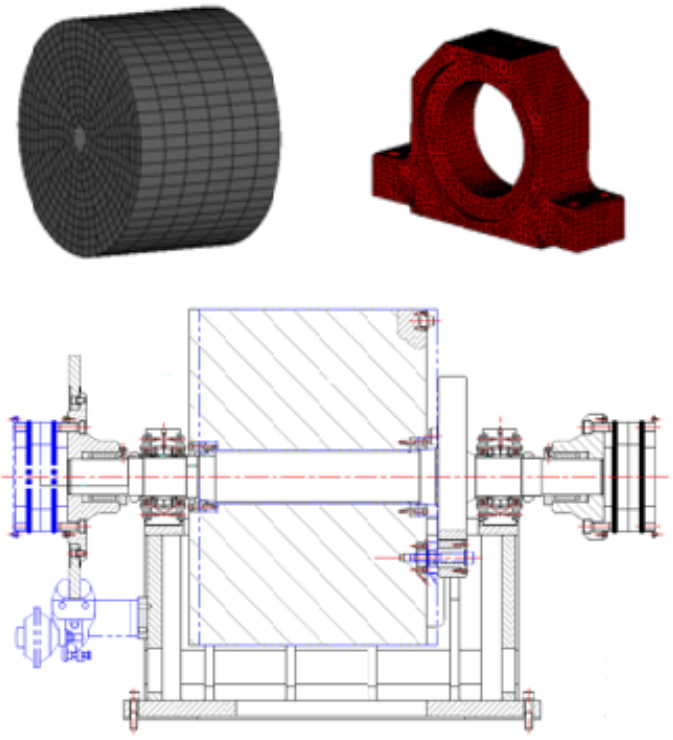

Fig. 3.8: Example of solid 3D elements to model complex components.

In the developed Rotordynamical Model shaft beam formulations may be employed to model in a general way massive elements to correctly reproduce their possible elastic effects on the rotor. Thus coaxial-rotors, particular mounted massive elements or distributed inertial components characterised by connections to shaft in multiple points (see Fig. 3.9) may be represented with a systematic approach with an high level of accuracy.

A distributed inertial element linked to the rotor by multi-point connections may be reproduced with classical beam or more advanced solid FE models connected to the rotor through general visco-elastic connections. The $p-th$ connection element is described by the interaction of the two connecting nodes,

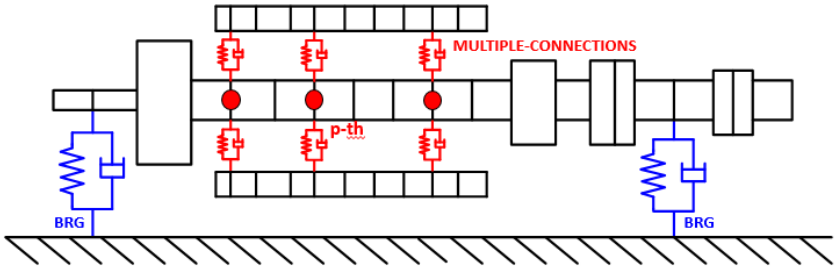

Fig. 3.9: Scheme of multi-point connections and distributed inertial element.

whose displacement vectors may be defined as:

$$\mathbf{q}_{p1}^{con} = \begin{bmatrix} u_{p1}^{con} & v_{p1}^{con} & w_{p1}^{con} & \theta_{p1}^{con} & \theta_{p1}^{con} & \theta_{p1}^{con} \end{bmatrix}^T \tag{3.18}$$

$$\mathbf{q}_{p2}^{con} = \begin{bmatrix} u_{p2}^{con} & v_{p2}^{con} & w_{p2}^{con} & \theta_{p2}^{con} & \theta_{p2}^{con} & \theta_{p2}^{con} \end{bmatrix}^T \tag{3.19}$$

where $\mathbf{q}_{p1}^{con}$ and $\mathbf{q}_{p2}^{con}$ are the connection nodes. The force acting between the two interconnected nodes may be evaluated as:

$$\mathbf{F}_p^{con} = K_p^{con}(N,\Omega)(\mathbf{q}_{p1}^{con} - \mathbf{q}_{p2}^{con}) + C_p^{con}(N,\Omega)(\dot{\mathbf{q}}_{p1}^{con} - \dot{\mathbf{q}}_{p2}^{con}) \tag{3.20}$$

where the matrices characterising the stiffness $K_p^{con}(N,\Omega)$ and damping $C_p^{con}(N,\Omega)$ properties of the $p-th$ connection element may depend on both the rotational regime (Ω) and the load (N) and their values are usually computed through previous more complex analysis, such as solid 3D or CFD analysis and then stored in look-up tables (LUT). The general expressions of the stiffness and damping matrices are:

$$K_p^{con} = \begin{bmatrix} k_{xxp}^{con} & k_{xyp}^{con} & k_{xzp}^{con} & k_{x\theta_x p}^{con} & k_{x\theta_y p}^{con} & k_{x\theta_z p}^{con} \\ k_{yxp}^{con} & k_{yyp}^{con} & k_{yzp}^{con} & k_{y\theta_x p}^{con} & k_{y\theta_y p}^{con} & k_{y\theta_z p}^{con} \\ k_{zxp}^{con} & k_{zyp}^{con} & k_{zzp}^{con} & k_{z\theta_x p}^{con} & k_{z\theta_y p}^{con} & k_{z\theta_z p}^{con} \\ k_{\theta_x xp}^{con} & k_{\theta_x yp}^{con} & k_{\theta_x zp}^{con} & k_{\theta_x\theta_x p}^{con} & k_{\theta_x\theta_y p}^{con} & k_{\theta_x\theta_z p}^{con} \\ k_{\theta_y xp}^{con} & k_{\theta_y yp}^{con} & k_{\theta_y zp}^{con} & k_{\theta_y\theta_x p}^{con} & k_{\theta_y\theta_y p}^{con} & k_{\theta_y\theta_z p}^{con} \\ k_{\theta_z xp}^{con} & k_{\theta_z yp}^{con} & k_{\theta_z zp}^{con} & k_{\theta_z\theta_x p}^{con} & k_{\theta_z\theta_y p}^{con} & k_{\theta_z\theta_z p}^{con} \end{bmatrix} \tag{3.21}$$

$$C_p^{con} = \begin{bmatrix} c_{xxp}^{con} & c_{xyp}^{con} & c_{xzp}^{con} & c_{x\theta_x p}^{con} & c_{x\theta_y p}^{con} & c_{x\theta_z p}^{con} \\ c_{yxp}^{con} & c_{yyp}^{con} & c_{yzp}^{con} & c_{y\theta_x p}^{con} & c_{y\theta_y p}^{con} & c_{y\theta_z p}^{con} \\ c_{zxp}^{con} & c_{zyp}^{con} & c_{zzp}^{con} & c_{z\theta_x p}^{con} & c_{z\theta_y p}^{con} & c_{z\theta_z p}^{con} \\ c_{\theta_x xp}^{con} & c_{\theta_x yp}^{con} & c_{\theta_x zp}^{con} & c_{\theta_x\theta_x p}^{con} & c_{\theta_x\theta_y p}^{con} & c_{\theta_x\theta_z p}^{con} \\ c_{\theta_y xp}^{con} & c_{\theta_y yp}^{con} & c_{\theta_y zp}^{con} & c_{\theta_y\theta_x p}^{con} & c_{\theta_y\theta_y p}^{con} & c_{\theta_y\theta_z p}^{con} \\ c_{\theta_z xp}^{con} & c_{\theta_z yp}^{con} & c_{\theta_z zp}^{con} & c_{\theta_z\theta_x p}^{con} & c_{\theta_z\theta_y p}^{con} & c_{\theta_z\theta_z p}^{con} \end{bmatrix} \tag{3.22}$$

Multi-rotor connections

In the Rotordynamical Model, the critical behaviour of multi-rotor layouts may be accurately studied. For sake of brevity, in the present work only coupling modelling is presented. A coupling is a device used to connect two shafts

together at their ends for the purpose of transmitting power. Couplings do not normally allow disconnection of shafts during operation, however there are torque limiting couplings which can slip or disconnect when some torque limit is exceeded.

Two main types of couplings are used in rotordynamics: *rigid* and *flexible*. Actually true *rigid* couplings do not exist on rotating machinery because all components exhibit a certain degree of flexibility, anyway the term *rigid* may be referred to those couplings designed when precise shaft alignment is required. Rigid couplings, shown in Fig. 3.10(a), are formed of two coupling halves connected by means of a set of bolts placed on a bolt circle diameter. Each coupling half may be realized as an integral part of the rotor end to be connected or it may be mounted onto the shaft through shrink-fit or keys.

(a) (b) (c)

Fig. 3.10: Types of coupling used in rotating machinery (a): rigid coupling (b): diaphragm flexible coupling (c): pin flexible coupling .

Some rotating machines exhibit substantial variations in the alignment passing from cold stand-still conditions to hot operating conditions thus requiring the adoption of flexible coupling to compensate a certain level of misalignment (radial, angular or axial) and to reduce the transmission of bending moments to minimize shaft bending stress and lateral vibration stability problems. Therefore, flexible couplings are adopted to introduce some features to produce a controlled amount of flexibility or damping in *multi-rotor* configurations to accommodate misalignment between centerlines of machine during operation, vibrations and shocks and axial loads.

Several types of couplings exist, such as diaphragm (illustrated in Fig. 3.10(b)), elastomeric, pin (see Fig. 3.10(c)), gear and disk coupling. The type to be selected for a certain application is chosen mainly depending on the rotational speed and the magnitude of steady-state or transient torque to be transmitted. Other important features for the selection of flexible couplings are represented by the required values of lateral and torsional, linear or nonlinear, stiffness and damping properties and also by the inertia and mass values of the coupling.

In standard uncoupled torsional models, the dynamical properties of couplings are usually taken into account as equivalent concentrated mass and inertia and with the corresponding torsional stiffness values that are provided by the coupling manufacturer.

In lateral analysis, ideally, couplings should have critical speeds much higher than the machine ones, thus resulting in a minor influence on the critical behaviour of machine. However, in some cases, the mass of the coupling halves

may represent a not negligible percentage of the total machine mass value, thus requiring an accurate modelling of such components to correctly predict the vibration behaviour of the investigated system. To this purposes couplings lateral models have been proposed in literature [21, 39] in the past. Due to the necessity of improving the accuracy of rotordynamical studies to predict critical speeds, also more accurate models of coupling are currently being developed to understand the influence of misalignment on the critical behaviour of rotating systems. Misalignment is the second most common malfunction cause in rotors (after unbalance) [10, 19, 75] and rotors often exhibit some residual misalignment even after they have been subjected to alignment operations. Furthermore, shaft misalignments may appear after continuous operating due to foundation movements or thermal heatings. Thus, such as unbalance, misalignment represents a prevailing malfunction cause in rotor dynamic systems and appropriate models are required to take into account couplings flexibility in rotordynamics studies and for understanding the coupling influence on the system, a correct estimation of the forces and the lateral moments generated in the coupling due to shaft misalignment is required. Couplings are critical elements also from the lateral-torsional coupling standpoint. Nowadays, several works may be found in literature describing accurate and innovative coupling models [19, 75]. In the Rotordynamical Model, couplings can be modelled according to three different formulations. The first one is the more general and it is based on an extended visco-elastic formulation. The displacement vectors of the two interconnected nodes of the generic $r-th$ flexible coupling model (Fig. 3.11) are:

$$\mathbf{q}_{r1}^{cplg} = \begin{bmatrix} u_{r1}^{cplg} & v_{r1}^{cplg} & w_{r1}^{cplg} & \theta_{r1}^{cplg} & \theta_{r1}^{cplg} & \theta_{r1}^{cplg} \end{bmatrix}^T \tag{3.23}$$

$$\mathbf{q}_{r2}^{cplg} = \begin{bmatrix} u_{r2}^{cplg} & v_{r2}^{cplg} & w_{r2}^{cplg} & \theta_{r2}^{cplg} & \theta_{r2}^{cplg} & \theta_{r2}^{cplg} \end{bmatrix}^T \tag{3.24}$$

and the force acting on the interconnected nodes may be evaluated as:

$$\mathbf{F}_p^{cplg}(N,\Omega) = K_p^{cplg}(N,\Omega)(\mathbf{q}_{r1}^{cplg} - \mathbf{q}_{r2}^{cplg}) + C_p^{cplg}(N,\Omega)(\dot{\mathbf{q}}_{r1}^{cplg} - \dot{\mathbf{q}}_{r2}^{cplg}) \tag{3.25}$$

where the matrices of stiffness $K_p^{cplg}(N,\Omega)$ and damping $C_p^{cplg}(N,\Omega)$ properties of the couplings depends both on the rotational regime (Ω) and the on load (N).

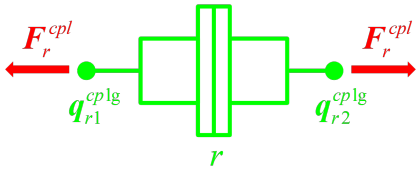

Fig. 3.11: Coupling element.

The extended stiffness and damping matrices are:

$$K_r^{cplg} = \begin{bmatrix} k_{xxp}^{cplg} & k_{xyp}^{cplg} & k_{xzp}^{cplg} & k_{x\theta_x p}^{cplg} & k_{x\theta_y p}^{cplg} & k_{x\theta_z p}^{cplg} \\ k_{yxp}^{cplg} & k_{yyp}^{cplg} & k_{yzp}^{cplg} & k_{y\theta_x p}^{cplg} & k_{y\theta_y p}^{cplg} & k_{y\theta_z p}^{cplg} \\ k_{zxp}^{cplg} & k_{zyp}^{cplg} & k_{zzp}^{cplg} & k_{z\theta_x p}^{cplg} & k_{z\theta_y p}^{cplg} & k_{z\theta_z p}^{cplg} \\ k_{\theta_x xp}^{cplg} & k_{\theta_x yp}^{cplg} & k_{\theta_x zp}^{cplg} & k_{\theta_x\theta_x p}^{cplg} & k_{\theta_x\theta_y p}^{cplg} & k_{\theta_x\theta_z p}^{cplg} \\ k_{\theta_y xp}^{cplg} & k_{\theta_y yp}^{cplg} & k_{\theta_y zp}^{cplg} & k_{\theta_y\theta_x p}^{cplg} & k_{\theta_y\theta_y p}^{cplg} & k_{\theta_y\theta_z p}^{cplg} \\ k_{\theta_z xp}^{cplg} & k_{\theta_z yp}^{cplg} & k_{\theta_z zp}^{cplg} & k_{\theta_z\theta_x p}^{cplg} & k_{\theta_z\theta_y p}^{cplg} & k_{\theta_z\theta_z p}^{cplg} \end{bmatrix} \tag{3.26}$$

$$C_r^{cplg} = \begin{bmatrix} c_{xxp}^{cplg} & c_{xyp}^{cplg} & c_{xzp}^{cplg} & c_{x\theta_x p}^{cplg} & c_{x\theta_y p}^{cplg} & c_{x\theta_z p}^{cplg} \\ c_{yxp}^{cplg} & c_{yyp}^{cplg} & c_{yzp}^{cplg} & c_{y\theta_x p}^{cplg} & c_{y\theta_y p}^{cplg} & c_{y\theta_z p}^{cplg} \\ c_{zxp}^{cplg} & c_{zyp}^{cplg} & c_{zzp}^{cplg} & c_{z\theta_x p}^{cplg} & c_{z\theta_y p}^{cplg} & c_{z\theta_z p}^{cplg} \\ c_{\theta_x xp}^{cplg} & c_{\theta_x yp}^{cplg} & c_{\theta_x zp}^{cplg} & c_{\theta_x\theta_x p}^{cplg} & c_{\theta_x\theta_y p}^{cplg} & c_{\theta_x\theta_z p}^{cplg} \\ c_{\theta_y xp}^{cplg} & c_{\theta_y yp}^{cplg} & c_{\theta_y zp}^{cplg} & c_{\theta_y\theta_x p}^{cplg} & c_{\theta_y\theta_y p}^{cplg} & c_{\theta_y\theta_z p}^{cplg} \\ c_{\theta_z xp}^{cplg} & c_{\theta_z yp}^{cplg} & c_{\theta_z zp}^{cplg} & c_{\theta_z\theta_x p}^{cplg} & c_{\theta_z\theta_y p}^{cplg} & c_{\theta_z\theta_z p}^{cplg} \end{bmatrix} \tag{3.27}$$

The second approach is based on the adoption of general ordinary differential equations (ODE) describing the dynamics of rigid parts of the couplings and interacting with the rotor FE model through load connections. Such formulations are particularly useful when nonlinear couplings characteristics must be taken into account in transient analysis. For flexible-couplings it can be written:

$$M_r^{cpl}\ddot{\mathbf{q}}_r^{cpl} + C_r^{cpl}\dot{\mathbf{q}}_r^{cpl} + K_r^{cpl}\mathbf{q}_r^{cpl} = \mathbf{F}_{r1}^{cpl} + \mathbf{F}_{r2}^{cpl} \tag{3.28}$$

where $M_r^{cpl} C_r^{cpl} K_r^{cpl} \in \Re^{6\times 6}$ and $\mathbf{F}_{r1}$ and $\mathbf{F}_{r1}$ are the load connections to the rotor FE model.

The third approach consists in using an equivalent shaft element, the material and geometrical properties of which are set to represent the equivalent torsional and bending stiffness properties of the coupling.

Assembly of the equations of motion

The general form of the equation of motion for the complete discretised rotor system can be formulated in matrix form as:

$$M\ddot{\mathbf{q}} + (C + \Omega G)\dot{\mathbf{q}} + K\mathbf{q} = \mathbf{F} \tag{3.29}$$

where M is the assembled mass matrix, G is the gyroscopic matrix, C and K represent respectively the damping and stiffness matrices of the considered system. $\mathbf{q}$ is the displacement and rotation vector of the nodes of the model ($\mathbf{q} \in \mathbb{R}^{6\cdot n_{tot}}$, with n_{tot} number of nodes of the analysed model) describing the position of each node of the discretised system, $\mathbf{F}$ is the applied load vector.

The Rotordynamical Model may be adopted to study the phenomenon of interaction between lateral and torsional vibrations in rotor systems. This can be reached thanks to finite element formulation that may vary in the number of degrees of freedom associated to each node. More specifically classical uncoupled finite element models (4 dofs for uncoupled lateral dynamics and 1 dof for torsional models) can be easily derived from the developed fully coupled lateral-torsional 6 dofs model. Hence, the proposed model may be employed to

evaluate the improvement and benefit of fully coupled model with respect to the classical uncoupled ones.

A number of different types of analyses can be performed starting from the previous equation: the prediction of critical speeds, harmonic response and transient analysis. The rotordynamical studies that can be performed through the developed model are briefly introduced in the following section.

3.4 The Rotordynamics Analysis

The third part of the general architecture, the *Rotordynamics analysis*, is the module responsible for the post-processing (i.e. the outputs of the Rotordynamical Model). The *Rotordynamics analysis* module has been implemented in the Matlab environment.

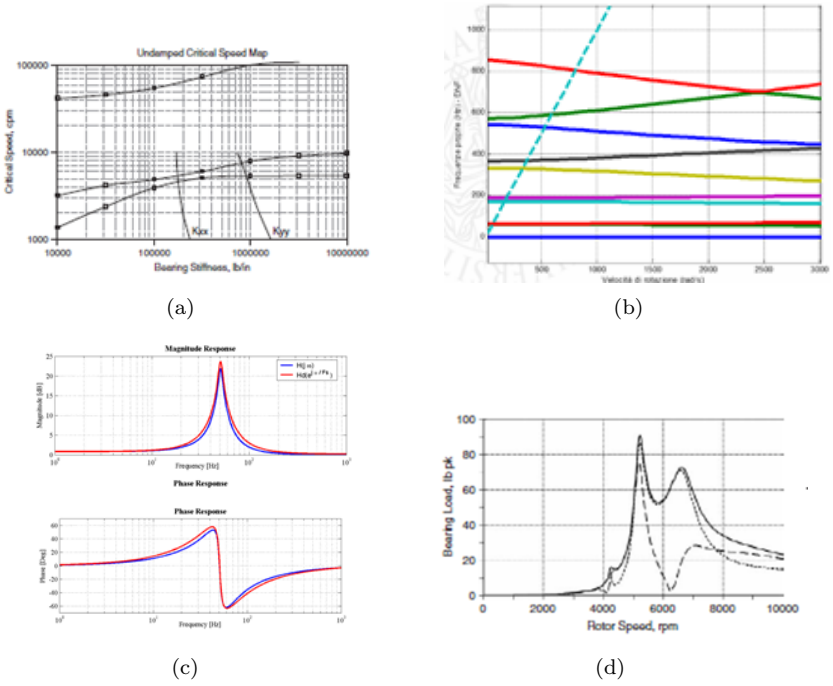

Fig. 3.12: Rotordynamics analysis (a): Undamped Critical Speed UCS (b): Damped Critical Speed DCS (c): Forced Response (d) Transient analysis.

The specific output of each feasible analysis can be assessed and the typical results are automatically generated. The analysis (Fig. 3.12) that can be easily performed are:

- *Undamped Critical Speed UCS* is performed to study how the critical speeds of a specified machine layout may vary w.r.t design parameters. For instance, this kind of analysis can be used for the selection of bearings to reach a good rotordynamics behaviour.

- *Damped Critical Speed DCS* that allows the Campbell's plot to be defined

and the evaluation of the lateral and torsional natural frequencies of the studied rotor;

- *Forced Response* to assess the amplitudes of synchronous, sub-synchronous and super-synchronous vibration caused by the rotor unbalance or other harmonic forcing functions;
- *Transient analysis* to study nonlinear or local effects can be performed.

3.5 Numerical validation

The Rotordynamical Model presented in this thesis has been specifically developed with the aim of modelling and investigating the dynamical behaviour of real complex machines. Before applying the model to experimental test-cases, it has been preliminary validated through the analysis of a numerical benchmark rotor. This kind of approach is a fundamental aspect and good practice in most of engineering research study, where software and experimental validation of theoretic studies are necessary for understanding both performance and limits of the research outputs.

In this section the numerical validation [76] is presented. The numerical validation has been performed considering two benchmark theoretical rotors described in [4, 9]. Friswell *et al.* developed a rotordynamical model for uncoupled lateral analysis based on a FE formulation characterised by 3D Timoshenko beams with 4 dofs per node. This model has been implemented in the MatLab enviroment. The capabilities of the model are extensively investigated in [9] through several rotor applications and one of those has been adopted for the numerical comparison of the model developed in the present thesis with the reference Friswell's model.

The investigated rotor-bearing system consists of a 1.5 m long shaft, shown in Fig. 3.13 , with a constant diameter of 0.05 m. Two disks are placed at the shaft locations 0.5 m and 1.0 m from the shaft extremity.

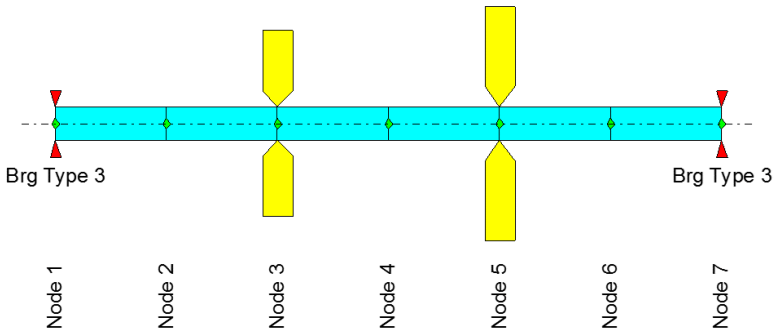

Fig. 3.13: Scheme of the two-disk, two-bearings rotor.

The first disk is 0.07 m thick with a diameter of a 0.28 m while the second has the same thickness values and a diameter of 0.35 m. Concerning shaft material properties, Young's E and tangential G modulus are respectively equal 211 GN/m^2 and 81.2 GN/m^2. No internal shaft damping has been considered

and for both the shaft and disks, the density ρ is equal to $7810\,\mathrm{kg/m^3}$. The response of the system at the disks due to an unbalance on the left disk equal to $0.001\,\mathrm{kg\,m}$ has been computed in two cases:

- *Case A*: isotropic bearings with stiffness values equal to $1\,\mathrm{MN/m}$ in both the lateral directions;
- *Case B*: anisotropic bearings with different stiffness values in the two lateral directions, respectively equal to $1\,\mathrm{MN/m}$ and $0.8\,\mathrm{MN/m}$.

The critical speed map and the harmonic response of the investigated rotor have been computed both with the Friswell's model through the Rotor Software V1 implemented in the Matlab environment and with the Rotordynamical Model developed in this thesis and implemented through the Comsol with Matlab environment. The following figures show that the results of the Rotordynamical Model match those computed through the Friswell's model in both cases. For sake of brevity, a subset of the available results of the two models are shown. These results represent a preliminary validation step of the model in the case of simple rotor system and for uncoupled lateral analysis. Extended analysis and extensive investigation are further required to validate the Rotordynamical Model application for real machine applications.

Case A

The modal response of the Friswell's model and of the Rotordynamical Model developed in this work are respectively illustrated in Fig. 3.14(a) and Fig. 3.14(b). The Campbell's plot shows a good agreement of the two models in calculating the modal response of the considered rotor (case A) in the entire operational regime.

Tab. 3.1: Case A - Isotropic rotor: Numerical Damped Natural Frequencies (Hz) at 0 and 3000 rpm.

	Friswell's model	Rotordynamical Model
0 rpm	13.79	13.79
	43.66	43.66
	43.66	43.66
3000 rpm	13.64	13.65
	13.93	13.93
	41.00	40.99
	46.13	46.13

Figs. 3.15 and 3.16 show that the Friswell's model and the Rotordynamical Model results are quite the same also concerning mode shapes determination.

Case B

Analogous considerations hold also for the anisotropic case (Case B). In this case the modal response of the Friswell's model and of the Rotordynamical model developed in this work are respectively illustrated in Fig. 3.17(a) and

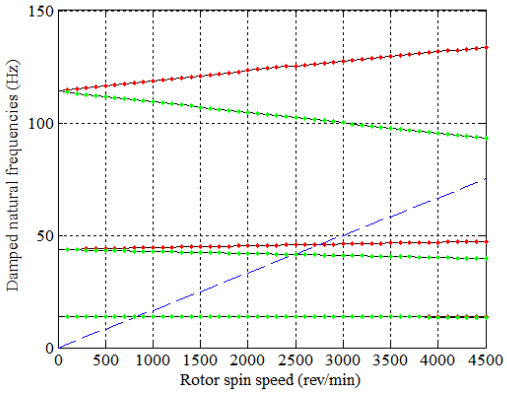

(a)

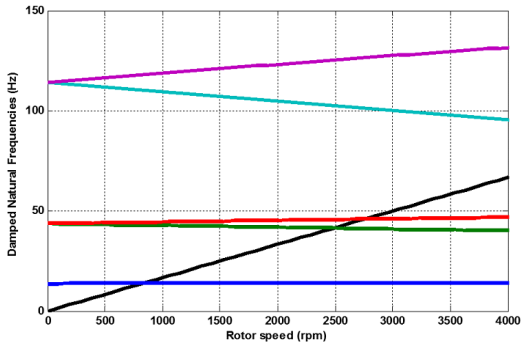

(b)

Fig. 3.14: Case A - Isotropic rotor: Campbell's plot (a): Friswell's model (b): Rotordynamical Model.

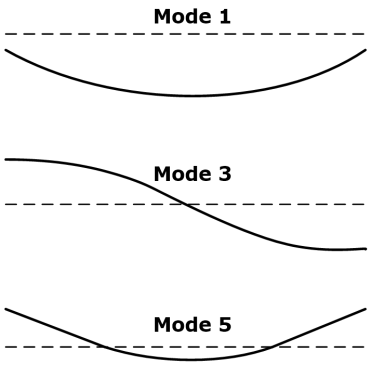

Fig. 3.15: Mode shapes in the yz plane at 0 rpm (Friswell's model).

.

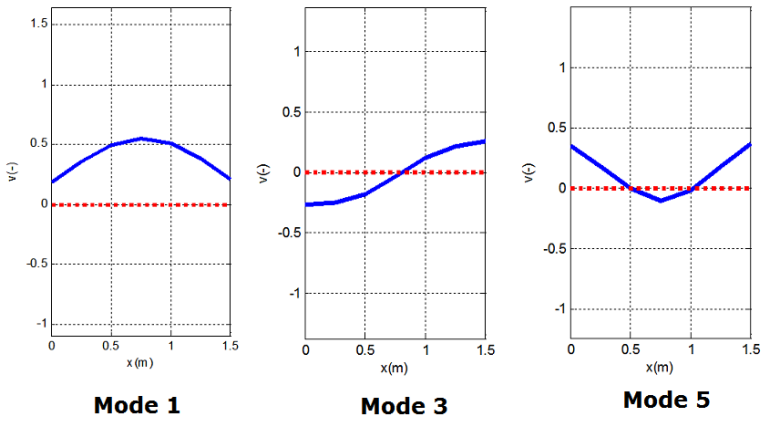

Fig. 3.16: Mode shapes in the xy plane at 0 rpm (Rotordynamical Model).

Fig. 3.17(b) where the Campbell's plots show good agreement of the two models in calculating the modal response of the considered rotor (case B) in the entire operational regime.

Tab. 3.2: Case B - Anisotropic rotor: Numerical Damped Natural Frequencies (Hz) at 0 and 3000 rpm.

	Friswell's model	Rotordynamical Model
0 rpm	13.15	13.15
	13.79	13.79
	40.51	40.51
	43.66	43.66
3000 rpm	13.12	13.12
	13.81	13.81
	38.96	38.98
	45.01	45.01

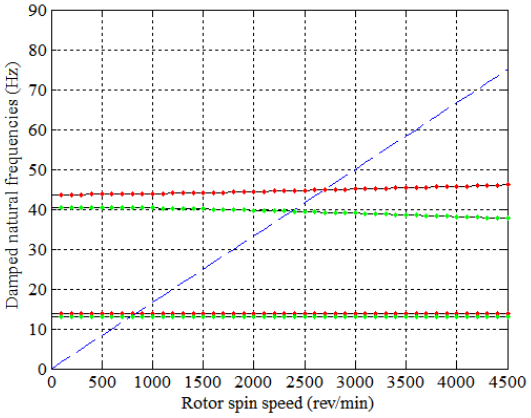

(a)

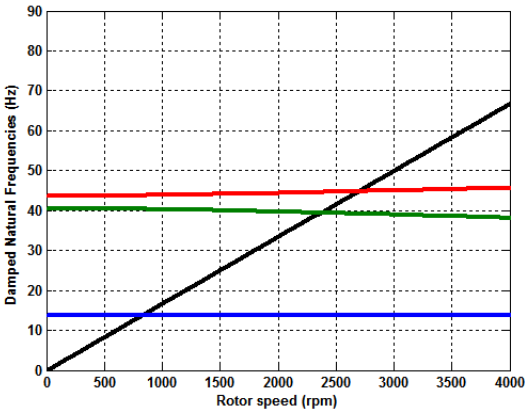

(b)

Fig. 3.17: Case B: Campbell's plot (a): Friswell's model (b): Rotordynamical Model.

Chapter 4

Test-case description

The rotor test-case studied in this work is a dynamometric flywheel test bench, designed for the acceptance tests of railway brake components. Thanks to different testing equipments both brake disks and brake shoes can be tested. The chosen case study presents several distributed inertial elements characterised by a multi-point connection inducing complex dynamical behaviours that are difficult to be investigated and predicted (especially in terms of later-torsional vibrations). During the verification tests performed in the acceptance phase the test bench exhibited some unpredicted vibrations phenomena.

4.1 Machine description

Dynamometric flywheel test bench are designed for the acceptance testing of railway brake components. The layout of such kind of machine must fulfill specific requirements that are provided in the ERRI B126/RP 18 report [77] that defines the general features and the approval tests for the validation of railway brake test-benches. To this aim, dynamometric test-benches are usually formed of a solid baseplate on which are mounted several movable flywheels, which, when appropriately combined, simulate the inertia of railways vehicles. Electrical motors are used to drive the flywheels up to the speed values required by the test cycles [78, 79, 80, 77]. In the opposite side of the shaft linking the motor to the flywheels, the mechanical and hydraulic components constituting the brake system to test are mounted by means of dedicated mechanical interfaces. Railway brake elements that can be tested are: brake disk, brake caliper and pads or wheel and brake blocks.

During the tests, brake components must dissipate the relative quota of the total kinetic energy characterising a single vehicle according to the railway standards [78, 79, 80, 77].
To this aim a dedicated test-bench has been built through a collaboration of RFI (Rete Ferroviaria Italiana) and Simpro S.P.A. To produce the required amount of energy the investigated test-bench is composed of a group of shafts, sustained by rolling bearings and linked each other through flexible couplings and driven by an electrical motor, and of five movable flywheel masses, which are used during tests to vary the simulated mass of vehicle.

Fig. 4.3 shows a scheme of the studied rotor. The whole train is formed of six

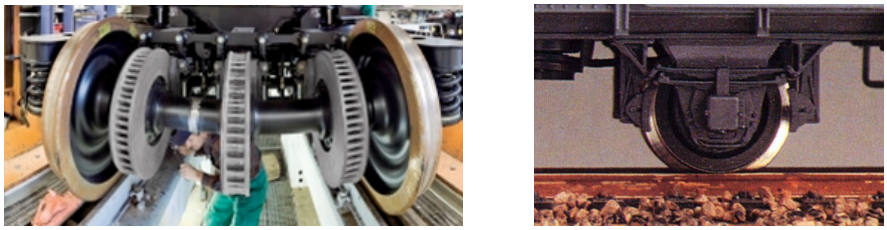

(a) (b)

Fig. 4.1: Railway braking systems (a): disk brake (b): block brake.

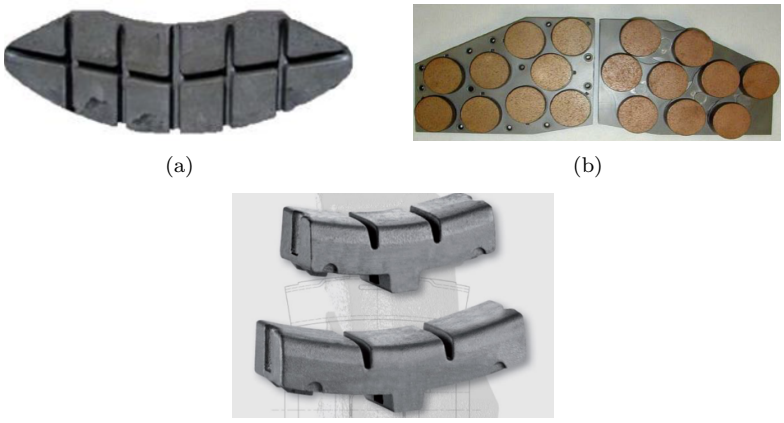

(a) (b)

(c)

Fig. 4.2: Brake pad types (a): organic pads (b): sintered pads (c): organic blocks.

parts linked by means of flexible couplings: the electrical motor group driving the train, the brake group supporting the disk brake to be tested and the four flywheel-shaft groups (denoted with the acronyms $K1$, $K2$, $K3$ and $K4-5$).

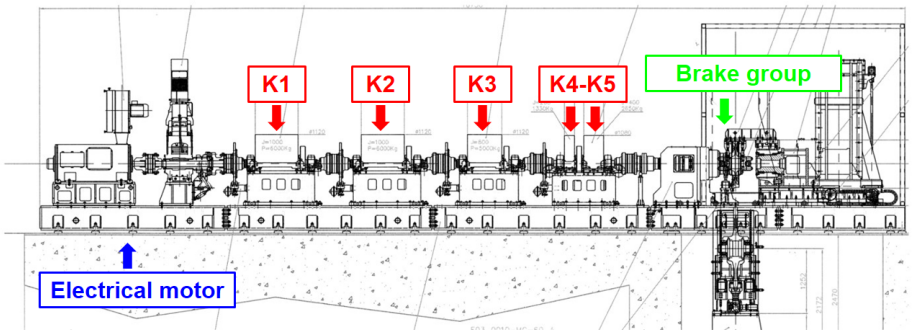

Fig. 4.3: View of the dynamometric flywheel test bench.

4.2 Motor group

The Motor group (MG) consists in the electrical motor driving the shaft line is a 500 kW asynchronous three-phases motor, which has been designed for this particular application. The maximum rotating speed of the motor is 3000 rpm, corresponding to a translational velocity equal to 500 km/h for vehicles with wheels characterised by a diameter equal to 890 mm.

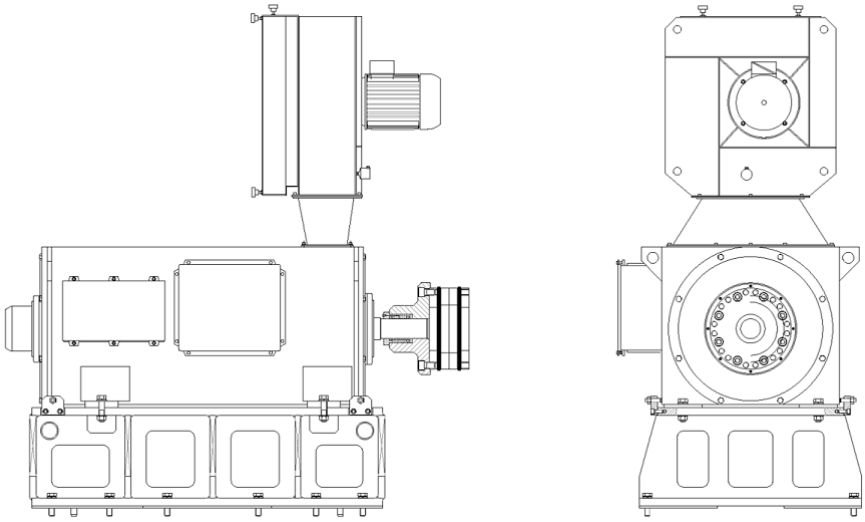

Fig. 4.4: Motor group.

The motor is equipped with an encoder to measure the rotational regimes and it may be controlled both in speed and torque (that is instantaneously measured), getting also the functionality of inertia simulator. This capability is

required to compensate the brake inertia when the mechanical inertia (provided by the combination of the flywheels) cannot exactly represent the brake mass value defined in the testing provision imposed by the reference standards [78, 79, 80, 77].

4.3 Flywheel-shaft groups

The part of the studied test-case responsible for the simulation of the mechanical inertia is based on a modular architecture, formed of four flywheel-groups, conventionally named K1, K2, K3 and K4 (see Fig. 4.3). The four modules present a similar geometrical layout and differ each other for the inertial properties. More specifically, the K1 and K2 groups are identical; the K3 module is characterised by the same layout but it exhibits different inertial values. The architecture of the K4 group is slightly different from the other ones since it carries on two flywheels (conventionally named K4-200 and K4-400). The total number N_{tot} of flywheel is five, thus allowing $2^{N_{tot}} = 32$ possible combinations of the simulated inertia.

The inertial properties of the five flywheels are listed in Tab. 4.1. As it can be seen from Tab. 4.1, since the shaft inertia is equal to $200\,\mathrm{kg\,m^2}$, the total mechanical inertia that can be simulated by the test bench is equal to $3600\,\mathrm{kg\,m^2}$.

Tab. 4.1: Mechanical inertia of the test bench.

Group name	**Rotatory Inertia** ($\mathrm{kg\,m^2}$)	**Total mass** (kg)
Shaft K0	200	2200
Flywheel K1	1000	6000
Flywheel K2	1000	6000
Flywheel K3	800	5000
Flywheel K4-200	200	1330
Flywheel K4-400	400	1650
Total	3600	19980

The layout of a flywheel-shaft group, which is illustrated in Fig. 4.6, is composed of:

- a steel forged flywheel;
- a steel transmission shaft with an in-built disk used to engage the corresponding flywheel;
- an emergency disk-brake operated by a fail-safe brake caliper;
- a manual locking system that allows the flywheel engagement on the shaft;
- two self-aligning roller bearings;
- a baseplate supporting the flywheel when it is not used for brake tests.

The flywheel is the element responsible for the simulation of the mechanical inertia. Each flywheel is made in steel through forging operations. The transmission shaft is realized in steel and it carries on an integral disk adopted to engage the flywheel when it is in the mounted position.

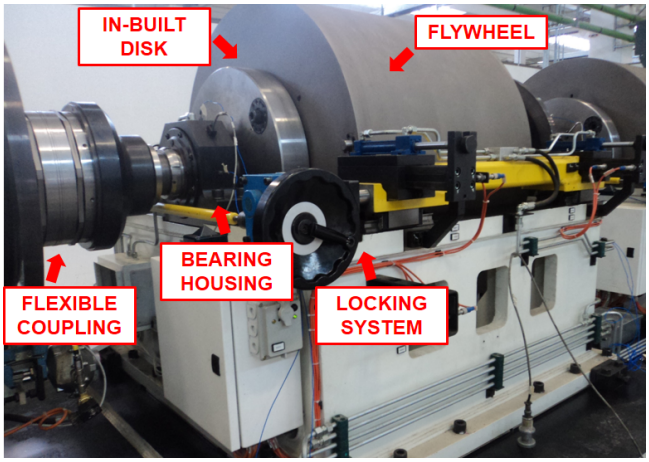

Fig. 4.5: The K2 flywheel-shaft group.

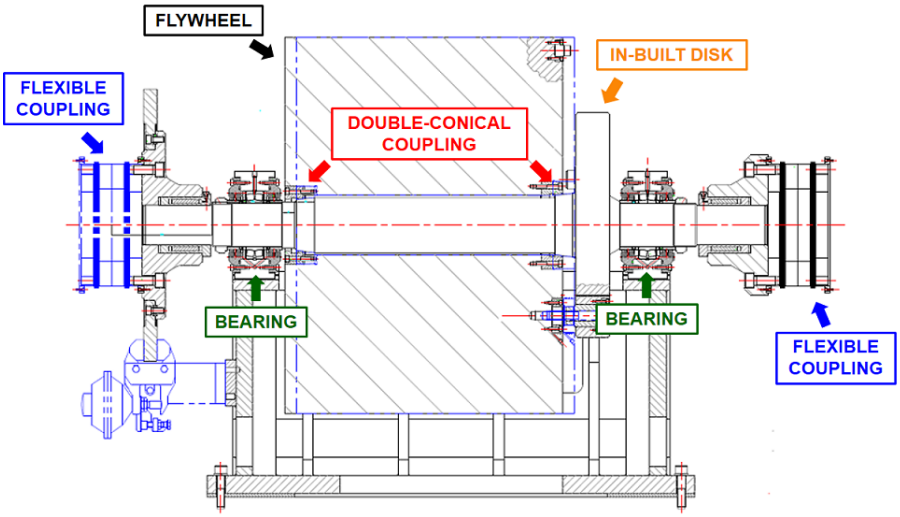

Fig. 4.6: Layout of the K1 and K2 flywheel-shaft group.

An appropriate manual locking device (see Fig. 4.5) is used to engage the flywheel to the shaft, allowing the modification of the mechanical inertia simulated during the test. Such manual device allows the engagement/disengagement of the flywheel with its relative shaft, through the flywheel axial translation. When the flywheel is translated to the engagement position (represented with the blue line in Fig. 4.6), it is axially coupled with its supporting shaft by means of a double-conical coupling. The rotational locking to the shaft is then assured by fastening the flywheel to the in-built disk by means of three screws. The flywheel represents a distributed inertial elements with several shaft-to-rotor point connections, thus defining a complex topology rotor system. This kind of elements are difficult to be described and their mathematical modelling requires the complete definition of stiffness $[K]$ and damping $[C]$ properties of the geometrical coupling. Stiffness properties have been evaluated through an appropriate 3D FE model of the considered components.

When the flywheel is disengaged (black line in Fig. 4.6) from the shaft it does not contribute to the simulated inertia and it is sustained by an appropriate steel structure. The main geometrical and inertial property of the K1 module are listed in Tab. 4.2.

Tab. 4.2: Main features of the K1 module.

Shaft diameter	165 mm
Flywheel external diameter	1120 mm
Flywheel inertia	1000 kg m^2
Axial distance between bearing locations	1173 mm
In-built disk diameter	670 mm
Static load acting on bearing DE	32.6 kN
Static load acting on bearing NDE	26.1 kN

The critical aspects of the particular flywheel-shaft coupling mechanism are the static indetermination of the coupling itself and the high distance between the two contact surfaces. Due to these issues a correct identification of the real contact points/surfaces between the flywheel and the shaft is very difficult. Hence, the action distribution between the two contact surfaces cannot be identified and large uncertainties on the influence of dynamical properties of the flywheels during the transient operating conditions arise This is a common problem that must be overcome for the study of distributed rotor elements.

It must be noticed that, due to the above-mentioned issues the dynamical analysis of the present test-case by means of classical models may lead to inaccurate results. More specifically, in the current application the classical assumptions made on the active surfaces do not hold, thus classical disk models cannot be employed to reproduce the flywheel dynamical behaviour and the introduction of distributed inertial elements is required.

The two ends of each flywheel-shaft module are supported on two identical self-aligning spherical roller bearings. These bearings are formed of a double-row roller bearings, a shared spherical outer ring raceway and two inner grooves. The center of the external groove sphere is located on axis of the bearing, enabling the inner ring and the rolling element set to make angular motions. Hence, this kind of bearing are self-aligning and insensitive to shaft misalignment due for example by the shaft deflection [81]. Self-aligning bearings have been adopted

to accommodate radial as well as thrust loads. Bearings may be mathematically modelled in rotor dynamics application either as ideal boundary condition for the shafts or as dynamic stiffness and damping elements [4]. In the latter case, the dynamical properties of bearings, characterised by the manufacturers through experimental setup or by means of dedicated simulation tools, must be known to achieve accurate rotor dynamics analysis results. A typical characteristic of a rolling element bearing is a high stiffness depending on the load [82], while they usually exhibit a very low damping. Furthermore, stiffness and damping values are almost constant for varying rotating speeds and exciting frequencies. Dynamical properties of the self-aligning spherical roller bearings adopted in the present test-case, have been provided by the bearing manufacturer according to the static load acting on them in the different configurations of the machine. It must be noticed that the stiffness values of the bearings are related to the static loads acting on them. Hence, in the investigated test-case, these values may vary according to the machine configuration. Stiffness properties relative to the K0 configuration (nominal load configuration wherein the total test inertia is given by the shaft inertia and none of the flywheels is mounted on the shaft-line) are listed in Tab. 4.3 where directions are defined according to the reference system shown in Fig. 4.7a and DE and NDE acronyms refer indicate respectively the motor (Drive End) and the brake-disk (Non Drive End) group side of each shaft-group. It must be noticed that for self-aligning rolling bearing only direct stiffness values (k_{xx}, k_{yy}, k_{zz}) exhibit significant values, while the indirect terms of the stiffness matrix are equal to zero. The listed values are the nominal ones, evaluated considering nominal loads acting on the bearings when none of the flywheel is engaged to the rotor shaft. Stiffness characteristics vary according to loads and rolling speed. In the present case the adoption of roller bearings set these features almost independent from the rolling speed [82].

Tab. 4.3: Bearings characteristics of the flywheel groups in nominal conditions.

Group	k_{xx} (N/m)	k_{yy} (N/m)	k_{zz} (N/m)
K1 DE	$9.5 \cdot 10^7$	$8.4 \cdot 10^8$	$3.3 \cdot 10^9$
K1 NDE	$9.5 \cdot 10^7$	$8.4 \cdot 10^8$	$3.3 \cdot 10^9$
K2 DE	$9.5 \cdot 10^7$	$8.4 \cdot 10^8$	$3.3 \cdot 10^9$
K2 NDE	$9.5 \cdot 10^7$	$8.4 \cdot 10^8$	$3.3 \cdot 10^9$
K3 DE	$9.5 \cdot 10^7$	$8.4 \cdot 10^8$	$3.3 \cdot 10^9$
K3 NDE	$7.9 \cdot 10^7$	$2.8 \cdot 10^8$	$6.9 \cdot 10^8$
K4 DE	$7.9 \cdot 10^7$	$2.8 \cdot 10^8$	$6.9 \cdot 10^8$
K4 NDE	$7.9 \cdot 10^7$	$2.8 \cdot 10^8$	$6.9 \cdot 10^8$

The data of the two bearings supporting the motor group and of the three bearings of the brake group are shown in Tab. 4.4.

In multi-rotor configurations flexible couplings are elements that transmit torque between two shafts, while compensating residual misalignments and minimizing their effect on the vibration response. Misalignment is accepted as the second most observed disturbance factor in rotating equipments [10, 19] and rotors often exhibit some residual misalignment even after they have been subjected to alignment operations. Furthermore, shaft misalignments may appear after continuous operating due to foundation movements or thermal heatings. Thus, such as unbalance, misalignment represents a prevailing malfunction cause

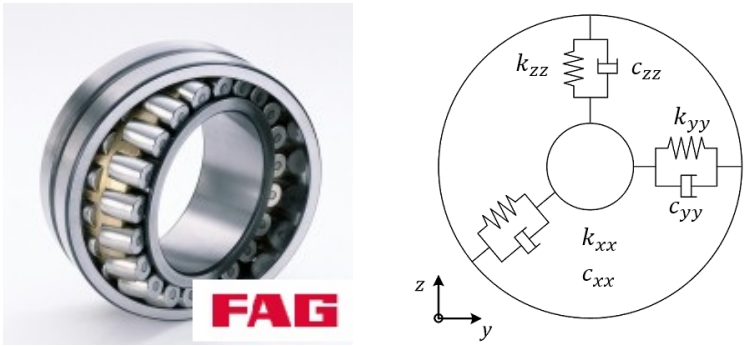

(a) (b)

Fig. 4.7: Self-aligning spherical rolling contact bearings (a): photo (b): rotor-dynamical scheme.

Tab. 4.4: Motor group and Brake group bearings characteristics.

Group	k_{xx} (N/m)	k_{yy} (N/m)	k_{zz} (N/m)
MG DE	$9.5 \cdot 10^7$	$8.4 \cdot 10^8$	$3.3 \cdot 10^9$
MG NDE	$9.5 \cdot 10^7$	$8.4 \cdot 10^8$	$3.3 \cdot 10^9$
BG 1	$9.5 \cdot 10^7$	$8.4 \cdot 10^8$	$3.3 \cdot 10^9$
BG 2	$9.5 \cdot 10^7$	$8.4 \cdot 10^8$	$3.3 \cdot 10^9$
BG 3	$9.5 \cdot 10^7$	$8.4 \cdot 10^8$	$3.3 \cdot 10^9$

in rotor dynamic systems and appropriate models are required to take into account couplings flexibility in rotordynamics studies. Couplings are critical elements also from the lateral-torsional coupling standpoint.

In the investigated test-case the shaft line is connected through torsionally-stiff flexible couplings. Couplings consist of two disk packs, two flanges (hubs) and one spacer. The flexible disk-pack is cardanically attached to both the hubs. The disk-pack consists of a number of thin disks made of stainless steel. Torsionally-stiff flexible couplings are adopted compensate for axial, angular and radial misalignment. The main geometrical and inertial property of the flexible couplings mounted in the investigated test-case are listed in Tab. 4.5.

Tab. 4.5: Main properties of the adopted flexible couplings.

Nominal torque	45 kN m
Maximum torque	80 kN m
Maximum Axial misalignment	3.6 mm
Maximum Radial misalignment	1.18 mm
Maximum Angular misalignment	0.75°
Torsional Spring Rate	$29.9 \cdot 10^6$ N m/rad
Moment of inertia	1.04 kg m^2
Weight	48 kg

4.4 Brake supporting group

The brake supporting group (BG) is the part of the test-case onto which the brake disk or train wheel to be braked are mounted. The devices to be tested are assembled to the shaft of the brake group by means of dedicated mechanical interfaces.

Brake calipers for brake disk or blocks are constrained to a dedicated supporting structure called Prony's system that is used for the measurement of the braking torque. It is formed of an oscillating beam to which calipers and their supports are assembled by means of slides. On the opposite side of the caliper support structure, the oscillating beam is substained by a load cell to measure the vertical load and then evaluate the equivalent braking torque.

When braking forces are applied to the overhang brake disk, the shaft is subjected to high bending and torsional loads and this aspect is particularly critical if combined with the presence of complex rotor elements.

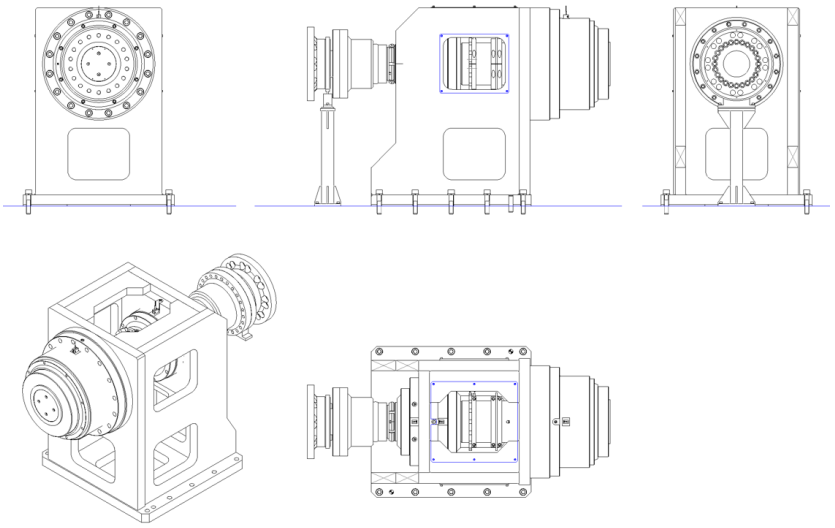

Fig. 4.8: Brake supporting group.

The shaft of the brake-group is supported by three bearings: a *slow-friction roller radial* bearing on the brake side, a *roller-radial* bearing and a *double-ball* bearing on the shaft line side. The brake supporting group (Fig. 4.8) is connected to the flywheels shaft line through a safety hydraulic coupling and of a torsiometer for the measurement of the braking torque.

4.5 Problem description

The investigated test-case is critical from the rotordynamic modelling standpoint both for several issues related to the particular adopted mechanical components and to the working conditions. The firs critical aspect is represented by the high dimensions of the rotating masses (i.e. the flywheels) with respect to the masses conventionally considered in rotordynamics models. Another aspect

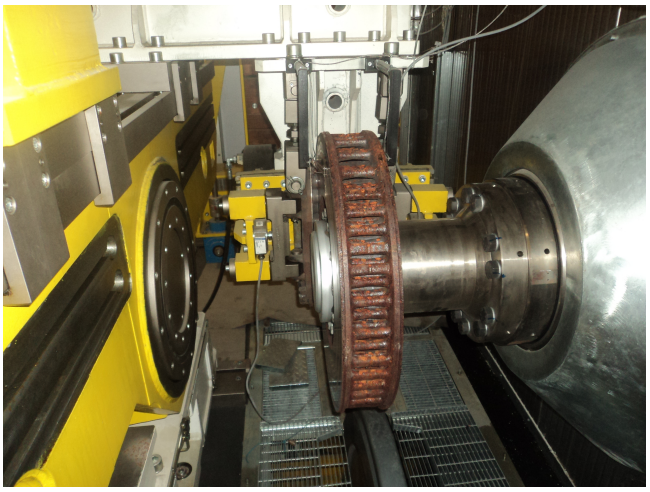

Fig. 4.9: A brake-disk mounted onto the brake supporting group.

related to the rotating masses is their particular assembly to the shaft (distributed rotor) that cannot be described with common disk or beam elements and require the adoption of distributed inertial elements with several shaft-to-rotor connections. The third issue consists in the influence of the flexible couplings on the shaft vibration, which gave rise to the necessity of correctly modelling such components. Furthermore, a correct representation of the misalignment between the shaft groups is fundamental to investigate its influence on the rotor line response.

Concerning the operating conditions it must be noticed that the studied test-case alway works in torsional and bending transient conditions, that are particularly critical for the lateral-torsional coupling, thus requiring an accurate prediction of its dynamical behaviour in order to avoid static or fatigue failure.

Furthermore, the brake testing standards [78, 79, 80] requires several brake mass value to be tested, imposing the utilisation of different flywheels for different tests. Each single flywheel configuration must be studied as a separate rotor system, hence requiring the adoption of an efficient rotordynamical model able to represent complex rotor and to perform the required analysis with a low computational effort.

Chapter 5

Experimental tests

This chapter deals with the experimental activity performed on the dynamometrical flywheel test bench for railway brakes. The experimental work on this particular test-case is part of a support activity for the acceptance of new test benches for railways components that has been committed to the DIEF - Applied Mechanics section of the University of Florence by Italcertifer S.p.A (FS group).

Due to the complexity of the dynamometrical flywheel test bench the activity on this particular machine lasted more than two years, during which the typical phases of an acceptance process have been executed. The undesired vibration phenomena firstly revealed theirselves during the emergency run tests, when the test bench exhibited some unpredicted vibration behaviours that have been identified through high noise, disturbs on the standard measurements as braking force, braking torque and pressure in the brake cylinder, (see Fig. 5.1) and as ground vibrations.

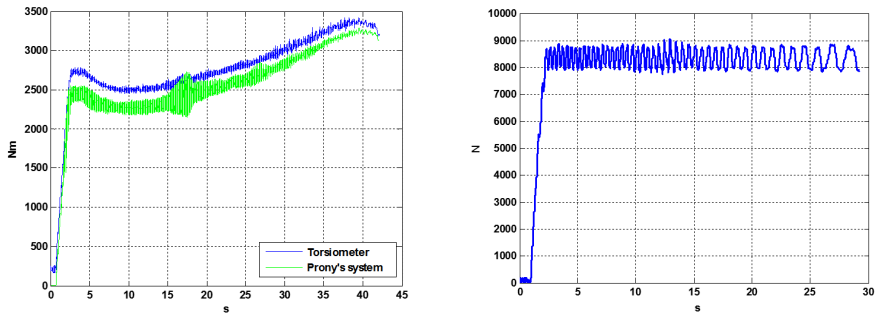

(a) (b)

Fig. 5.1: Disturbs on the standard acquired measurements (a): brake torque (b): brake force.

A correct assessment and mapping of the vibration levels was hence required to identify safe operating conditions for all the machine configurations to preserve the machine integrity, to guarantee operators safety and to assure the goodness of acceptance test on brake components.

Different test campaigns have been then executed with the aim of evaluating

the machine vibration levels by measurements on non-rotating parts (housings of the bearings, baseplates and foundation). Three measurement campaigns have been executed over time in collaboration with Politecnico of Milano and they can be classified and conventionally named:

- *Test campaign 1*: the first one has been executed on November 2012 when both impulsive and free run tests of few machine configurations were executed;
- *Test campaign 2*: the second campaign has been performed on September 2013 with the same instrumentation set and tested configurations of the first one after some structural interventions on the baseplate anchorage;
- *Test campaign 3*: during the third test campaign, executed on January 2014, a comprehensive set of machine configurations has been tested in both free and brake run tests.

The measurement have been performed according to the guidelines provided by the ISO 10816 series *Mechanical vibration Evaluation of machine vibration by measurements on non-rotating parts* [18], that is one of the ISO (International Organization for Standardization) reference standards in the field of machinery vibration monitoring and analysis.

In the following sections the evaluation criteria, the experimental setup and the different test campaigns are briefly described.

5.1 Evaluation criteria

The evaluation criteria adopted for the assessment of the vibration severity of the test bench configurations is provided by the ISO 10816 Standard [18] and it is based on the magnitude of observed vibration. The dynamometrical flywheel test bench is a peculiar machine that cannot be classified in a specific machine type, thus, in this case, evaluation criteria specified in Appendix B of [18] of general type machine have been employed. The maximum vibration magnitude measured at each pedestal is classified according to the various classes of machines and to the different evaluation zones for the support class where the evaluation zones have been established from international experience to permit a qualitative evaluation on a specific machine. The different machine classes are:

- Class I: Small machines up to 15 kW;
- Class II: Machines with power in the range 15 - 75 kW on light foundations;
- Class III: Machines with power above 300 kW on heavy and rigid foundations;
- Class IV: Machines with power above 300 kW on flexible foundations (soft mount).

Four evaluation zones have been defined:

- Zone A: relative to new commissioned machines;

- Zone B: containing vibration values acceptable for long-term operation;
- Zone C: defining vibration values unsatisfactory for long-term operation and the necessity of suitable remedial actions;
- Zone D: relative to vibration values high enough to cause damage to the machine.

Obviously, numerical values assigned to the zone boundaries are not mandatory, and specific values must be agreed by the machine manufacturer and customer. However, these values provide guidelines for avoiding gross deficiencies or unrealistic requirements.

In several studies it has been found that vibration velocity is sufficient to characterise the zone boundary values of vibration over a wide range of machine types and machine operating speeds. The main evaluation quantity is therefore the overall *root-mean-square* (r.m.s.) value of vibration velocity in mm/s.

The numerical limit values of the evaluation quantity are shown in Fig. 5.2

RANGES OF VIBRATION SEVERITY	QUALITY JUDGEMENTS			
RMS Velocity (mm/s RMS)	I	II	III	IV
0.28	A	A	A	A
0.45				
0.71				
1.12	B			
1.80		B		
2.80	C		B	
4.50		C		B
7.10	D		C	
11.2		D		C
18.0			D	
28				D
45				

Fig. 5.2: Evaluation of vibration severity.

Since the dynamometrical test bench belongs to Class III, the following upper limits on the r.m.s value of vibration velocity have been considered to assess the vibration severity in the machine configurations:

- Zone A: 1.8 mm/s;
- Zone B: 4.5 mm/s;
- Zone C: 11.2 mm/s;

5.2 Description of the experimental setup

According to the different executed test campaigns, the test bench has been instrumented by means of

- a set of vertical and lateral piezo-electric accelerometers;
- vertical and lateral servo-accelerometers;

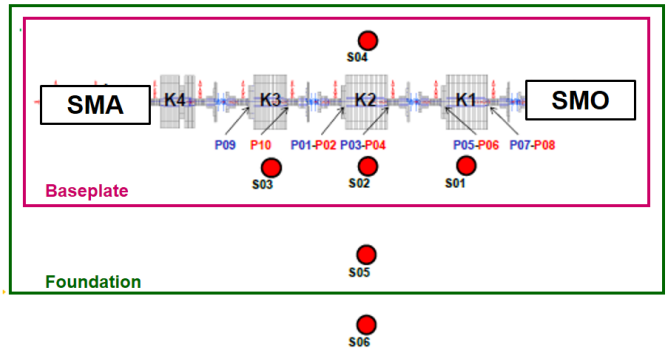

Fig. 5.3: An example of the positioning of the accelerometers.

- an encoder.

The positioning of the accelerometers during *Test Campaign 1* is illustrated in Fig. 5.3. The set of piezo-electric accelerometers has been used for the measurement of the radial (vertical and horizontal) vibration on the bearings housings (see Fig. 5.4) of the shafts group in compliance with the regulation of the ISO 10816 Standard. The accelerometers have been installed by stick method.

Servo-accelerometers have been installed in several location of the test bench to evaluate the vibration of the baseplates and of the supporting foundation (see Fig. 5.5).

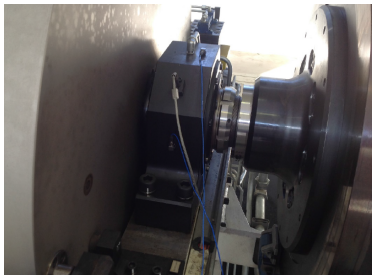

Fig. 5.4: Accelerometers sticked on the bearing housing.

5.3 Configurations of the test-case

The dynamic behaviour of the studied test-case has been investigated in different configurations of the machine and for several operating conditions.

The possible machine configurations are 32 according to the number of possible combination of mounted flywheels. Moreover, the vibration of the test bench have been measured according to different working conditions: free and braking conditions. The tests executed during the measurement test campaigns are:

- impulsive excitation tests;

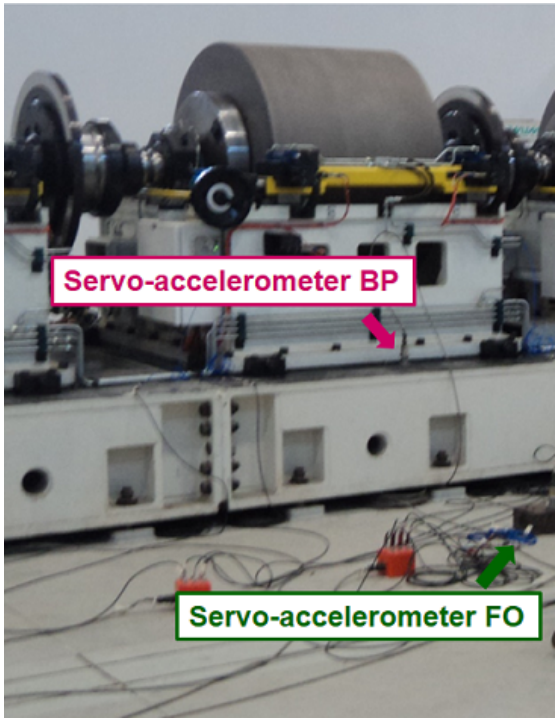

Fig. 5.5: Position of the servo-accelerometers on baseplate and foundation.

- run tests that can be distinguished in free and braking runs. The free case consists of three different phases: a ramp-up test wherein the test bench accelerates from the zero-velocity condition to the maximum angular speed value, a regime test during which the investigated machine rotates at the maximum angular speed value, a ramp-down test wherein the test bench decelerates from the regime condition until it reaches zero-velocity condition. Braking tests consist of the first two phases of the free ones, followed by a braking-test that is a ramp down in which the test bench brakes according to specific braking conditions applied to the test railway brake disk in compliance with railway standards [77, 78, 79].

During *Test campaign 1* impulsive (hammer) and free tests considering the machine configurations listed in Tab. 5.1 have been performed. The aim of this test campaign consists in the evaluation of the rms-values of the velocity of the vibration measured on the bearing housings during the regime phase. This value is taken by the ISO 10816 Standard as the evaluation criterion to assess vibration severity in terms of vibration magnitude. According to this parameter, evaluation zones are defined to permit a qualitative assessment of the vibration, and to provide guidelines on possible actions [18].

Test campaign 2 has been performed to verify a possible improvement of the dynamic behaviour. Impulsive and free tests executed in *Test campaign 1* have been repeated and other machine configurations have been investigated (see Tab. 5.2).

Test campaign 3 has been executed to study the influence of the braking

Tab. 5.1: List of tests performed in *Test Campaign 1*.

	Mounted flywheels	Test type	Total Inertia ($kg\,m^2$)	Operating conditions	Regime speed (rpm)
Hammer 1	K2	Impulsive test	1200	ET K1	-
Hammer 2	K2	Impulsive test	1200	ET K2	-
Hammer 3	K1+K2	Impulsive test	2200	ET K3	-
Hammer 4	K1+K2	Impulsive test	2200	ET BD	-
Run 1	-	Run Test	200	Free	3000
Run 2	K2	Run Test	1200	Free	3000
Run 3	K1+K2	Run Test	2200	Free	3000
Run 4	K3+K4+K5	Run Test	1600	Free	3000

Tab. 5.2: List of tests performed in *Test Campaign 2*.

	Mounted flywheels	Test type	Total Inertia ($kg\,m^2$)	Operating conditions	Regime speed (rpm)
Hammer 1	K2	Impulsive test	1200	ET K1	-
Hammer 2	K2	Impulsive test	1200	ET K2	-
Hammer 3	K1+K2	Impulsive test	2200	ET K1	-
Hammer 4	K3+K4 200-400	Impulsive test	1600	ET K3	-
Hammer 5	K3+K4 200-400	Impulsive test	1600	ET BP	-
Run 1	K5	Run Test	600	Free	3000
Run 2	K2	Run Test	1200	Free	3000
Run 3	K4 200-400	Run Test	800	Free	3000
Run 4	K1+K2	Run Test	2200	Free	3000
Run 5	K3+K4 200-400	Run Test	1600	Free	3000
Run 6	K1+K2+K3+K4 200-400	Run Test	1600	Free	3000

conditions on the vibration behaviour of the machine. Thus, a set of the braking tests required by the railways standards for the acceptance and the validation of this kind of test bench [77] have been performed. A subset of the executed braking tests is listed in Tab. 5.3. The listed tests are the ones characterised by values of the angular speed, mechanical inertia and brake application force, that are meaningful for the evaluation of the dynamics behaviour of the studied test bench.

During *Test campaign 3* also further free tests, limited for the maximum value of the angular speed, have been executed to investigate the vibration behaviour of the entire set of machine configurations (see Tab. 5.4).

Figs 5.6-5.11 show the results of a subset of the regime tests in terms of the the r.m.s values of the velocity vibration in mm/s that is the evaluation quantity according to the ISO 10816 Standard [18]. The limit values respectively for Zone A and Zone B are plotted as horizontal red lines.

Tab. 5.3: A subset of the braking tests performed in *Test Campaign 3*.

	Mounted flywheels	Total Inertia ($kg\,m^2$)	Brake Inertia ($kg\,m^2$)	Maximum speed (rpm)	Brake force (kN)
Run 1	K3+K4 400	1400	1485	1192	46
Run 2	K4 400	600	1485	1490	18
Run 3	K4 400	600	792	2682	14/18
Run 4	K4 400	1000	1210	2170	14/18
Run 5	K4 400	600	1210	2170	14/18
Run 6	K4 400	600	792	2980	14/18
Run 7	K4 400	1000	1210	2411	14/18
Run 8	K4 400	600	1210	2411	14/18
Run 9	-	200	792	2682	14/18
Run 10	-	200	792	2980	14/18

Tab. 5.4: List of free tests performed in *Test Campaign 3*.

	Mounted flywheels	Test type	Total Inertia ($kg\,m^2$)	Maximum speed (rpm)
Run 1	-	Run Test	200	3000
Run 2	K4 400	Run Test	600	3000
Run 3	K4 200	Run Test	400	3000
Run 4	K4 200-400	Run Test	800	2800
Run 5	K3	Run Test	1000	3000
Run 6	K3+K4 400	Run Test	1400	2900
Run 7	K3+K4 200	Run Test	1200	2900
Run 8	K3+K4 K4 400	Run Test	1600	2800
Run 9	K2	Run Test	1200	2400
Run 10	K1	Run Test	1200	2400
Run 11	K1+K3	Run Test	2000	2500
Run 12	K1+K2	Run Test	2200	2300
Run 13	K1+K2+K3	Run Test	3000	2300
Run 13	K1+K2+K3+K4 400	Run Test	3000	2300
Run 13	K1+K2+K3+K4 200-400	Run Test	3000	2300

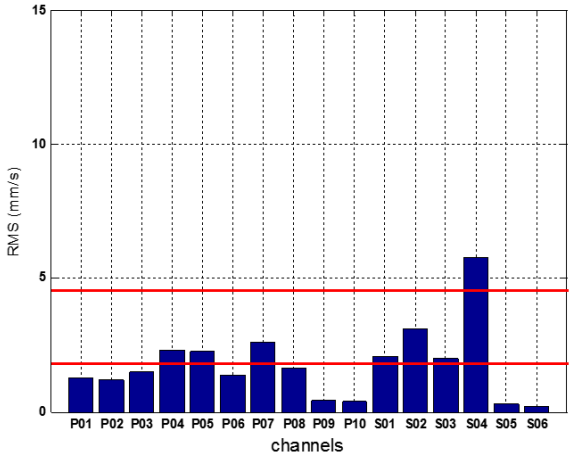

Fig. 5.6: Test Campaign 1 - Run 1 (K0 - 3000 rpm): r.m.s. value of the vibration velocity.

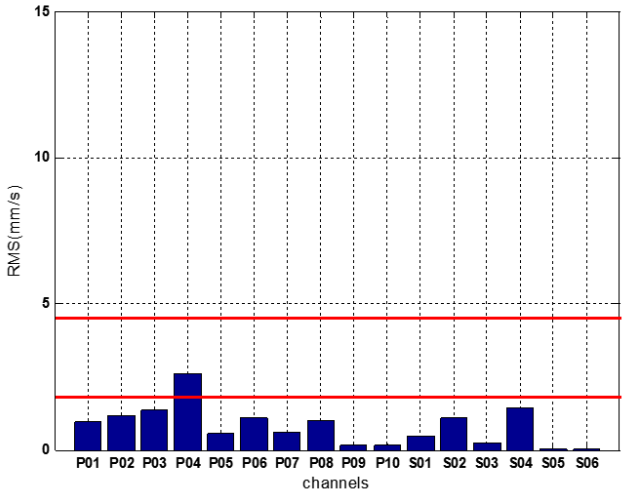

Fig. 5.7: Test Campaign 1 - Run 2 (K2 - 1500 rpm): r.m.s. value of the vibration velocity.

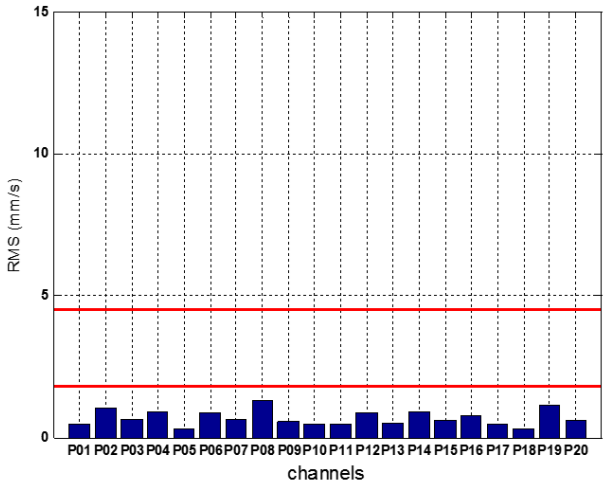

Fig. 5.8: Test Campaign 3 - Run 1 (K0 - 3000 rpm): r.m.s. value of the vibration velocity.

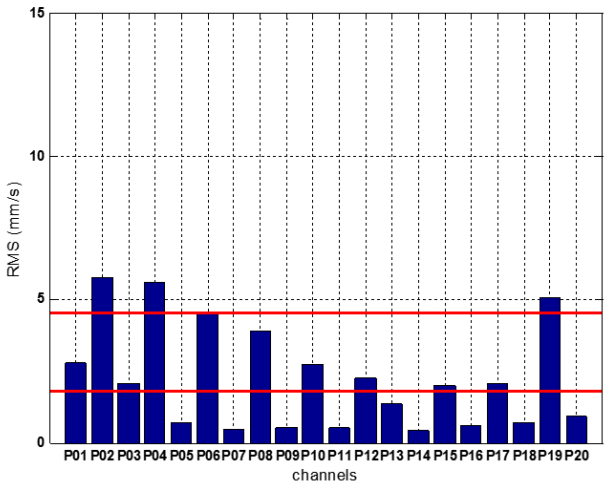

Fig. 5.9: Test Campaign 3 - Run 10 (K1 - 2000 rpm): r.m.s. value of the vibration velocity.

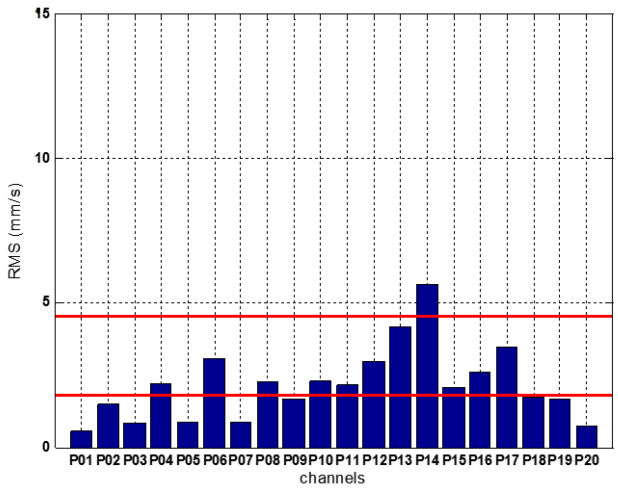

Fig. 5.10: Test Campaign 3 - Run 3 (K4 - 3000 rpm): r.m.s. value of the vibration velocity.

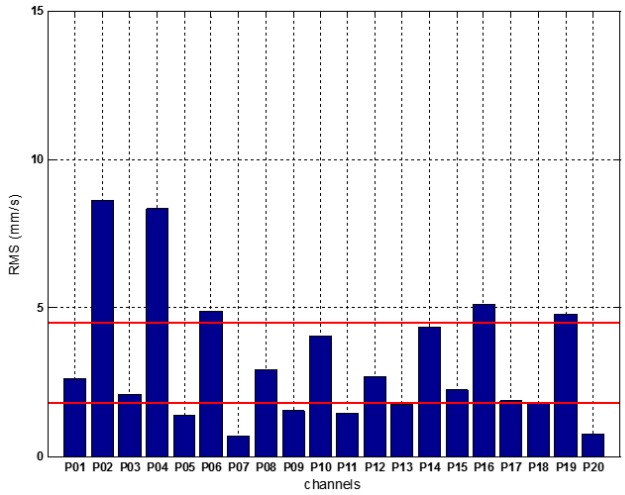

Fig. 5.11: Test Campaign 3 - Run 13 (K1-K2-K3-K4-K5 - 2300 rpm): r.m.s. value of the vibration velocity.

As it can be deduced from the Figs. 5.6-5.11, the measurements performed on the non-rotating parts of the machine (bearing pedestals) had shown that vibration values usually falls in Zone B of severity evaluation. Moreover, several channels exhibit r.m.s velocity vibration values that fall in Zone C, and this behaviour is unacceptable for a new machine. Only one machine configuration respects the limits of Zone A, this configuration is the K0 configuration, when none of the five flywheels is engaged to the shaft.

The realisation and validation of an accurate mathematical model of the test bench is highly recommended to investigate the cause of these vibrations and to evaluate in reasonable times and costs, the benefit of possible modifications to the structure of the machine in terms of reduction of vibrations severity. Since the test bench has 32 configurations, a systematic approach for the machine modelling is highly needed.

Chapter 6

Numerical Results

The dynamometric test bench presented in the previous chapter has a modular structure formed of five movable flywheels that can be engaged to the rotor shaft and contribute to the rotating masses. Therefore, the test bench can be operated in 32 different configurations ($N_{config} = 2^5$), which can cover all the rotating inertia values required by testing standards [78, 79, 80]. The dynamical behaviour of each configuration must be investigated and predicted as a separate rotor system; thus, in this case, the adoption of an efficient and systematic rotordynamical model is fundamental to analyse all the complex rotor configurations and to perform the required analysis with a low computational effort. Thanks to its systematic architecture, the Rotordynamical Model developed in this thesis, results particularly efficient in such kind of task.

In this chapter the application of the Rotordynamical Model to the test-case is firstly introduced, focusing on those modelling features and issues that are the same for all the studied configurations. Then the numerical results of the studied machine configurations are compared to the experimental data to assess and validate the Rotordynamical Model performance in predicting the critical behaviour of real complex rotating machines.

For sake of brevity, in the present chapter the comparison between numerical results and experimental data relative to a subset of the machine configurations is shown. The presented configurations (see Fig. 6.1) are:

- K1+K2 configuration ($J_{eq} = 2200$ kg m^2): the results of this configuration are particularly meaningful because its dynamical behaviour has been tested in all the different Test Campaigns;

- K3+K4 200-400 configuration ($J_{eq} = 1600$ kg m^2): this configuration is studied to test the Rotordynamical Model for the different layout of the K4 200-400 shaft;

- K2 configuration ($J_{eq} = 1200$ kg m^2): this configuration is characterised by one of the rotational inertial value usually required by railway braking standards.

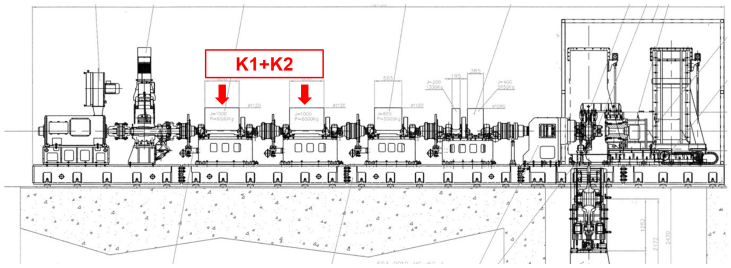

(a)

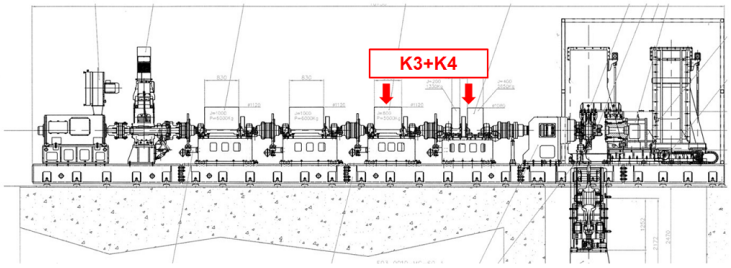

(b)

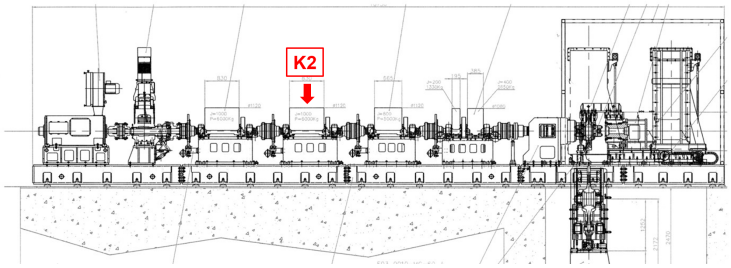

(c)

Fig. 6.1: The investigated configurations (a): K1+K2 (b): K3+K4 200-400 (c) K2.

6.1 Test-case modelling

The starting point for the rotordynamical analysis is the creation of the model representing the investigated test-case. To this purpose, the complex structure of the dynamometric brake test bench has been discretised and represented through several meaningful elements characterising the rotordynamical behaviour of the machine components. The discretised models of the considered machine configurations are based on the following assumptions:

- for the investigation of the lateral-torsional vibration behaviour of the considered test-case, the significant lateral and torsional properties (material, stiffness, damping and inertias) of the elements have been taken into account;
- axial motions have not be taken into account;
- at this step of the research activity vibrations due to the shaft line dynamics have been investigated; other critical behaviours of the machine resulting from the dynamics properties of the baseplate, of the foundation and of the brake supporting structure are not studied;
- since detailed geometrical and bearing property of the motor group shaft missed, a theoretical discretisation of the motor shaft line has been adopted for the model;
- since detailed geometrical and material property of the motor group shaft missed, a theoretical discretisation of the motor shaft line has been adopted for the model;

The studied machine configurations present common features that have been represented through a subset of the elements defined by the Rotordynamical Model. Both standard and non-standard elements have been employed to represent the mechanical components of the test-bench.

Standard components

Classical rotordynamical models are used to represent the dynamical characteristics of some inertial elements and several components of the test bench have been thus modelled by means of lumped disk elements. Such components are:

- four emergency disk-brakes (Fig. 6.2);
- four in-built disks for the engagement of the flywheels (Fig. 6.2);
- the tested rail disk-brake (Fig. 6.3);
- the flanges of the flexible couplings (Fig. 6.2).

The inertial properties introduced in the Rotordynamical Model are listed in Tab. 6.1.

The test-bench shaft line is the same for all the machine configurations. It is formed of six shaft linked each other through flexible-couplings: one motor shaft, the brake group shaft and four flywheel module shafts (see Fig. 6.4(a)-(c)).

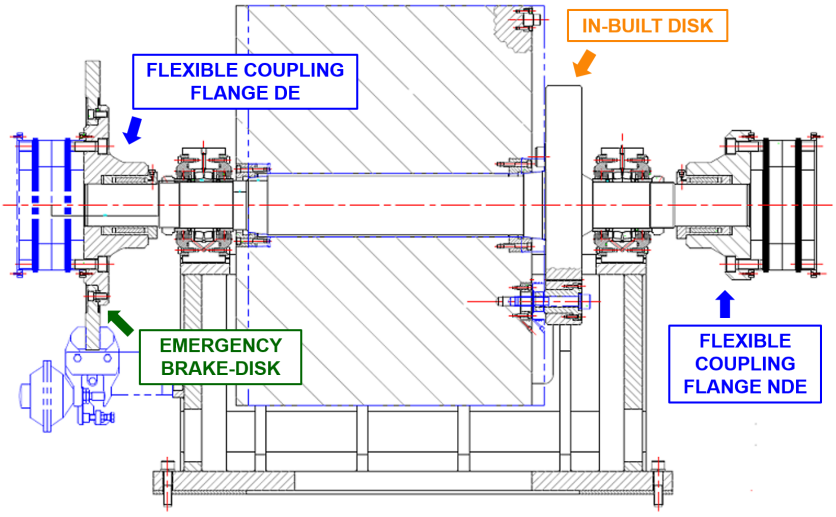

Fig. 6.2: Components of the flywheel modules modelled as disk elements.

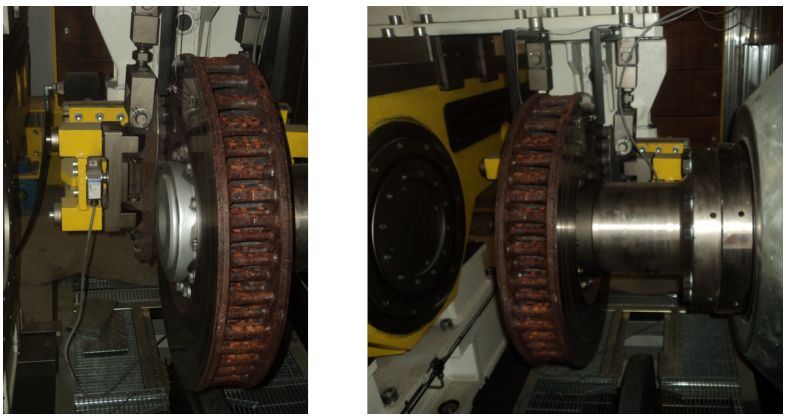

Fig. 6.3: A railway brake disk mounted on the shaft of the brake group.

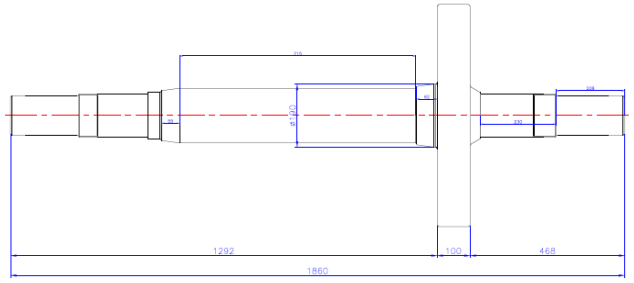

(a)

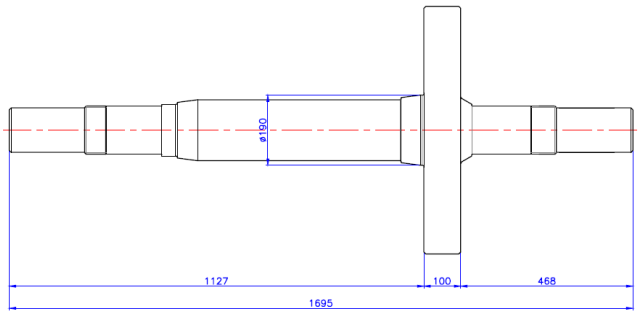

(b)

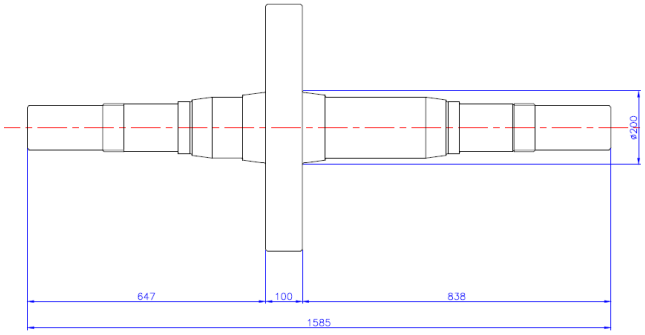

(c)

Fig. 6.4: Rotors shafts geometry (a): K1 and K2 modules shaft (b): K3 module shaft (c) K4 200-400 module shaft.

Tab. 6.1: Main properties of disk elements.

	Mass m^D (kg)	Polar inertia J_P^D (kg m^2)	Transverse inertia J_T^D (kg m^2)
Emergency brake-disk	203	15.48	7.08
Engagement in-built disk	254	15.33	7.88
Tested brake-disk	123.2	6.3	3.15
Flexible-coupling flange DE	36	0.83	0.42
Flexible-coupling flange NDE	60	1.3	0.78
Flexible-coupling	42	1	0.63

Each shaft module is discretised into several shaft beam elements characterised by circular sections.

Thirteen standard bearing elements based on the elasto-damping approach have been considered in each configuration and the values of the stiffness matrices have been provided by the bearing manufacturer as a function of the static load acting on each bearing. The bearing elements are introduced and modelled according to Eq. 3.13.

Non-standard components

In this specific application, non-standard elements are used to model the massive flywheels when they are engaged to the corresponding shaft and to represent the dynamical properties of flexible-couplings forming the multi-rotor configuration of the test bench.

A correct representation of the flywheel dynamical properties is the most critical issue from a modelling standpoint due to its complex topology. The flywheel is in fact a distributed inertial element assembled to the shaft by means of the complex connections that have been previously described in Sec. 4.3. Investigations performed by means of classical rotordynamical elements (flywheels modelled as lumped disks) showed the limitation of such kind of approach in predicting the critical behaviour of the test-case [83]. Also full solid 3D models (see Fig. 6.1) failed in the prediction of the dynamical critical speeds because of its limitation in the modelling of the complex flywheel-to-shaft connection. Furthermore, the high computational load required by such kind of approach is too expensive in this application where 32 different machine configurations must be investigated thus increasing the necessity of a simpler and systematic approach.

The non-standard elements of the Rotordynamical Model developed in the present research activity are particularly useful for the mathematical modelling of distributed rotors with complex rotor-to-shaft connections. In this specific application, a distributed inertial element is used to represent the inertial and stiffness contribution of each flywheel to rotordynamics behaviour. The complex connection of the flywheel to the shaft, which consists in a double conical coupling and a torsional coupling, is modelled through two visco-elastic elements (previously described in sec.3.3), connecting the distributed element and the rotor shaft in the midpoints of the double-conical surfaces, as illustrated in Fig. 6.6. The values of the stiffness matrices K_{DE}^{con} and K_{NDE}^{con} are derived

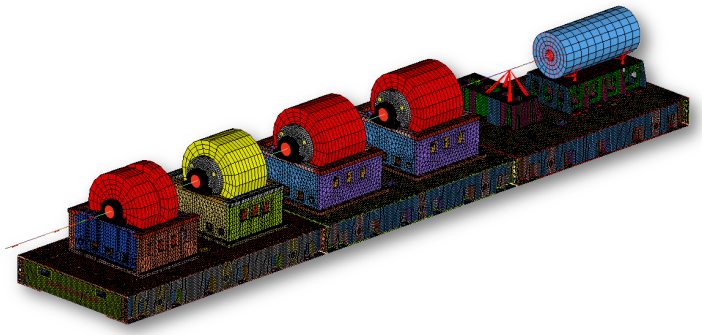

Fig. 6.5: Complete 3D model of the test bench.

from preliminary FEM analysis of the geometrical coupling for different values of the load acting on the midpoints and for speeds values covering the entire operation range of the machine ($0 - 3000$ rpm). The values are then stored in equivalent look-up tables (LUT) as function of the load N and rotational speed Ω. The torsional coupling between the flywheel and the rotor shaft through the in-built disk has not been directly modelled; it has been taken into account by modifying the values of the K_{NDE}^{con} stiffness matrice on the NDE side of the flywheel.

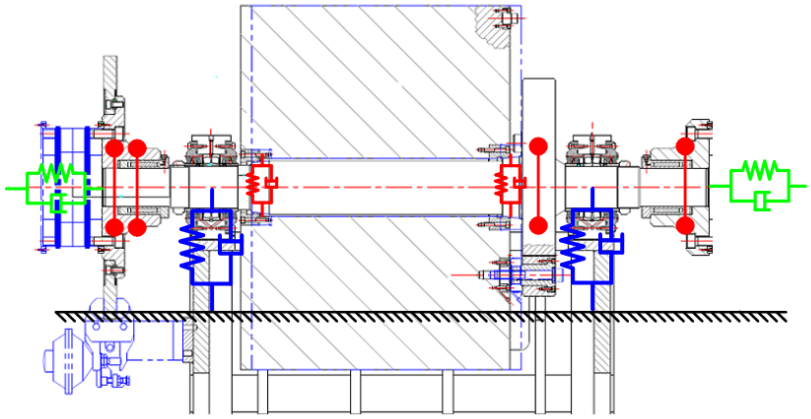

Fig. 6.6: Flywheel groups: modelling of the flywheel to shaft connections.

Fig. 6.7 shows a schematic representation of the implemented model for the K1+K2 configuration where K1 and K2 flywheels are both modelled as distributed inertial elements linked to the main shaft by means of two connection elements characterised by different values of the matrices K_{DE}^{con} and K_{NDE}^{con}. In this way the asimmetry of the double-conical and torsional coupling can be correctly reproduced.

An analogous approach has been used for modelling flexible-disk couplings.

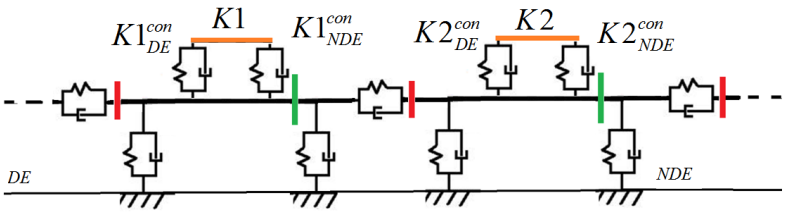

Fig. 6.7: Schematic representation of the implemented model for the K1+K2 configuration.

The inertial properties of the two coupling halves are introduced as classical lumped masses, while the stiffness properties K^{cpl} of the flexible disk are computed by previous solid FEM analysis.

6.2 K1-K2 configuration results

The FE model of the K1+K2 configuration is characterised by a shaft discretisation formed of 141 3D shaft elements that mathematically describes the multi-rotor shaft line formed by the motor group (MG), the flywheel-shaft groups and the brake supporting group (BG). The section properties are attributed according to real geometries of the shafts.

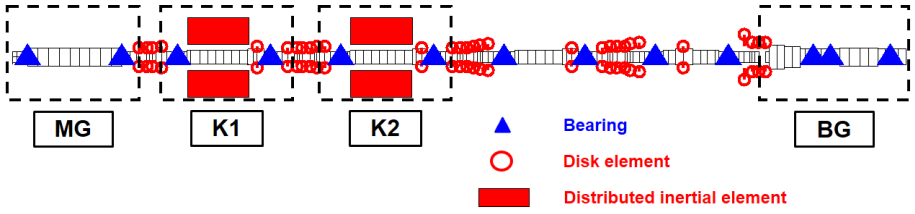

Fig. 6.8: Discretisation of the K1+K2 configuration.

Two distributed inertial elements are used to model both K1 and K2 flywheels that are mounted on the rotor line. The K1 and K2 flywheel are introduced in the model as distributed inertial elements connected to the shaft by means of visco-elastic elements with the properties stored in the matrices $K^{con}_{K1DE}(\Omega)$, $K^{con}_{K1NDE}(\Omega)$, $K^{con}_{K2DE}(\Omega)$, $K^{con}_{K2NDE}(\Omega)$ and $C^{con}_{K1DE}(\Omega)$, $C^{con}_{K1NDE}(\Omega)$, $C^{con}_{K2DE}(\Omega)$, $C^{con}_{K2DE}(\Omega)$.

A total of 13 bearings elements are introduced and modelled according to Eq. 3.13 in the K1+K2 configuration model. A schematic representation of the discretised rotor system is illustrated in Fig. 6.8.

In this application axial vibrations are small if compared to lateral ones, thus axial motions have been neglected. Firstly, to validate the Rotordynamical Model results by means of real experimental data (only lateral vibrations measurement have been performed on the test-case), the lateral behaviour of the K1-K2 configuration is studied through an uncoupled lateral FE formulation

with 4 dofs for each node.

The matching with the experimental data in terms of modal response is investigated by means of a damped natural frequency analysis in the entire operational regime of the machine ($0 - 3000$ rpm). The values of the first ten computed natural frequencies relative to the K1+K2 configuration at 0 rpm are listed in Tab. 6.2.

Tab. 6.2: K1+K2 Configuration - Computed natural frequencies at 0 rpm (Uncoupled lateral analysis).

Number	Mode	Value (Hz)	Element
1	$f^{com\ st}_{K1+K2\ m1}$	58.3	Flywheel K1
2	$f^{com\ st}_{K1+K2\ m2}$	58.3	Flywheel K1
3	$f^{com\ st}_{K1+K2\ m3}$	63.8	Flywheel K2
4	$f^{com\ st}_{K1+K2\ m4}$	63.8	Flywheel K2
5	$f^{com\ st}_{K1+K2\ m5}$	89.2	K1-K2 Flexible-Coupling
6	$f^{com\ st}_{K1+K2\ m6}$	89.2	K1-K2 Flexible-Coupling
7	$f^{com\ st}_{K1+K2\ m7}$	90.3	MG-K1 Flexible-Coupling
8	$f^{com\ st}_{K1+K2\ m8}$	90.3	MG-K1 Flexible-Coupling
9	$f^{com\ st}_{K1+K2\ m9}$	101.2	K2 Shaft
10	$f^{com\ st}_{K1+K2\ m10}$	101.2	K1 Shaft

The first two natural frequencies $f^{com\ st}_{K1+K2\ m1}$ and $f^{com\ st}_{K1+K2\ m2}$ are relative to the horizontal and vertical bending modes of the K1 flywheel-shaft group; analogously, the modes at natural frequencies $f^{com\ st}_{K1+K2\ m3}$ and $f^{com\ st}_{K1+K2\ m4}$ are bending modes in the horizontal and vertical plane of the K2 flywheel-shaft group. Modes involving the flexible-couplings are characterised by the natural frequencies values $f^{com\ st}_{K1+K2\ m5}$ and $f^{com\ st}_{K1+K2\ m6}$ for the coupling linking the K1 and K2 modules and $f^{com\ st}_{K1+K2\ m7}$ and$f^{com\ st}_{K1+K2\ m8}$ for the coupling between the motor group and the K1 module.

The static computed damped natural frequencies values $f^{com\ st}_{K1+K2\ mi}$ are compared to the experimental measurements coming from an impulsive test performed on the K1+K2 configuration. More specifically, results relative to the Hammer 3 - impulsive test obtained through an impulsive excitation on the in-built disk of the K1 flywheel in the vertical direction during the Test Campaign 2 are considered. The results of the considered experimental impulsive test in terms of vertical displacement of the bearing housings of the K1 and K2 flywheel-shaft groups are illustrated in Figs. 6.9(a) and (b) and listed in Tabs. 6.3 and 6.4.

Comparing the experimental data with the results coming from the the modal analysis of the Rotordynamics Model of the K1+K2 configuration, it can be noticed that the value of the experimental frequency corresponding to the main peak of the K2 NDE vertical accelerometer response ($f^{exp-st}_{K2-NDE-m2} = 62.19$ Hz) is very close to the value of the static frequency of the 3^{rd} and 4^{th} computed mode $f^{com\ st}_{K1+K2\ m3} = f^{com\ st}_{K1+K2\ m4} = 63.8$ Hz. Furthermore, the computed vertical modal response of the K1 bearings matches the experimental data in terms of natural frequency values ($f^{comst}_{K1+K2\ m1} = f^{com\ st}_{K1+K2\ m2} = 58.3$ Hz

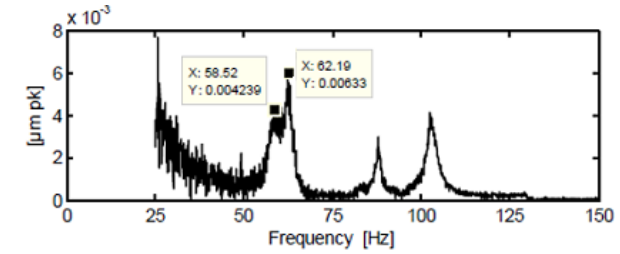

(a)

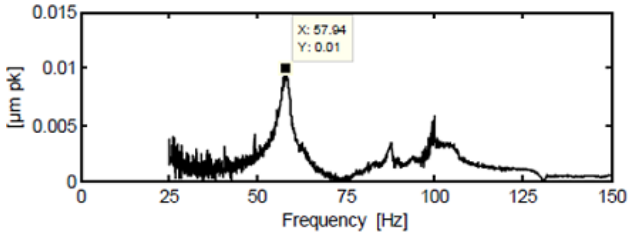

(b)

Fig. 6.9: K1+K2 Configuration - Hammer 3: Impulsive test - Excitation on K1 flywheel - (a): K2 NDE Vertical accelerometer (b): K1 NDE Vertical accelerometer.

vs. $f^{exp-st}_{K1-NDE-m1} = 57.94$ Hz). The K2+K1 (see Tab. 6.2) configuration model has two modes characterised by a static frequency $f^{com}_{K1+K2\ m9} = f^{com}_{K1+K2\ m10} = 101.2$ Hz that match the peaks in the experimental response characterised by frequency values near 104 Hz and present in accelerometric data of each experimental tests Fig. 6.9, independently from the particularly mounted flywheel, thus meaning that it characterise modes of the shaft-line regardless the specific mounted flywheel.

Tab. 6.3: K1+K2 Configuration- Hammer 3 Impulsive test: Peak frequencies in the hammer displacement response K2-NDE.

Number	Mode	Value (Hz)
1	$f^{exp-st}_{K2-NDE-m1}$	58.52
2	$f^{exp-st}_{K2-NDE-m2}$	62.19
3	$f^{exp-st}_{K2-NDE-m3}$	88.3
4	$f^{exp-st}_{K2-NDE-m4}$	104.2

The numerical modal response in the whole operating range of the test bench ($0 - 3000$ rpm) is presented in the Campbell's plot (Fig. 6.10), derived considering a step of 100 rpm. The Campbell's plot individuates two possible harmonic resonances in the operating regime of the machine. The resonance predicted by means of the Rotordynamical Model relative to the 1^{st} mode ($f^{comp\ res}_{K2\ m1} = 47.38$ Hz) is approximately equal to the experimental resonance that the K2 flywheel shaft group exhibits for a rotational regime corresponding

Tab. 6.4: K1+K2 Configuration - Hammer 3 Impulsive test: Peak frequencies in the hammer displacement response K1-NDE.

Number	Mode	Value (Hz)
1	$f^{exp-st}_{K1-NDE-m1}$	57.94
2	$f^{exp-st}_{K2-NDE-m3}$	89.8
3	$f^{exp-st}_{K2-NDE-m4}$	100.3

to $f^{exp-res}_{K2-NDE\ m1} = 48.8$ Hz (see Fig. 6.11) in the Run 4 test performed during Test Campaign 2.

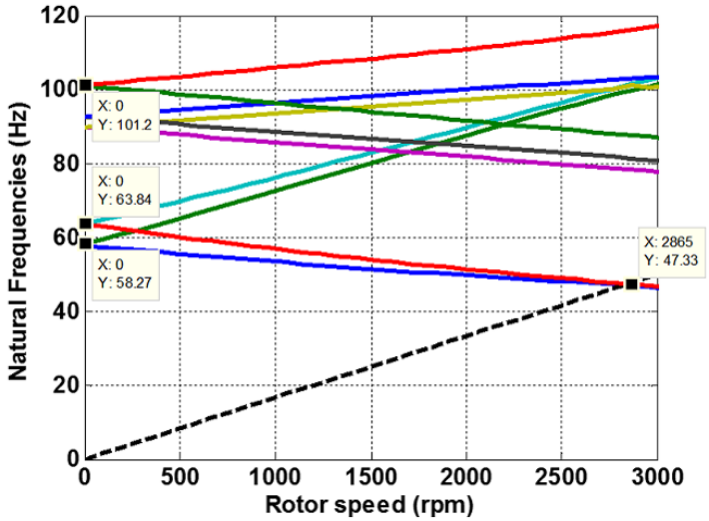

Fig. 6.10: K1+K2 configuration - Campbell's plot (Uncoupled lateral analysis).

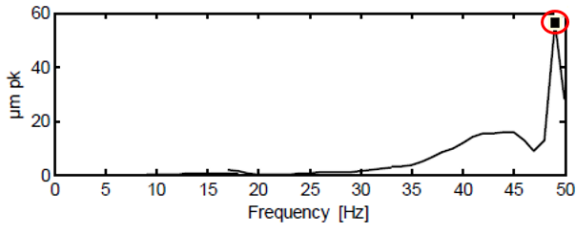

Fig. 6.11: K1+K2 Configuration - Run 4 Free run test: K2 NDE vertical accelerometer.

6.3 K3+K4 200-400 configuration results

The capability of the Rotordynamical Model in predicting the critical behaviour of complex real rotating machines is further investigated by applying it to the machine configuration with K3 and both K4-200 and K4-400 flywheels engaged to the shaft, for a total inertial value J_{eq} equal to 1600 kg m^2. The peculiarity of this configuration consists in the shaft geometry of the K4 flywheel group that differs from the ones of the K1, K2 and K3 groups (see Fig. 6.4c). In the K4 group, two flywheels can be engaged or disengaged to the shaft and, to this purpose, the in-built disk for the engagement is placed in the mid-span of the shaft instead of being at the NDE side.

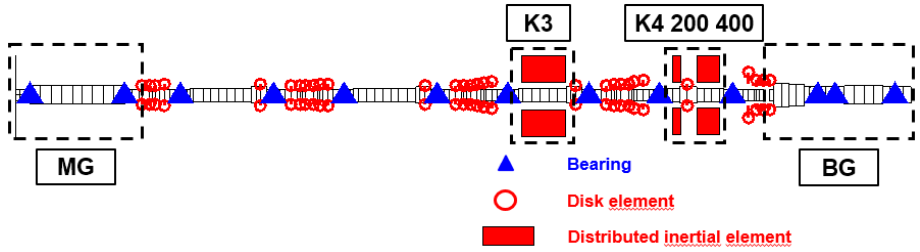

Fig. 6.12: Discretisation of the K3+K4 200-400 configuration.

To further validate the Rotordynamical Model results by means of real experimental data (only lateral vibrations measurement have been performed on the test-case), the lateral behaviour of the K3-K4 200-400 configuration is studied through an uncoupled lateral FE formulation with 4 dofs for each node.

The FE model of the K3+K4 configuration is characterised by a shaft discretisation formed of 148 3D shaft elements that mathematically describes the multi-rotor shaft line formed by the motor group (MG), the flywheel-shafts groups and the brake supporting group (BG). The section properties are attributed according to real geometries of the shafts.

Three distributed inertial elements are used to model K3, K4-200 and K4-400 flywheels that are mounted on the rotor line. These flywheels are introduced in the model as distributed inertial elements connected to the shaft by means of visco-elastic elements with the properties stored in the matrices $K^{con}_{K3DE}(\Omega)$, $K^{con}_{K3NDE}(\Omega)$, $K^{con}_{K4200DE}(\Omega)$, $K^{con}_{K4200NDE}(\Omega)$, $K^{con}_{K4400DE}(\Omega)$, $K^{con}_{K4400NDE}(\Omega)$ and $C^{con}_{K3DE}(\Omega)$, $C^{con}_{K3NDE}(\Omega)$, $C^{con}_{K4200DE}(\Omega)$, $C^{con}_{K4200NDE}(\Omega)$, $C^{con}_{K4400DE}(\Omega)$, $C^{con}_{K4400NDE}(\Omega)$.

A total of 13 bearings elements are introduced and modelled according to Eq. 3.13 in the K1+K2 configuration model. A schematic representation of the discretised rotor system is illustrated in Fig. 6.12.

As it has been done for the K1+K2 configuration analysis, the matching with the experimental data in terms of modal response is investigated by means of a damped natural frequency analysis in the entire operational regime of the machine ($0 - 3000$ rpm). The values of the first ten computed damped natural frequencies relative to the K3+K4 200-400 configuration at 0 rpm are listed in Tab. 6.5.

The first two natural frequencies $f^{com\ st}_{K3+K4\ m1}$ and $f^{com\ st}_{K3+K4\ m2}$ are relative

Tab. 6.5: K3+K4 200-400 Configuration - Computed natural frequencies at 0 rpm (Uncoupled lateral analysis).

Number	Mode	Value (Hz)	Element
1	$f^{com\ st}_{K3+K4\ m1}$	61.5	Flywheel K3
2	$f^{com\ st}_{K3+K4\ m2}$	61.5	Flywheel K3
3	$f^{com\ st}_{K3+K4\ m3}$	65.2	Flywheels K4
4	$f^{com\ st}_{K3+K4\ m4}$	66.6	Flywheels K4
5	$f^{com\ st}_{K3+K4\ m5}$	87.2	K3-K4 Flexible-Coupling
6	$f^{com\ st}_{K3+K4\ m6}$	87.2	K3-K4 Flexible-Coupling
7	$f^{com\ st}_{K3+K4\ m7}$	90.5	K3-K4 Flexible-Coupling
8	$f^{com\ st}_{K3+K4\ m8}$	91.5	K3-K4 Flexible-Coupling
9	$f^{com\ st}_{K3+K4\ m9}$	116.3	K3-K4 Shaft
10	$f^{com\ st}_{K3+K4\ m10}$	116.3	K3-K4 Shaft

to the horizontal and vertical bending modes of the K3 flywheel-shaft group; analogously, the modes at natural frequencies $f^{com\ st}_{K3+K4\ m3}$ and $f^{com\ st}_{K3+K4\ m4}$ are bending modes in the horizontal and vertical plane of the K4 flywheel-shaft group. Modes involving the flexible-couplings are characterised by the natural frequencies values $f^{com\ st}_{K3+K4\ m5}$, $f^{com\ st}_{K3+K4\ m6}$, $f^{com\ st}_{K1+K2\ m7}$ and $f^{com\ st}_{K1+K2\ m8}$.

The static computed damped natural frequencies values $f^{com\ st}_{K3+K4\ mi}$ are compared to the experimental measurements coming from an impulsive test performed on the K3+K4 configuration. More specifically, results relative to the Hammer 4 - impulsive test obtained through an impulsive excitation on the in-built disk of the K3 flywheel in the vertical direction during the Test Campaign 2 are considered. The results of the considered experimental impulsive test in terms of vertical displacement of the bearing housings of the K3 and K4 groups are illustrated in Figs. 6.13 - 6.15 and listed in Tabs. 6.3 and 6.4.

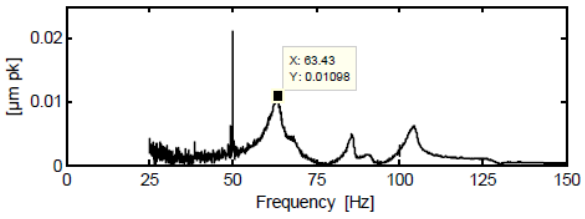

Fig. 6.13: K3+K4 Configuration - Hammer 4: Impulsive test - Excitation on K3 flywheel: K3 NDE Vertical accelerometer.

Comparing the experimental data with the results coming from the the modal analysis of the rotordynamics model of the K3+K4 configuration, it can be observed that the value of the experimental frequency corresponding to the main peak of the K3 NDE vertical accelerometer response $f^{exp-st}_{K2-NDE-m2} = 63.4$ Hz is close to the value of the static frequency of the 1^{st} computed mode

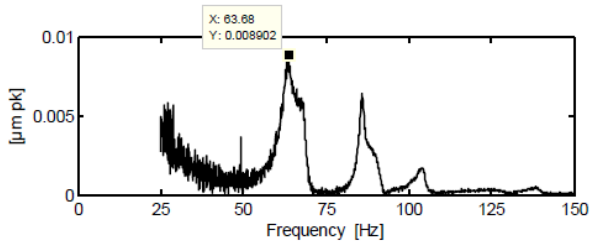

Fig. 6.14: K3+K4 Configuration - Hammer 4: Impulsive test - Excitation on K3 flywheel: K4 DE Vertical accelerometer.

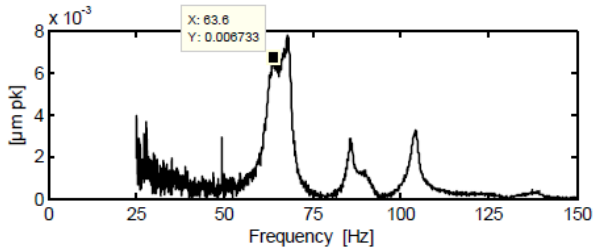

Fig. 6.15: K3+K4 Configuration - Hammer 4: Impulsive test - Excitation on K3 flywheel: K4 NDE Vertical accelerometer.

$f^{com\ st}_{K3+K4\ m1} = f^{com\ st}_{K3+K4\ m4} = 61.5$ Hz. Furthermore, also the computed vertical modal response of the K4 bearings matches the experimental data in terms of frequency response ($f^{comst}_{K3+K4\ m2} = 65.2$ Hz vs. $f^{exp-st}_{K4-NDE-m2} = 67.2$ Hz). The K3+K4 configuration model has two modes characterised by a static frequency $f^{com}_{K3+K4\ m9} = f^{com}_{K3+K4\ m10} = 116.3$ Hz that may correspond to the peaks in the experimental response characterised by frequency values near 103.6 Hz representing modes of the shaft-line. It must be noticed that the discrepancy between computed and experimental data in the frequency values may be caused by the particular geometrical arrangement of the K3+K4 shaft. A more detailed discretised model is hence required to match shaft bending modes.

The numerical modal response in the whole operating range of the test bench ($0 - 3000$ rpm) is presented in the Campbell's plot (Fig. 6.16), derived considering a step of 100 rpm.

The Campbell's Diagram individuates one possible harmonic resonance in the operating regime of the machine ($f^{comp\ res}_{K2\ m1} = 45.8$ Hz). The experimental response of the K3 flywheel shaft is illustrated in 6.17 in terms of r.m.s. value of the vertical vibration velocity of the K3 NDE bearing housing. It can be noticed that the dynamical response exhibits a dynamical amplification starting from a speed equal to 45 hertz, thus assessing the predicting capability of the Rotordynamical Model with a good degree also in this machine configuration.

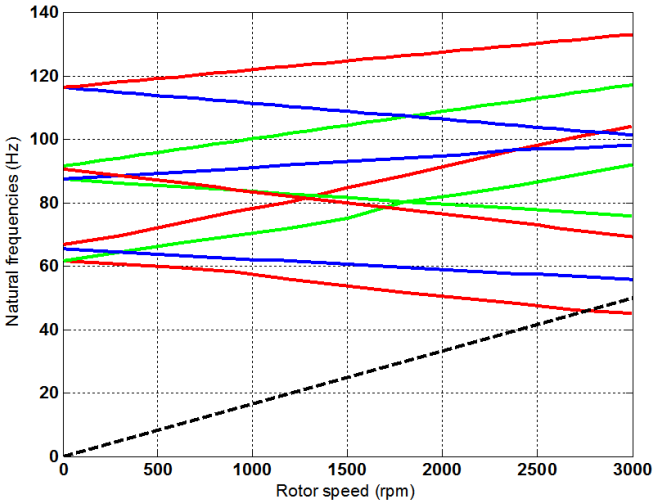

Fig. 6.16: K3+K4 200-400 Configuration - Campbell's plot (Uncoupled lateral analysis).

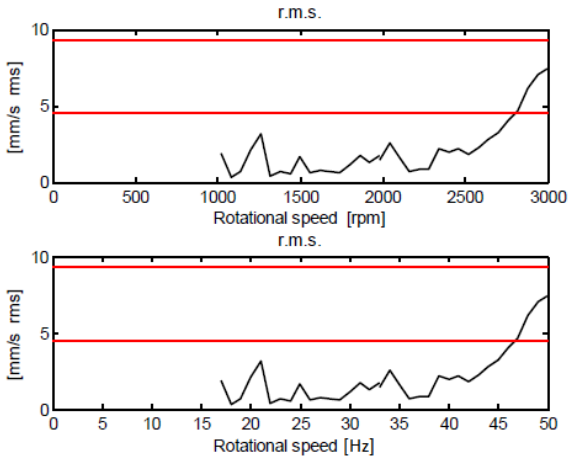

Fig. 6.17: K3+K4 200-400 Configuration: Test Campaign 2 - Run 5: r.m.s. value of the vibration velocity (K3 NDE vertical accelerometer).

Tab. 6.6: K3+K4 Configuration - Hammer 4 Impulsive test: Peak frequencies in the hammer displacement response K3-NDE.

Number	Mode	Value (Hz)
1	$f^{exp-st}_{K3-NDE-m1}$	63.4
2	$f^{exp-st}_{K3-NDE-m2}$	67.4
3	$f^{exp-st}_{K3-NDE-m3}$	85.3
4	$f^{exp-st}_{K3-NDE-m4}$	103.3

Tab. 6.7: K3+K4 Configuration - Hammer 4 Impulsive test: Peak frequencies in the hammer displacement response K4-DE.

Number	Mode	Value (Hz)
1	$f^{exp-st}_{K4-NDE-m1}$	63.7
2	$f^{exp-st}_{K4-NDE-m2}$	67.7
3	$f^{exp-st}_{K4-NDE-m3}$	87.9
4	$f^{exp-st}_{K4-NDE-m4}$	103.6

6.4 K2 configuration results

To investigate the performance of the Rotordynamical Model in describing coupled bending-torsional vibrations, the K2 configuration is analysed using of a coupled lateral torsional FE formulation with 5 dofs for each node. The K2 shaft line is modelled analogously to the previous configuration: 141 3D shaft are used with the section properties attributed according to real geometries of the shafts.

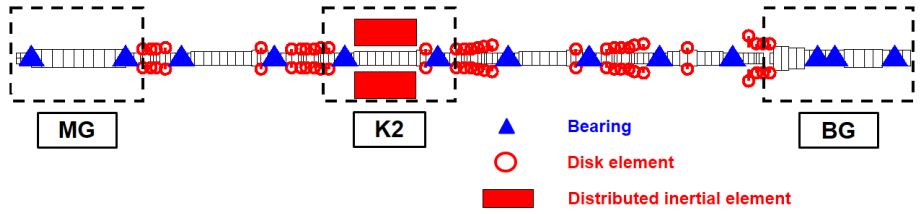

Fig. 6.18: Discretisation of the K2 configuration.

Concerning rigid disk elements, for the entire set of rotor units a total of 30 lumped mass have been added to nodes to take into account the inertial influence of the emergency brake disks, the in-built disks, the tested brake-disk and the flanges of the flexible-couplings. The lumped masses are placed in the nodes corresponding to their location on the corresponding shaft. The K2 flywheel is modelled as a distributed inertial element connected to the shaft in two points. The geometry coupling both axially and torsionally the K2 flywheel to the shaft is described with different values of the $K^{con}_{K2SNDE}(\Omega, N)$, $K^{con}_{K2DE}(\Omega, N)$ and $C^{con}_{K2DE}(\Omega, N)$, $C^{con}_{K2NDE(\Omega,N)}$ matrices. To consider the influence of the centrifugal forces on the double-conical coupling the stiffness matrices is speed

Tab. 6.8: Peak frequencies in the hammer vertical displacement response: K4-NDE.

Number	Mode	Value (Hz)
1	$f^{exp-st}_{K4-NDE-m1}$	63.7
2	$f^{exp-st}_{K4-NDE-m2}$	67.7
3	$f^{exp-st}_{K4-NDE-m3}$	87.5
4	$f^{exp-st}_{K4-NDE-m4}$	103.6

dependent.

In the developed model 13 bearings elements are introduced and modelled according to Eq. 3.13.

The torsionally-stiff flexible-couplings are introduced as general elasto-damping elements linking the single *Rotor units* according to the approach described by Eq. 3.25. The inertial properties of the flexible-couplings are introduced by means of classical disk massive elements.

A schematic representation of the rotor system is illustrated in Fig. 6.18.

The modal response of the K2 configuration is obtained from a coupled lateral-torsional damped natural frequency analysis in the entire operational regime of the machine $0 - 3000$ rpm. The values of the first six computed damped natural frequencies relative to the K2 configuration at 0 rpm are listed in Tab. 6.9.

Tab. 6.9: K2 Configuration - Computed natural frequencies at 0 rpm (Coupled torsional-lateral analysis).

Number	Mode	Value (Hz)	Element
1	$f^{com\ st}_{K2\ m1}$	13.1	Torsional
2	$f^{com\ st}_{K2\ m2}$	20.2	Torsional
3	$f^{com\ st}_{K2\ m3}$	36.2	Torsional
4	$f^{com\ st}_{K2\ m4}$	63.9	Lateral
5	$f^{com\ st}_{K2\ m5}$	89.4	Lateral
6	$f^{com\ st}_{K2\ m6}$	101.2	Lateral

The first three natural frequencies $f^{com\ st}_{K2\ m1} = 13.1$ Hz, $f^{com\ st}_{K2\ m2} = 20.2$Hz are $f^{com\ st}_{K2\ m3} = 36.2$ Hz are characteristic of torsional modes. The modes at natural frequencies $f^{com\ st}_{K2\ m4} = 63.9$ Hz, $f^{com\ st}_{K2\ m5} = 89.4$ Hz and $f^{com\ st}_{K2\ m6} = 101.2$ Hz are the bending modes relative respectively to the flywheel-shaft K2 module, the K1-K2 flexible coupling and the K2 shaft.

The numerical results relative to lateral modes can be directly compared to the experimental measurements coming from an impulsive test performed on the K2 configuration. More specifically, results relative to the Hammer 2-impulsive test obtained through an impulsive excitation on the in-built disk of the K2 flywheel in the vertical direction during the Test Campaign 2 are considered.

The results of the considered experimental impulsive test in terms of vertical displacement of the bearing housings of the K2 NDE bearing are illustrated in

Fig. 6.19 and listed in Tab. 6.10. Comparing the experimental data with the results coming from the the modal analysis of the rotordynamics model of the K2 configuration, it must be noticed that the value of the experimental frequency corresponding to the main peak of the K2 NDE vertical accelerometer response ($f^{exp-st}_{K2-NDE-m2} = 63.35$ Hz) is very close to the value of the static frequency of the 4^{th} computed mode $f^{com\ st}_{K2\ m4} = 63.9$ Hz.

The other two peaks in the experimental response ($f^{exp-st}_{K2-NDE-m2} = 86.9$ Hz and $f^{exp-st}_{K2-NDE-m2} = 101.1$ Hz) are matched by the computed static frequencies $f^{com-st}_{K2-NDE-5} = 89.4$ Hz and $f^{com-st}_{K2-NDE-6} = 101.2$ Hz relative respectively to flexible-coupling and shaft modes and they are predicted with a good approximation by the discretisation developed with the Rotordynamical Model.

Tab. 6.10: Peak frequencies in the hammer displacement response: K2-NDE.

Number	Mode	Value (Hz)
2	$f^{exp-st}_{K2-NDE-m1}$	63.35
3	$f^{exp-st}_{K2-NDE-m2}$	86.9
4	$f^{exp-st}_{K2-NDE-m2}$	101.1

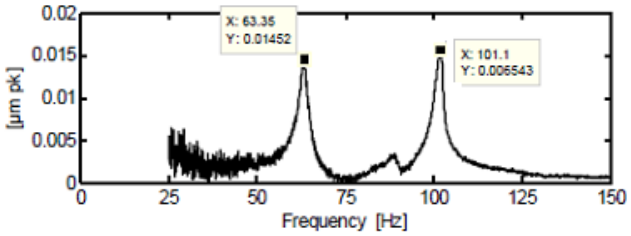

Fig. 6.19: K2 Configuration - Hammer 2: Impulsive test - Excitation on K2 flywheel.

It must be noticed that the Campbell's plot (see Fig. 6.20) highlights one possible lateral synchronous resonance ($f^{comp\ res}_{K2\ m} = 47.4$ Hz) of the 4^{th} lateral mode in the entire operating range of the test bench. The predicted resonance value is approximately equal to the experimental resonance frequency that the K2 flywheel shaft group exhibits for a rotational regime corresponding to $f^{exp-res}_{K2-NDE\ mI} = 48.6$ Hz (see Fig. 6.21) in the Run 2 test performed during Test Campaign 2.

The Campbell's plot individuates also three possible torsional resonance speed ($f^{comp\ res}_{K2\ t1} = 13.1$, $f^{comp\ res}_{K2\ t1} = 13.1$, $f^{comp\ res}_{K2\ t2} = 20.2$ and $f^{comp\ res}_{K2\ t2} = 36.2$ Hz). Since direct measurements on torsional vibrations are not available (dedicated tests to evaluate the torsional vibrations behaviour of the machine have not been performed), some considerations have been performed from indirect vibration lateral data.

More specifically, Test-Campaign 3-Run 9 data are considered; this test is formed of a ramp-up frome 0 rpm to 2400 rpm, a regime phase 2400 rpm and a run-down to 0 rpm. Figs. 6.22(a) and 6.22(b) illustrate the vertical acceleration response respectively on the K2 NDE and K2 DE housings. Responses are

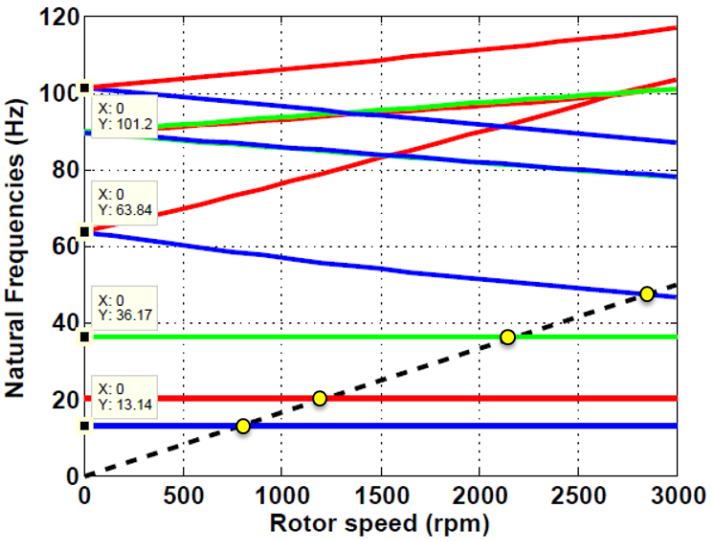

Fig. 6.20: K2 Configuration - Campbell's plot (Coupled torsional-lateral analysis).

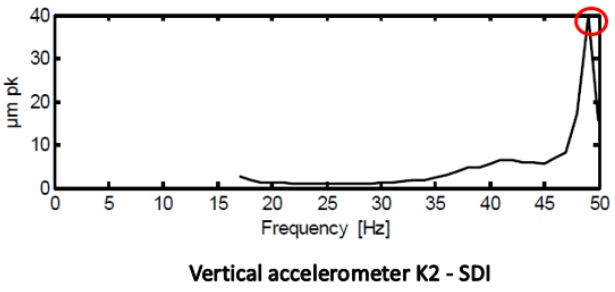

Fig. 6.21: K2 Configuration - Run 2: Free run test: vertical accelerometers on K2 flywheel-shaft group.

plotted as a visual representation of the spectrum of frequencies of the accelerometric data as they vary with time during a free run test.

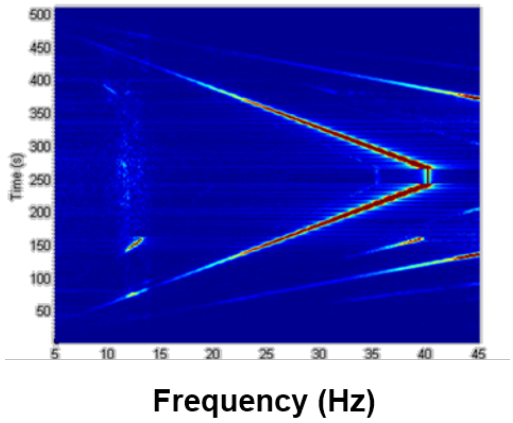

(a)

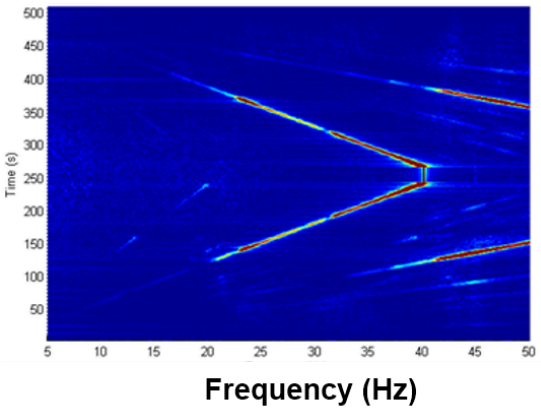

(b)

Fig. 6.22: K2 Configuration - Test campaign 3 run 9: Vertical acceleration on K2 bearing supports (a): NDE (b): DE .

As it can be seen from the figures, both the plots present the typical synchronous response and other non-harmonic dynamical amplifications probably due to shaft-line misalignments. The spectrum of the vertical acceleration of the K2 NDE housing exhibit a weak amplification zone at a constant frequency in the band around 13 Hz. Such kind of response can be explained as the influence on the lateral response of a torsional vibration at a value of about 13 Hz, that is close to the value of the first torsional frequency predicted by the numerical model $f_{K2\ t1}^{comp\ res} = 13.1$. It must be noticed that the K2 NDE housing is on the side of the K2 module where there is the torsional coupling between the K2 flywheel and its in-built disk, which represents a possible torsional excitation source; the constant frequency amplification band is in fact not present in the response on the K2 DE housing where such torsional coupling is absent.

Conclusions

In the present thesis a general-purpose Rotordynamical Model has been developed for the systematic analysis of multi-rotor systems. The aim of the work consists in modelling complex rotors through a systematic and practical approach for the study of coupled lateral and torsional dynamics. The model is based on a finite element rotordynamics formulation and it is able to manage long rotors characterised by complex topology, such as rotor with distributed inertias or elements with complex connections. A correct modelling of this kind of rotor is a fundamental aspect for the prediction of the critical behaviour of the rotordynamics systems, particularly when lateral-torsional vibration couplings arise. Through the developed model, complicated shaft-to-rotor connections or particular mounted parts, otherwise not representable with classical models, may be mathematically described. The main innovative characteristics of the model consists in its general topology: it may reproduce rotor features by means of both standard and non-standard rotor finite element (FE) models. Multi-rotor linking elements (such as couplings) may be implemented and non-standard elements may be also used for describing rotor non-standard components. The finite element formulation is derived considering for shafts 3D beams with 6 degrees of freedom (dofs) per node. The numerical efficiency of the presented model set it as a good compromise between accuracy and computational effort, thus it may be used to perform common rotordynamical investigation performed in rotating machinery design.

The test-case investigated in this research activity is a dynamometric flywheels test bench for railways brakes, designed for the acceptance dynamical testing of railways brake components. This particular test bench has been chosen as case study for its complex configuration characterised by distributed rotors requiring a correct identification of the critical speeds of the machinery in order to assure safe working conditions and to prevent the system from working with large amplitude vibrations that may be harmful for the system integrity (rolling bearings, flexible couplings) and for the operation of the test bench.

The Rotordynamical Model developed during the Ph.D activity has been validated by means of experimental data coming from a test campaign aimed at the evaluation of the vibration levels of the machinery. The test campaign has been performed by Politecnico di Milano, in collaboration with Italcertifer (FS) and Simpro S.p.A thanks to the instrumentation of the test bench through a set of accelerometers to measure mechanical vibration signals in terms of acceleration characterising the non-rotating parts of the machinery.

The Rotordynamical Model turned out to be particularly useful for the rotordynamical systematic analysis of the investigated machine, enabling the definition of models and analysis of several machine configurations through a simple

procedure. Thanks to its efficiency, it represents a good compromise between accuracy and computational load and it exhibited good capabilities in predicting lateral and torsional dynamics behaviour of the complex machine chosen as test-case.

Future developments of the present work will be based both on the modal analysis of other tested machine configurations of the present case study and on the comparison of the results coming from transient simulations with the vibration levels acquired during brake test. The entire set of tests performed in Test Campaign 1, 2 and 3 will be analysed in detail. Frequency responses and transient analysis will be performed to make a quantitative investigation of the contribution of the complex components on the vibration behaviour of the test-bench. Furthermore, thanks to the developed model, the effects due to the misalignment of the flexible-couplings will be studied. Models of the base-plate and foundation will also be introduced to reproduce modes relative to the anchoring structure. Simultaneously, other test-cases, such as multi-rotor machines equipped with gearboxes, will be studied with the developed model. From a modelling stand-point more complex finite-element or flexible-multibody formulations will be studied and possibly introduced in the general architecture of the developed model. Furthermore, the modelling of other coupling mechanisms will be enabled in the Rotordynamical Model.

Appendix A

Shape Functions

$$N_{v1} = \frac{1}{1+\Phi}\left[1 - 3\xi^2 + 2\xi^3 + \Phi(1-\xi)\right] \tag{A.1}$$

$$N_{v2} = \frac{1}{1+\Phi}\left[\xi - 2\xi^2 + \xi^3 + \frac{\Phi}{2}(\xi - \xi^2)\right] \tag{A.2}$$

$$N_{v3} = \frac{1}{1+\Phi}\left[3\xi^2 - 2\xi^3 + \Phi\xi\right] \tag{A.3}$$

$$N_{v4} = \frac{l}{1+\Phi}\left[-\xi^2 + \xi^3 + \frac{\Phi}{2}(-\xi + \xi^2)\right] \tag{A.4}$$

$$N_{\theta_{y1}} = \frac{6}{l\,(1+\Phi)}\left[\xi^2 - \xi\right] \tag{A.5}$$

$$N_{\theta_{y2}} = \frac{1}{1+\Phi}\left[1 - 4\xi + 3\xi^2 + \Phi\,(1-\xi)\right] \tag{A.6}$$

$$N_{\theta_{y3}} = \frac{6}{l\,(1+\Phi)}\left[\xi^2 - \xi\right] \tag{A.7}$$

$$N_{\theta_{y4}} = \frac{1}{1+\Phi}\left[-2\xi + 3\xi^2 + \Phi\xi\right] \tag{A.8}$$

$$N_{\theta_{x1}} = 1 - \xi \tag{A.9}$$

$$N_{\theta_{x1}} = \xi \tag{A.10}$$

Appendix B

ERRI B 126/RP 18

ERRI B 126/RP 18			PROGRAMME D'ESSAIS POUR LA VERIFICATION PERIODIQUE DES BANCS D'ESSAIS Programme 3.1			Page 7/8
Programme d'essais général			Type de garniture : métal fritté			
Masse par disque :	m = 4/7,5 t		Type de disque :		Acier, puissance de ventilation réduite	
Vitesse max. :	v = 300 à 350 km/h				640 x 80 mm	
			Dimensions du disque :		890 mm	
			Diamètre de la roue :		max. 30 mm	
			Epaisseur de garniture :			
Régime de freinage	Nombre de freinages	Essai n°	Vitesse [km/h]	Effort d'application F_B [kN]	Température initiale θ_0 [°C]	Observations
Str	x	R1 à Rx	120	31 [1])	20-100	Rodage avec x freinages jusqu'à 70% de portée
Str	5		30	8	20-60	
"	5		30	46	20-60	
"	5		120	8	50-60	m = 7,5 t/disque
"	5		120	46	"	
"	5		160	16	"	
"	5		160	46	"	
"	5		200 (175)	16	"	
"	5		200 (175)	46	"	
Dtr	1		60	-	20-30	25 kW/20 min
Str	10		120	31	20-100	m = 4 t/disque
Str	5		30	8	20-60	
"	5		30	25	20-60	
"	5		120	8	50-60	m = 4 t/disque
"	5		120	18	"	
"	5		120	25	"	
"	5		200 (175)	18	"	
			200 (175)	25		
Sn	5		30	8		m = 4 t/ disque
"	5		30	25		Freinages humides
"	5		120	8		
"	5		120	18		
"	5		120	25		
Str	10		120	25		Freinages pour le séchage des garnitures
Rtr	5		200-100	8		Freinages de régulation de 200 km/h à 100 km/h
	5		200-100	18		
"	5		250	18	"	m = 4 t/disque
"	5		250	25	"	**Observation :**
"	5		300	14/18 [2])	"	Entre 450 et 500 km/h:
"	5		300	19/25 [2)]	"	Le diamètre de roue peut être augmenté jusqu'à 1100 mm maximum pour atteindre la vitesse.
"	3		350	14/18 [2)]	"	
"	3		350	19/25 [2)]	"	
"	3		400	14/18 [2)]	"	
"	3		450	14/18 [2)]	"	
	3		500	14/18 [2)]	"	
						Str: Freinage (d'arrêt) à sec **Dtr:** Freinage de maintien (sur pente) à sec **Sn:** Freinage (d'arrêt) sous conditions humides **Rtr:** Freinage de régulation, en vue de réduire la vitesse

Fig. B.1: Programme pour les essais comparatifs et pour les verifications periodiques - Projet

Bibliography

[1] J. Vance, Rotordynamics of Turbomachinery, A Wiley-Interscience Publication, Wiley, 1988.

[2] H. Jeffcott, The lateral vibration of loaded shafts in the neighbourhood of a whirling speed the effect of want of balance, Philosophical Magazine Series 6 Vol. 37 (1919) 304314.

[3] A. Stodola, Steam and Gas Turbines, Dekker Mechanical Engineering, Mc Graw-Hill, New York, 1927.

[4] G. Ferraris, Rotordynamics prediction in engineering, no. v. 1 in Rotordynamics prediction in engineering, Wiley, 1990.

[5] M. Mohiuddin, Y. Khulief, Coupled bending torsional vibration of rotors using finite element, Journal of Sound and Vibration 223 (2) (1999) 297 – 316.

[6] D. Childs, Turbomachinery rotordynamics: phenomena, modeling, and analysis, Wiley-Interscience publication, Wiley, 1993.

[7] C. X. Mao, Q. H. Qin, Coupled torsional-flexural vibration of shaft systems in mechanical engineeringii. fe-tm impedance coupling method, Computers and Structures 58 (4) (1996) 845 – 849.

[8] J. Rao, History of Rotating Machinery Dynamics, History of mechanism and machine science, Springer, 2011.

[9] I. Friswell, Dynamics of Rotating Machines, Cambridge Aerospace Series, Cambridge University Press, 2010.

[10] A. Muszynska, Rotordynamics, Dekker Mechanical Engineering, Taylor & Francis, Dordrecht, Netherlands, 2010.

[11] B. Al-Bedoor, Modeling the coupled torsional and lateral vibrations of unbalanced rotors, Computer Methods in Applied Mechanics and Engineering 190 (45) (2001) 5999 – 6008.

[12] M. Kita, T. Hataya, Y. Tokimasa, Study of a rotordynamic analysis method that considers torsional and lateral coupled vibrations in compressor trains with a gearbox, Proceedings of the thirty-sixth turbomachinery symposium 299 (12) (2007) 31 – 37.

[13] Y. J. Chiu, D.-Z. Chen, The coupled vibration in a rotating multi disk rotor system, International Journal of Mechanical Sciences 53 (1) (2011) 1 – 10.

[14] Z. Gosiewski, Analysis of coupling mechanism in lateral/torsional rotor vibrations, Journal of theoretical and applied mechanics 46 (4) (2008) 829–844.

[15] D. Walker, Torsional Vibration of Turbo-Machinery, McGraw-Hill engineering reference, McGraw-Hill Education, 2003.

[16] Api 617, Axial and Centrifugal Compressors and Expander-compressors for Petroleum, Chemical and Gas Industry Services (August 2005).

[17] Api 684, Second Edition Tutorial on the API Standard Paragraphs Covering Rotor Dynamics and Balancing: An Introduction to Lateral Critical and Train Torsional Analysis and Rotor Balancing (August 2005).

[18] I. 10816-1, Mechanical vibration, evaluation of machine vibration by measurements on non-rotating parts - part 1: General guidelines (December 1995).

[19] P. Pennacchi, A. Vania, S. Chatterton, Nonlinear effects caused by coupling misalignment in rotors equipped with journal bearings, Mechanical Systems and Signal Processing 30 (0) (2012) 306 – 322.

[20] T. H. Patel, A. K. Darpe, Coupled bending torsional vibration analysis of rotor with rub and crack, Journal of Sound and Vibration 326 (35) (2009) 740 – 752.

[21] A. T. Tadeo, K. L. Cavalca, A comparison of flexible coupling models for updating in rotating machinery response, Journal of the Brazilian Society of Mechanical Sciences and Engineering 25 (2003) 235 – 246.

[22] J. Rao, T. Shiau, J. Chang, Theoretical analysis of lateral response due to torsional excitation of geared rotors, Mechanism and Machine Theory 33 (6) (1998) 761 – 783.

[23] A. Lee, J. Ha, D. Choi, Coupled lateral and torsional vibration characteristics of a speed increasing geared rotor bearing system, Journal of Sound and Vibration 263 (4) (2003) 725 – 742.

[24] P. Girdhar, C. Scheffer, 5 - Machinery fault diagnosis using vibration analysis, in: P. Girdhar, C. Scheffer (Eds.), Practical Machinery Vibration Analysis and Predictive Maintenance, Newnes, Oxford, 2004, pp. 89 – 133.

[25] G. Genta, Dynamics of Rotating Systems, no. v. 1 in Dynamics of Rotating Systems, Springer, 2005.

[26] M. E. Leader, Time transient analysis and non-linear rotordynamics.

[27] H. Diken, Non linear vibration analysis and subharmonic whirl frequencies of the jeffcott rotor model, Journal of Sound and Vibration.

[28] C. Agostini, E. C. Souza, Complex modal analysis of a vertical rotor by finite elements method, Proceedings of the 9th Brazilian Conference on Dynamics, Control and their Applications.

[29] Y. Luo, An efficient 3d timoshenko beam element with consistent shape functions, Advanced Theoretical Applied Mechanics.

[30] M. Prohl, A general method of calculating critical speeds of flexible rotors, Journal of Applied Mechanics, Trans. ASME, Series E 67 (1945) 142.

[31] P. Toni, Dispense del corso di dinamica dei rotori, University of Florence.

[32] N. Myklestad, Vibration Analysis, Mc Graw-Hill Book Co., 1944.

[33] N. Myklestad, Fundamental of Vibration Analysis, Mc Graw-Hill Book Co., 1956.

[34] R. Ruhl, J. Booker, A finite element model for distributed parameter turborotor systems, Journal of Engineering for Industry, Trans. ASME 94 (1972) 126.

[35] H. Nelson, J. McVaugh, The dynamics of rotor bearing systems using finite elements, Journal of Engineering for Industry, ASME 98 (1976) 593.

[36] H. Nelson, Finite rotating shaft element using timoshenko beam theory, Journal of Mechanical Design, ASME, 102 (1980) 793.

[37] H. Nelson, Finite rotating shaft element using timoshenko beam theory, Journal of Mechanical Design 102 (1980) 793.

[38] S. Falomi, Torsional electro-mechanical interaction in compression trains with a synchronous motor fed by a load commutated inverter, Ph.D. thesis, University of Florence, Engineering Faculty (2011).

[39] J. Vance, F. Zeidan, B. Murphy, Machinery Vibration and Rotordynamics, Wiley, 2010.

[40] A. V. Paolo Pennacchi, F. Frattaroli, Torsional vibrations caused by geared coupling in a shaft train driven by a steam turbine, Journal of Engineering for Gas Turbines and Power 133 (1).

[41] Z. Yuan, F. Chu, Y. Lin, External and internal coupling effects of rotor's bending and torsional vibrations under unbalances, Journal of Sound and Vibration 299 (12) (2007) 339 – 347.

[42] R. Sukkar, A. Yigit, Analysis of fully coupled torsional and lateral vibrations of unbalanced rotors subjected to axial loads, Kuwait J. Sci. Eng (35) (2008) 143 – 170.

[43] A. Tondl, Some problems of rotor dynamics, Cambridge Aerospace Series, Publishing House of the Czechoslovak Academy of Sciences, 1965.

[44] M. Rabkin, Combined flexural-torsional vibrations of multi disk rotors, Soviet Applied Mechanics (1972) 310 – 315.

[45] D. Smith, The dynamics of synchronous whirl in turbine rotors, Proceedings of IUTAM Symposium on Dynamics of Rotors (1972) 524 – 545.

[46] H. Diken, I. G. Tadjbakhsh, Unbalance response of flexible rotors coupled with torsion, Journal of Vibration and Acoustics 111 (2) (1989) 179 – 186.

[47] O. Bernasconi, Bisynchronous torsional vibrations in rotating shafts, Journal of Applied Mechanics 54 (1987) 893 – 897.

[48] R. Cohen, I. Porat, Coupled torsional and transverse vibration of unbalanced rotor, Journal of Applied Mechanics 52 (3) (1989) 701 – 705.

[49] C. Nataraj, On the interaction of torsion and bending in rotating shafts, Journal of Applied Mechanics 60 (1993) 239–241.

[50] R. Plaut, J. Wauer, Parametric, external and combination resonances in coupled flexural and torsional oscillations of an unbalanced rotating shaft, Journal of Sound and Vibration 183 (5) (1995) 889 – 897.

[51] A. Yigit, A. Christoforou, Coupled torsional and bending vibrations of actively controlled drillstrings, Journal of Sound and Vibration 234 (1) (2000) 67 – 83.

[52] N. Bachschmid, P. Pennacchi, E. Tanzi, Cracked Rotors: A Survey on Static and Dynamic Behaviour Including Modelling and Diagnosis, Springer-Verlag, 2010.

[53] C. A. Papadopoulos, A. D. Dimarogonas, Coupling of bending and torsional vibration of a cracked timoshenko shaft, Ingenieur-archive 57 (1987) 257 – 266.

[54] Y. Zhao, Q. Li, Q. Xu, Analysis on bending-torsional coupled vibration of cracked rotor, Chinese Journal of Applied Mechanics 16 (1) (1999) 60–64.

[55] H. Zhu, M. Zhao, A study on coupled vibration of a cracked rotor, Journal of Vibration Engineering 14 (3) (2001) 349–353.

[56] W. M. Ostachowicz, M. Krawczuk, Coupled torsional and bending vibrations of a rotor with an open crack, Applied Mechanics 62 (1992) 191 – 201.

[57] H. Ozguven, D. Houser, Mathematical models used in gear dynamics a review, Journal of Sound and Vibration 121 (3) (1988) 383 – 411.

[58] P. Schwibinger, R. Nordmann, The influence of torsional lateral coupling on the stability behavior of geared rotor systems, Journal of Engineering for Gas Turbines and Power 110 (1988) 563 – 571.

[59] M. LI, H. Hu, P. Jiang, L. Yu, Coupled axial lateral torsional dynamics of a rotor bearing system geared by spur bevel gears, Journal of Sound and Vibration 254 (3) (2002) 427 – 446.

[60] B. Kishor, S. K. Gupta, On dynamic gear tooth loading due to coupled torsional lateral vibrations in a geared rotor-hydrodynamic bearing system, Journal of Tribology 111 (3) (1989) 418 – 425.

[61] B. AlBedoor, Dynamic model of coupled shaft torsional and blade bending deformations in rotors, Computer methods in Applied Mechanics and Engineering 169 (1999) 177 – 190.

[62] B. Al-Bedoor, Transient torsional and lateral vibrations of unbalanced rotors with rotor-to-stator rubbing, Journal of Sound and Vibration 229 (3) (2000) 627 – 645.

[63] Z. Sun, J. Xu, T. Zhou, N. Tan, Study on influence of bending-torsion coupling in an impacting-rub rotor system, Applied Mathematics and Mechanics 24 (11) (2003) 1316 – 1323.

[64] T. Szolc, On the discrete-continuous modeling of rotor system for the analysis of coupled lateral torsional vibrations*, International Journal of Rotating Machinery 6 (2) (2000) 135 – 435.

[65] D. Huang, L. Zhu, Z. Jiang, Numerical simulation of unbalanced rotor with bending-torsion coupling, Steam turbine technology 37 (6) (1995) 346 – 348.

[66] D. Huang, Characteristics of torsional vibrations of a shaft with unbalance, Journal of Sound and Vibration 308 (35) (2007) 692 – 698.

[67] Liu, Cui, Huang, al., Study of non-linear dynamic characteristics of a rotor with coupled bending and torsional vibrations, Computers and Structures 58 (4) (1996) 845 – 849.

[68] S.-C. Hsieh, J.-H. Chen, A.-C. Lee, A modified transfer matrix method for the coupled lateral and torsional vibrations of asymmetric rotor-bearing systems, Journal of Sound and Vibration 312 (45) (2008) 563 – 571.

[69] C. X. Mao, Q. H. Qin, Coupled torsional-flexural vibration of shaft systems in mechanical engineering i. finite element model, Computers and Structures 58 (4) (1993) 835 – 843.

[70] O. Bachau, S. Han, Three-dimensional beam theory for flexible multibody dynamics, Journal of Computational and Nonlinear Dynamics 9 (4).

[71] M. Brown, A. Shabana, Application of multibody methodology to rotating shafts problem, Journal of Sound and Vibration 204 (3) (1997) 439 – 458.

[72] E. Zorzi, H. Nelson, The dynamics of rotor bearing systems with axial torque: A finite element approach, ASME Journal of Mechanical Design 102 (1980) 158.

[73] O. Zienkiewicz, R. Taylor, J. Zhu, The Finite Element Method: Its Basis and Fundamentals: Its Basis and Fundamentals, Elsevier Science, 2005.

[74] COMSOL Multiphysics®: Reference Manual, `www.comsol.com` (1998–2013).

[75] T. H. Patel, A. K. Darpe, Vibration response of misaligned rotors, Journal of Sound and Vibration 325 (3) (2009) 609 – 628.

[76] F. Cangioli, Development and validation of innovative models for the analysis of coupled lateral-torsional vibrations in rotating machines, University of Florence Master's Degree Thesis.

[77] ERRI 126 RP-18 Problemes de freinage — exigences requises des bancs de freinage pour l'homologation internationale des matriaux de frottement (2003).

[78] UIC 540 Brakes — Air brakes for freight and passenger train characteristics of railway vehicles (2002).

[79] UIC 541-1 Brakes — regulations concerning the manufacture of different brake parts (2003).

[80] EN 15734-2 Railway applications — Braking systems of high speed trains — Part 2: Test Methods (2011).

[81] Shigley'S Mechanical Engineering Design (Sie) 8E, McGraw-Hill Education (India) Pvt Limited.

[82] T. Lim, R. Singh, Vibration transmission through rolling element bearings, part i: Bearing stiffness formulation, Journal of Sound and Vibration 139 (2) (1990) 179 – 199.

[83] Report on the rotordynamical modelling of a flywheel test bench using rotlab, University of Florence.

Acknowledgements

This thesis is the result of my research activity during the Ph.D in Industrial Engineering at the University of Florence. I would like to thank each and every person who helped me in this challenging activity to which I like to refer as the final part of a great adventure.

Firstly, I thank my advisor Dr. Andrea Rindi for the encouragement and advice provided during the Ph.D activity. A special thanks to Prof. Benedetto Allotta for his great support during the Master's degree thesis. A debt of gratitude must go to Dr. Enrico Meli who provided the vision, encouragement and advice necessary to complete the Ph.D research. I would like to thank Prof. Paolo Toni, to whom I'll always think about as my mentor as he always gave to me brilliant comments and suggestions and he deeply encouraged me letting me grow as researcher and engineer. A special thanks also to my friend Dr. Lorenzo Marini, whose friendship and support has really meant to me. I wish to thank all the colleagues, researchers, Ph.D students and students of the MDMLab for sharing these years with me. A special thanks to Benedetta and Elisa for the really good time spent together and to Filippo and Giulia, for their worthy, helpful and serious works. A huge thanks to my dear friend Eng. Rosa Schina for being the most precious treasure I found in Santa Marta.

I want to express my huge professional respect to Prof. Paolo Pennacchi, who supported my research activity providing experimental data and worthy advice and suggestions.

I wish to thank everyone I studied or worked with and from whom I learned during this lifetime adventure spent in school and University. A preliminary and promising thank you to the CAMD Rotordynamic team at GE Oil&Gas, for the wish of starting a new adventure as much interesting and challenging as the just finished one.

I would like to thank all my family (human beings and animals) for all their unconditioned love and for giving me that gift that a great scientist called the *enviable opportunity to learn to know the liberating influence of beauty in the realm of the spirit for your own personal joy and to the profit of the community to which your later work belongs.* Particularly, I want to thank my grand-father Adolfo and my aunt Simona for being such great models to me.

Finally, I wish to thank Fabio for his patience, support and love throughout all these years.